Regulation of Cerebral Cortex Folding by Controlling Neuronal Migration and Progenitor Expansion

Dissertation an der Fakultät für Biologie

der Ludwig-Maximilians-Universität München

zur Erlangung des akademischen Grades

eines Doktor der Naturwissenschaften (Dr. rer. nat.)

Seung Hee Chun

Munich, 26. July 2023

Diese Dissertation wurde angefertigt

unter der Leitung von Prof. Dr. Rüdiger Klein

in der Abteilung Moleküle – Signale – Entwicklung am Max-Planck-Institut für Biologische Intelligenz in Martinsried, Deutschland.

Erstgutachter*in:	Prof. Dr. Rüdiger Klein
Zweitgutachter*in:	Prof. Dr. Laura Busse

Tag der Abgabe:	26. July 2023
Tag der mündlichen Prüfung:	23. Jan 2024

Eidesstattliche Erklärung

Ich versichere hiermit an Eides statt, dass die vorgelegte Dissertation von mir selbständig und ohne unerlaubte Hilfe angefertigt ist.

München, den ……26. July 2023…… ……Seung Hee Chun……..

(Unterschrift)

Erklärung

Hiermit erkläre ich,

☒ dass die Dissertation nicht ganz oder in wesentlichen Teilen einer anderen Prüfungskommission vorgelegt worden ist.

☒ dass ich mich anderweitig einer Doktorprüfung ohne Erfolg nicht unterzogen habe.

München, den ……26. July 2023…… ……Seung Hee Chun……..

(Unterschrift)

ABSTRACT

Cerebral cortex folding represents a highly important evolutionary mechanism, one that remains, as yet, not fully understood. Present evidence suggests that cortex folding is caused by two cellular mechanisms: (1) expansion of progenitor cells, and (2) divergent radial migration of neurons. We previously generated a genetic deletion mouse model in which two cell adhesion molecules were ablated: *Flrt1/Flrt3* double knockout mice. This model showed sulci-like cortex folding induced by divergent radial neuronal migration without expansion of progenitor cells. We used this 'cell migration' model to ask if the two folding mechanisms synergize, and whether the expansion of certain types of progenitors leads to qualitatively different cortical folds. In this thesis, I describe the generation and phenotypic analysis of two different triple knockout (TKO) mouse lines. I found that overproduction of intermediate progenitors by deletion of the centrosomal protein 83 (Cep83) in this 'cell migration' model (*Cep83/Flrt1/Flrt3*^{TKO} mice, in short *Cep83*^{TKO} mice) lead to cortical folding with an increased sulci-like appearance. In a separate mouse model, increasing the length of the early cortical stem cell expansion phase by deletion of fibroblast growth factor 10 (FGF10) in the 'cell migration' model (*Fgf10/Flrt1/Flrt3*^{TKO} mice, in short *Fgf10*^{TKO} mice) lead to cortical folding with a much increased penetrance and, interestingly, gyrus-like protrusions. These results indicate that expansion of progenitor cells and divergent radial migration of neurons synergize *in vivo* to induce cortical folding. They further suggest that expanding different types of progenitors leads to qualitatively different folding, raising the possibility that the formation of gyri and sulci requires the timely expansion of distinct progenitors.

TABLE OF CONTENTS

LIST OF TABLES

LIST OF FIGURES

LIST OF ABBREVIATIONS

AKNA	AT-hook transcription factor
AP	apical progenitor
aRG	apical radial glia
bIP	basal intermediate progenitor
BP	basal progenitor
BrdU	bromodeoxyuridine
bRG	basal radial glia
BSA	bovine serum albumin
CGE	caudal ganglionic eminence
Cep83	centrosomal protein 83
$Cep83^{DKO}$	$Cep83^{KO}Flrt1^{-/-}Flrt3^{het}$
$Cep83^{TKO}$	$Cep83/Flrt1/Flrt3^{TKO}$
cKO	conditional knock out
CNS	central nervous system
CP	cortical plate
CTL	littermate control, $Flrt1^{-/-}Flrt3^{het}$
DAP	distal appendage
DAPI	4',6-diamidino-2-phenylindole
DBE	dibenzylether
DCM	dichloromethane

DCX	doublecortin
Di	diencephalon
DKO	double knock-out
dNTP	deoxynucleotide triphosphate
E	embryonic day
ECM	extracellular matrix
EDTA	ethylenediaminetetraacetic acid
EOMES	eomesodermin
FB	Forebrain
FGF	fibroblast growth factor
$Fgf10^{DKO}$	$Fgf10^{KO}Flrt1^{-/-}Flrt3^{het}$
$Fgf10^{TKO}$	$Fgf10/Flrt1/Flrt3^{TKO}$
FLRT	fibronectin leucine rich transmembrane protein
GE	ganglionic eminence
GFP	green fluorescent protein
GI	gyrification index
HB	hindbrain
HCL	hydrochloric acid
ISVZ	inner subventricular zone
ISH	*in situ* hybridization
INM	interkinetic nuclear migration
IP	intermediate progenitor
IUE	*in utero* electroporation

IZ	intermediate zone
lCP	lower cortical plate
LGE	lateral ganglionic eminence
LIS1	lissencephaly-1
LRR	leucine-rich repeat
MT	microtubule
MTOC	microtubule organizing canter
MB	Midbrain
Met	metencephalon
MGE	medial ganglionic eminence
Myel	myelencephalon
MZ	marginal zone
NBN	newborn neuron
NE	neuroepithelia
NEC	neuroepithelial cells
NSC	neural stem cell
NSPC	neural stem/progenitor cell
O.C.T.	optimal cutting temperature compound
OSVZ	outer subventricular zone
PCR	polymerase chain reaction
PBS	phosphate-buffered saline
PBST	phosphate-buffered saline with triton X-100
PFA	paraformaldehyde

RELN	reelin
RGP	radial glia progenitor cells
Satb2	special AT rich sequence binding protein 2
SC	spinal cord
shRNA	short hairpin RNA
Sox2	SRY-box transcription factor 2
SVZ	subventricular zone
TAE	tris-acetate-ethylenediaminetetraacetic acid
Tbr2	T-box brain protein 2
TBS	tris-buffered saline
TBST	tris-buffered saline with triton X-100
TdTomato	tandem dimer tomato
Tel	telencephalon
THF	tetrahydrofurane
TKO	triple knock out
Trnp1	TMF1 regulated nuclear protein 1
uCP	upper cortical plate
VZ	ventricular zone
WT	wild-type

1. INTRODUCTION

Based on cortical folding, mammals can be categorized into two groups: gyrencephalic species (ferrets and most primates), which are characterized by brains that exhibit folds consisting of gyri and sulci; and lissencephalic species (such as mice), which are characterized by smooth-surfaced cortices, lacking pronounced folding patterns.

The neocortex is the brain structure which is mainly responsible for the cognitive abilities of the higher vertebrates is responsible. During evolution, the surface of the cerebral cortex becomes folded and is thus greatly enlarged. It is this surface enlargement and the associated increase in number of neurons that enable the advanced brain and memory abilities of primates such as pronounced social behavior. (Lohmann et al., 2007; Fernández et al., 2016). The prevailing hypothesis proposes that it is the combination of progenitor expansion with divergent radial migration that contributes to the expansion and folding of the cerebral cortex. However, the relative contribution of both mechanisms is not known.

Our lab previously showed that genetic deletion of Flrt1/3 in mice resulted in sulcus formation in the normally smooth mouse neocortex (Del Toro et al., 2017). This process happened due to changes in the migration of cortical neurons, independent of changes in cell proliferation.

Based on studies in gyrencephalic species, cortical folding could take place in two stages: In a first stage, more cortical neurons are formed, which then show characteristic migratory behavior in a second stage. In FLRT mouse mutants, the first stage (multiplication of neurons) is absent, while the second stage takes place. Overall, cortex folding in the FLRT mouse mutants is still quite subdued due to the lack of the first stage, with only a few (one to two) wrinkles per brain, often only one-sided, and pronounced in only about one third of the FLRT mouse mutants (Del Toro et al., 2017).

Therefore, I hypothesize that the combined alteration of different cellular mechanisms (higher migration speed and increased number of cortical neurons, which produces cortex expansion) may lead to an increase of folds and/or to an increase of the phenotypic penetrance. To investigate whether all of these cellular processes are needed to promote cortex folding, I generated new mouse models to strengthen cortex folding by combining the FLRT mutations with other proteins that could promote an increase of neuronal pools, namely Cep83 and Fgf10, and thereby reveal how folding occurs (Figure1.1.1).

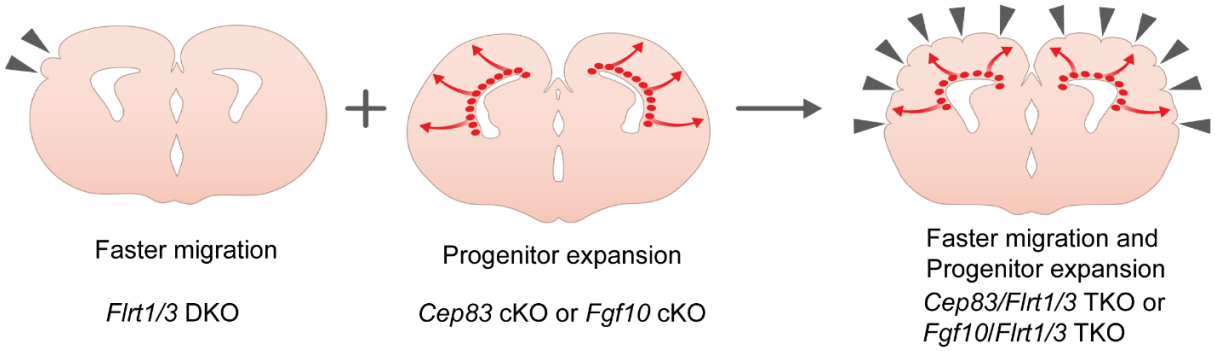

Figure 1.1.1 Graphical summary of generation of *Cep83/Flrt1/Flrt3*^{TKO} (*Cep83*^{TKO}) and *Fgf10/Flrt1/Flrt3*^{TKO} (*Fgf10*^{TKO}) mice.

1.1 Cortical folding

The expansion and folding of the mammalian cerebral cortex are responsible for higher brain functions such as cognition, memory, language, and decision-making. The folding of the mammalian cortex is composed of two major structures, sulci i.e., fissures which are invaginations or grooves (sulcal fundus) of cortical tissue, and gyri, i.e., folds or convolutions which are protrusions of rounded elevations (Gyral crown) of cortical tissue between two sulci (Figure 1.1.2; Llinares-Benadero et al., 2019; Borrell, 2018; Garcia et al., 2018).

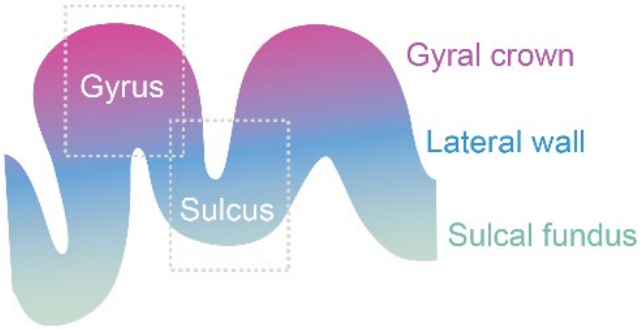

Figure 1.1.2 Anatomy of cortical folding

Schematic illustration of cortical folding, showing gyrus, convex folds, sulcus, and valleys (Graphic adapted from Llinares-Benadero et al., 2019).

Depending on the existence of cortical folding, mammalian species can be classified into gyrencephalic (such as primates, dolphin, cat, and ferret), which have folding in the cortex, and lissencephalic (such as rodents), which exhibit smooth cortices. In general, cortical size plays a crucial role in inducing cortical folding (Figure 1.1.3; Kelava et al., 2013).

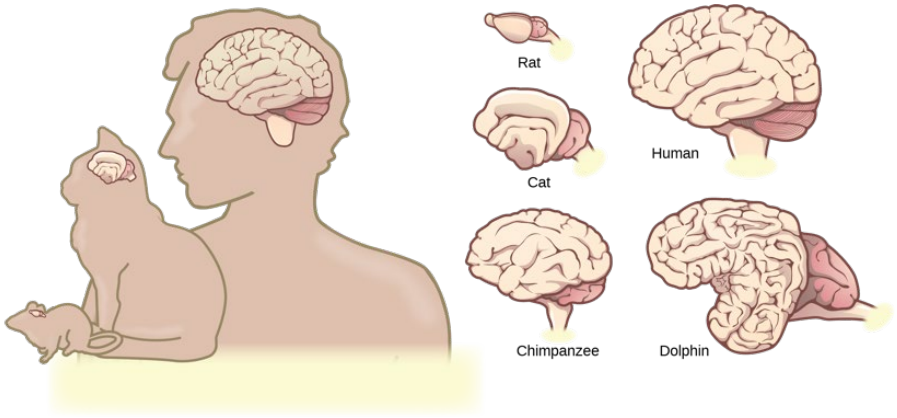

Figure 1.1.3 Gyrencephalic and lissencephalic species

Graphical illustration of representative gyrencephalic species such as human, chimpanzee, dolphin, and cat, and lissencephaly such as rodent (Figure adapted from OpenEd CUNY).

1.2 Development of the neocortex

The mammalian cerebral cortex is a highly dynamic complex composed of many different cell types. Sophisticated coordination of a variety of developmental processes is necessary to generate proper brain function. Development of the neocortex starts when the neural tube closes and develops into three primary vesicles: the forebrain, the midbrain, and the hindbrain.

The forebrain and hindbrain further develop into secondary vesicles: the telencephalon/diencephalon and myelencephalon/metencephalon, which further develop into specific brain structures in the neocortex (Figure 1.2.1). The cerebral cortex occupies the majority of the brain, and mainly forms from the smooth sheet of the dorsal part of the telencephalic proliferative zone (Meyer et al., 1998; Wilson et al., 2004; Ishikawa et al., 2012; Agirman et al., 2017).

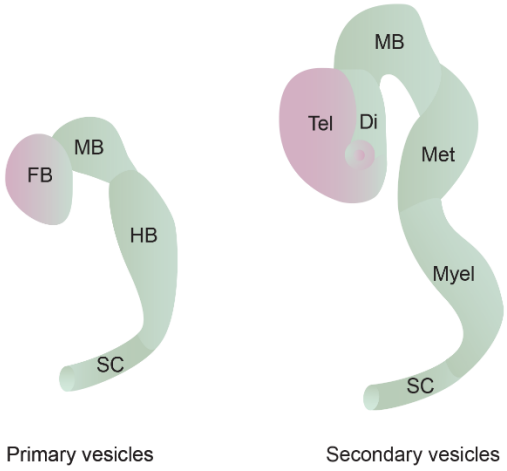

Figure 1.2.1 Cerebral cortex development

The rostral region of neural tubes develops into three distinct primary brain vesicles: the forebrain (FB), midbrain (MB), and hindbrain (HB). These three primary vesicles go on to subdivide into a series of five secondary brain vesicles: the Telencephalon (Tel), Diencephalon (Di), metencephalon (Met), myelencephalon (Myel), and the spinal cord (SC).

The developing cortex is organized into distinct zones and layers with specific cell types. The ventricular/subventricular zone (VZ/SVZ) is the region where neurons are born. It contains radial glia cell bodies, which serve as scaffolds for neuronal migration. Above the VZ/SVZ is the intermediate zone (IZ), followed by the cortical plate (CP), which is subdivided into six layers, I-VI. Layer I, is the most superficial layer and contains few neuronal cell bodies. However, it is densely packed with the apical dendrites of cortical pyramidal neurons and axons from cortical and thalamic neurons (Rubio-Garrido et al., 2009), indicating its role in integrating information from different brain regions. Layers II/III contain pyramidal neurons that predominantly project their axons to the opposite hemisphere via the anterior commissure and the corpus callosum, forming callosal projections (Molyneaux et al., 2007). Layer IV mainly receives input from subcortical regions, especially the thalamus, and serves as a relay station for sensory information processing. Deep-layer neurons in layers V and VI project their axons mostly to subcortical regions. Layer V neurons extend their axons to the brainstem and the spinal cord, while layer VI neurons provide input to thalamic nuclei from the cortex. The excitatory neurons in the cortex, including pyramidal neurons in layers II-VI, are glutamatergic and use glutamate as their primary neurotransmitter (Figure 1.2.2; Gilmore et al, 1997; Cadwell et al., 2019).

Excitatory neurons are generated from neural stem cells located in the VZ of the dorsal telencephalon and migrate radially toward the CP to establish long-range connections with other brain regions (Figure 1.2.3). Inhibitory GABAergic interneurons, another major cell type in the cortex, are generated from neural progenitors located in the ganglionic eminence (GE) of the ventral telencephalon and migrate tangentially to the developing cortical wall to reach their final positions (Figure 1.2.3; Molnár et al, 2019**;** Mukhtar et al, 2018).

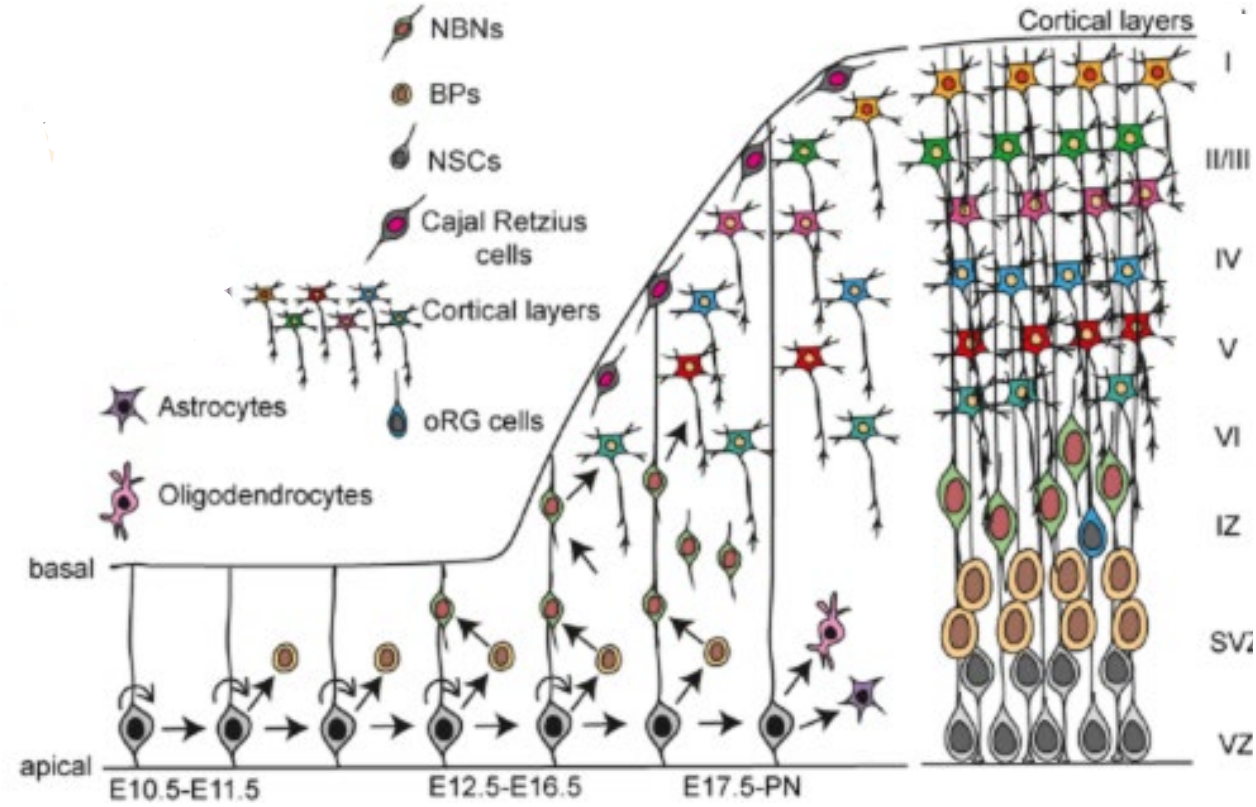

Figure 1.2.2 Schematic diagram of the developing cortex

During the early stages of cerebral cortical development, (E10.5-E11.5), neural stem cells (NSCs) mainly undergo symmetric cells divisions to expand the NSC pool, which is referred to as the expansion phase. During late embryogenesis, (E12-E16.5), NSCs promote asymmetric divisions to generate one NSC (self-renewal) and one BP, which is referred to as the neurogenic phase. Neurons are generated sequentially, and settle down in an inside-out fashion. At later stages of development, NSCs generate the other cell types, such as astrocytes and oligodendrocytes, which is referred to as the gliogenic phase. BPs, basal progenitors; NBNs, newborn neurons; NSCs, neural stem cells; IZ, intermediate zone; SVZ, subventricular zone; VZ, ventricular zone (Figure 1.3.2 adapted from Mukhtar et al.,2018).

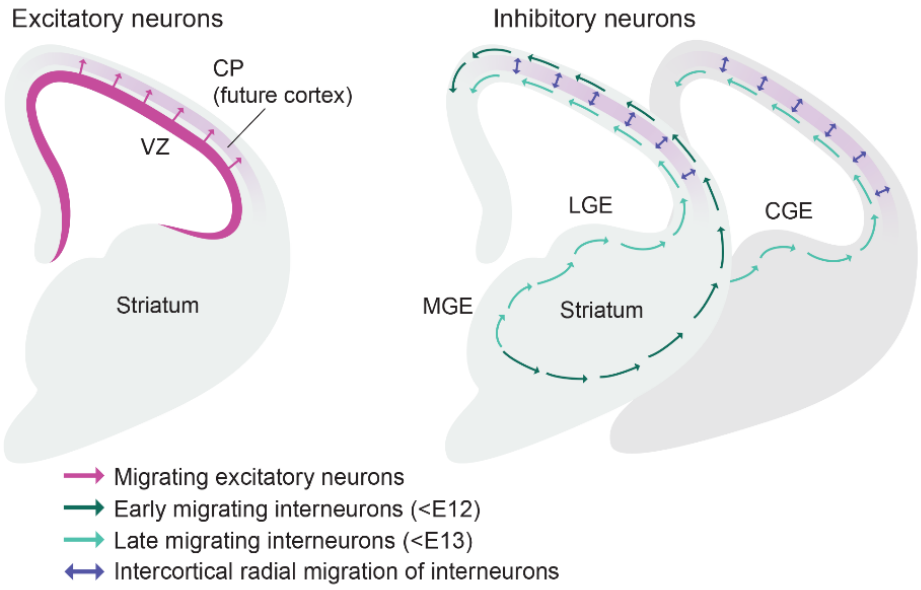

Figure 1.2.3 Origin and migration path of cortical neurons in the developing cortex

Excitatory cortical neurons have their origin in the ventricular zone (VZ, depicted in magenta), located in the dorsal telencephalon. These newborn neurons migrate radially along the radial fiber scaffold (depicted by magenta arrows), towards the cortical plate (CP, depicted in light magenta). In contrast, inhibitory cortical interneurons are generated in the ventricular zone of the medial ganglionic eminence (MGE) in the ventral telencephalon. These interneurons migrate over long distances, taking two different routes: one closer to the ventricular surface, and the other closer to the pial surface. Both paths bypass the striatum (depicted in dark and light green arrows). Upon reaching the cortex, interneurons change their direction and radially invade the cortical plate (CP) where they settle. Lateral ganglionic eminence (LGE), Caudal ganglionic eminence (CGE).

1.3 Neurogenesis: progenitor subtypes

The proper growth and formation of the cortex in neurogenesis is highly dependent on the precise regulation of neural progenitor cell proliferation and differentiation. Distinct subtypes of neural progenitor cells, which arise at specific time points during cortical development, are critical for proper brain functioning. Neuroepithelial cells (NECs, yellow in Figure 1.3) are the earliest type of neural progenitor cells during cortical development. They are organized in a single pseudostratified layer and possess a high capacity for proliferation. NECs exhibit a bipolar morphology, with their apical domains attached the ventricle and their basal domains in contact with the basement membrane. NECs exclusively undergo symmetrical division, generating more NECs but at a later time point, it switches mode to generate radial glial progenitors (RGPs). RGPs are the classical neural stem cells (NSCs) responsible for producing the majority of cortical excitatory neurons. RGPs have a distinct bipolar morphology, with a short apical endfoot attached to the ventricular surface, and a long basal fiber extending to the pial membrane. The apical endfeet of RGPs are connected through adherens junctions, forming the ventricular surface, and the nuclei of RGPs are arranged in a pseudostratified manner, creating the VZ adjacent to the lateral ventricle of the brain. RGPs are capable of dividing in different modes at different stages of cortical development. During early embryonic cortical development, RGPs initially undergo symmetrical divisions, expanding the neural progenitor pool. Later, RGPs undergo a transition into asymmetric cell divisions that generate neurons directly or indirectly through intermediate progenitors (IPs) or basal radial glia cells (bRGCs). IPs are generated from the asymmetric cell division of RGPs. After their birth, IPs detach from the ventricular surface and migrate to the SVZ. They have limited proliferative potential and typically undergo one round of terminal symmetric cell division, resulting in the production of two neurons. In mice, IPs are responsible for generating the majority of both deep and superficial layer neurons in the cortex. (Figure 1.3; Götz et al., 2005; Wang et al., 2011; Arai et al., 2017; Martínez-Cerdeño et al., 2018).

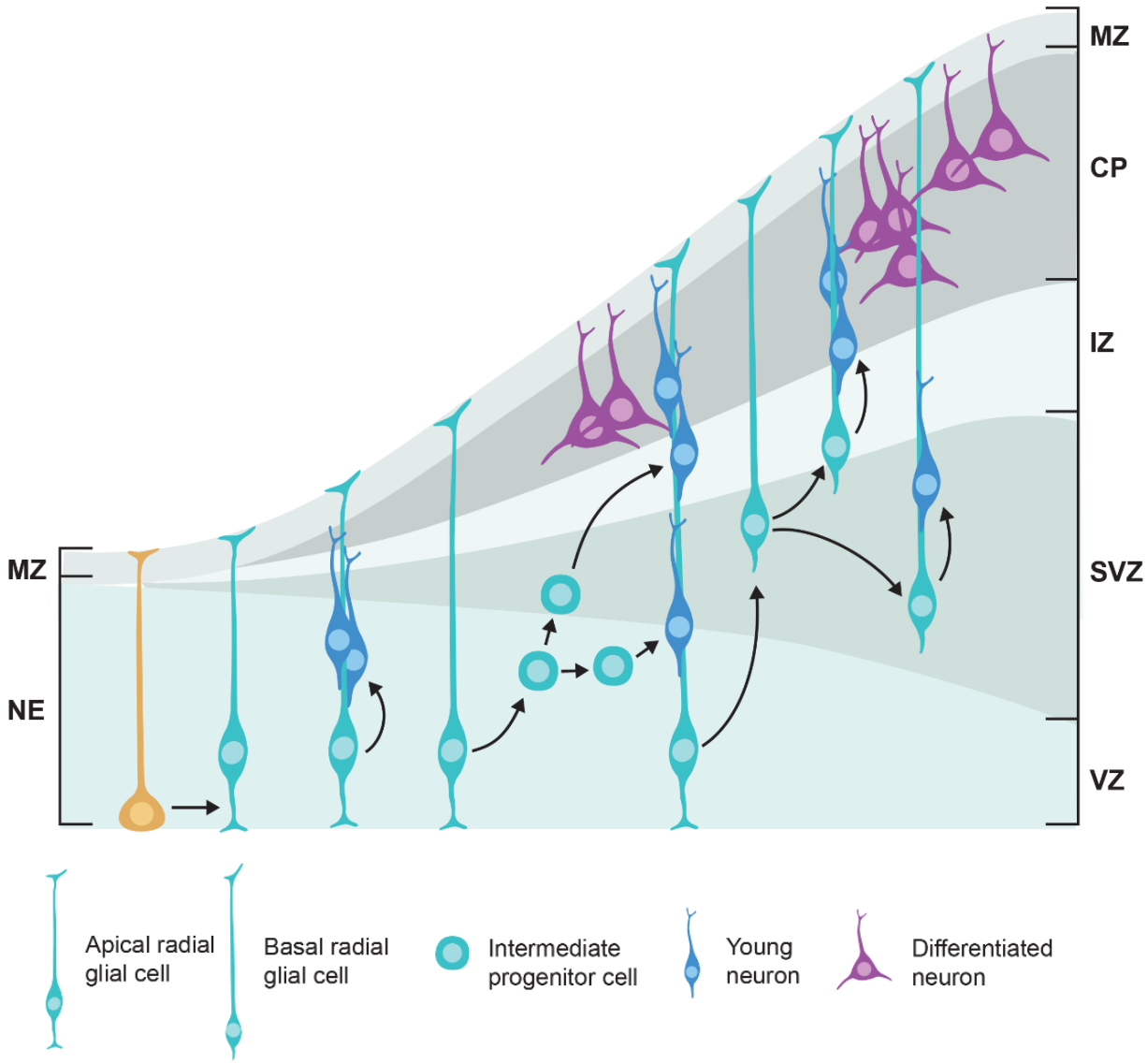

Figure 1.3 Schematic diagram of neurogenesis

Illustration depicting the main types of progenitor cells and their lineage relationships in the developing cerebral cortex. Arrows indicate lineage relationships. NE, Neuroepithelia; MZ, Marginal zone; VZ, ventricular zone; SVZ, subventricular zone; IZ, intermediate zone; CP, cortical plate.

1.4 Cell cycle progression

Previously, proliferating progenitor cells in the VZ of cultured human fetal cortical slices were identified using 3H-thymidine labeling which tracks DNA synthesis (Rakic et al.,1968). The progenitor cells in the VZ of the developing cortex exhibit distinct patterns of nuclear movement during different phases of the cell cycle. The VZ is a region in the developing brain that contains neural progenitor cells, which are responsible for generating various types of neurons and glial cells. During the cell cycle, which consists of distinct phases such as G1 (gap 1), S (synthesis), G2 (gap 2), and M (mitosis), progenitor cells in the VZ undergo nuclear movement that is tightly regulated and coordinated with cell cycle progression. In the G1 phase, progenitor cell nuclei in the VZ are often observed near the ventricular surface, where they actively undergo interkinetic nuclear migration (INM) (Figure 1.4). INM is the characteristic movement of progenitor cell nuclei in a basal-to-apical direction during the cell cycle, where the nuclei migrate away from the ventricular surface during the G1 phase and return towards the ventricular surface during G2. (Taverna et al, 2010; Kosodo et al, 2011; Azzarelli et al, 2015). During S phase, when DNA replication occurs, progenitor cell nuclei typically remain close to the ventricular surface, and their movement is limited compared to the G1 and G2 phases. After DNA replication is completed in S phase, progenitor cells enter the G2 phase, where the nuclei migrate back towards the ventricular surface in preparation for mitosis. During mitosis (M phase), progenitor cell nuclei undergo complex movements that involve rounding up, followed by division, leading to the generation of two daughter cells. These daughter cells can then either remain as progenitor cells or differentiate into neurons or glial cells, contributing to the development of the nervous system. The characteristic pattern of nuclear movement during different phases of the cell cycle in progenitor cells of the VZ is essential for proper development of the brain and regulation of cell proliferation, differentiation, and distribution in the developing cortex (Sauer and Walker, 1959; Farkas et al, 2008; Spear et al.,2012; Sun et al., 2014).

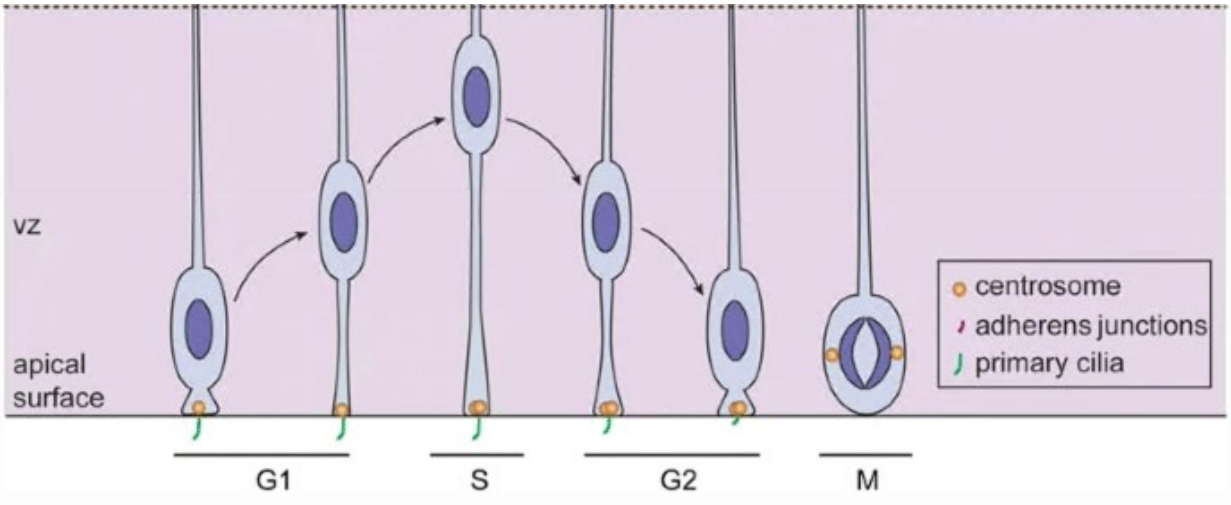

Figure 1.4 Interkinetic nuclear migration of radial glial cells.

Radial glial cells (RGs), which are progenitor cells in the ventricular zone (VZ) of the developing nervous system, undergo characteristic nuclear movements during different phases of the cell cycle.

1.5 Neuronal migration

Neuronal migration is the movement of neurons from their birthplace to their final destination in the developing cerebral cortex. Neuronal migration plays a fundamental role in establishing the complex layered structure of the cortex, which is critical for its proper function. The process of neuronal migration can be divided into several stages (Cooper, 2013; Kawauchi et al., 2006; Tabata and Nakajima, 2003; Hatanaka et al., 2016). Neurons are generated from progenitor cells in the VZ of the developing brain. These progenitor cells divide and produce post-mitotic neurons, which then begin their journey towards their final destination in the cortex. Newly generated neurons transition to a multipolar stage, where they extend multiple processes, and form neurites. These neurites serve as guides for neuronal migration and help neurons navigate through the developing brain tissue. Most cortical neurons migrate radially, guided by a specialized type of glial cell, apical radial

glia cells (aRGCs), which extend from the VZ to the pial surface of the developing cortex. Neurons use these radial glial fibers as a scaffold, climbing up or down along them to reach their final position in the cortical layers. This type of migration is known as radial migration and is a characteristic feature of cortical development (Figure 1.2.3, migration of excitatory neurons). In addition to radial migration, some neurons in the cortex also migrate tangentially, that is, they move horizontally within specific cortical layers (Figure 1.2.3, migration of inhibitory neurons). Tangential migration contributes to the diversity of cell types and their distribution within the cortex. Once neurons reach their final destination, they stop migrating and start establishing synaptic connections with other neurons, ultimately forming the complex neural circuits that underlie cortical function (Figure 1.6.2). The precise regulation of neuronal migration is critical for proper cortical development, and disruptions in this process can lead to various neurodevelopmental disorders, such as lissencephaly, periventricular heterotopia, and cortical dysplasia (Spalice et al., 2009; Gressens et al., 2000; Lambert de Rouvroit et al., 2001; Rahimi-Balaei et al., 2018).

1.6 Gyrencephaly vs Lissencephaly : Neurogenesis and Neuronal migration

Cortical size is highly related to folding phenotypes in many gyrencehpalic species. The growth of the neocortex is strongly regulated by the proliferation and differentiation of neural stem/progenitor cells (NSPCs) and neuronal migration. These factors are highlighted when we compare cellular composition and organization of the developing cortex between gyrencephalic, i.e. ferret, and lissencephalic species, i.e. mouse. Progenitor expansion is a crucial aspect that induces cortical expansion and folding. During neurogenesis, there are two distinct types of cell division: direct, and indirect neurogenesis. The number and type of neurons produced in each neurogenesis differ significantly. Direct neurogenesis involves the direct production of a single neuron from the division of an aRGC. In indirect neurogenesis, an intermediate progenitor is produced from RGCs, which leads to the production of two neurons (Figure 1.6.1; Homem et al., 2012). The robust progenitor expansion in gyrencephalic species, specifically through indirect neurogenesis, can produce more neurons and lead to cortical expansion as compared to direct neurogenesis, which is typical in lissencephalic species (Albert et al., 2015 Cárdenas et al., 2018; Borrell and Götz, 2014). Furthermore, the gyrencephalic cortex expands greatly in the SVZ, specifically in the inner subventricular zone (ISVZ) and outer subventricular zone (OSVZ). The ISVZ and OSVZ are highly occupied by bRGCs and IPs, which can lead to tangential expansion of the cortex. bRGCs are neural stem cells generated from aRGCs. Unlike aRGCs, a classic RGC is attached to the apical endfeet of the VZ, bRGCs are not anchored to the apical surface of the VZ, but only attached to the basal endfeet of the pial surface, and their cell soma is located in the ISVZ or OSVZ. Structurally, bRGCs provide a wider scaffold divergence that means neurons can migrate towards CP. Therefore, the abundance of bRGCs allows lateral dispersion of radial migrating neurons. Furthermore, it is known in ferret that migrating neurons are able to laterally switch several radial glial fibers, so in that sense their lateral dispersion is higher but the mechanisms are not known

(Kornack, D. & Rakic, P, 1999; and Gertz, C. et al., 2015). As a result, the surface area of the cortex expands with folding in gyrencephalic species, whereas lissencephalic species have relatively small cortices with smooth brains (Figure 1.6.2; Striedter et al., 2015; Floria et al., 2015; Ju et al., 2016; Llinares-Benadero et al., 2019; Borrell and Götz, 2014).

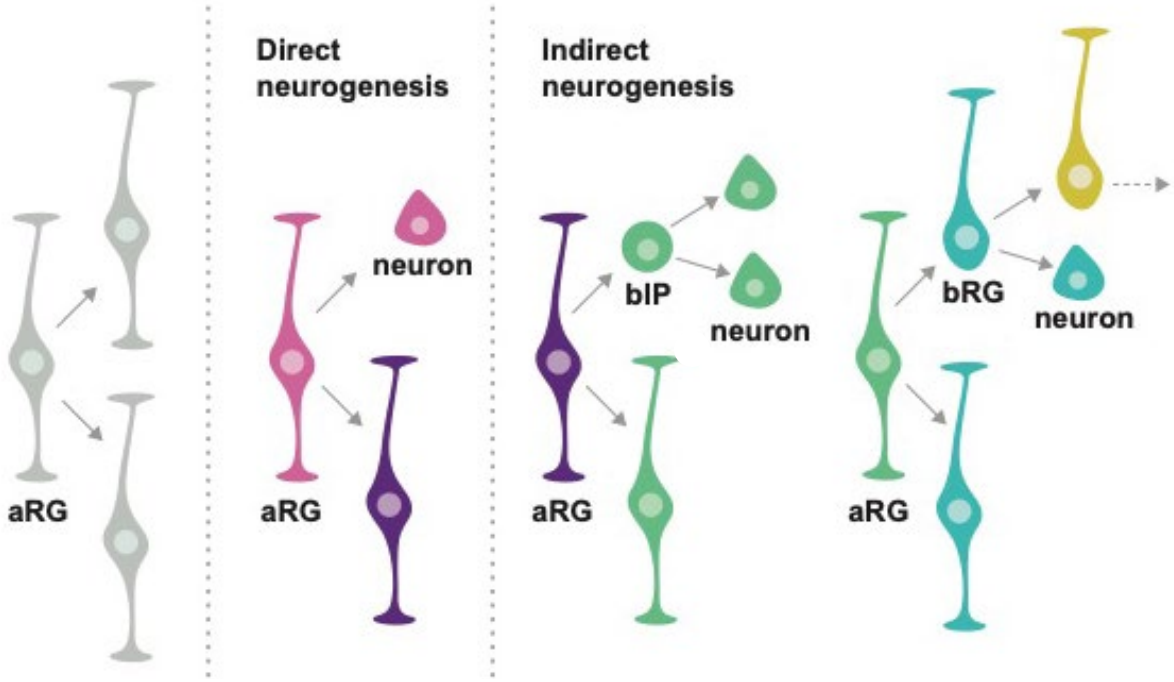

Figure 1.6.1 Schematic illustration of progenitor lineages in direct and indirect neurogenesis

Radial glial cells (aRGCs, shown in pink) undergo asymmetric division during direct neurogenesis, resulting in both self-renewal and the generation of differentiated neurons (shown in purple). During indirect neurogenesis, RGCs can divide obliquely towards the ventricular surface, leading to self-renewal and the generation of intermediate precursor cells (IPCs, shown in green). IZ, intermediate zone; VZ, ventricular zone; aRG, apical radial glia; bIP, basal intermediate progenitor; bRG, basal radial glia.

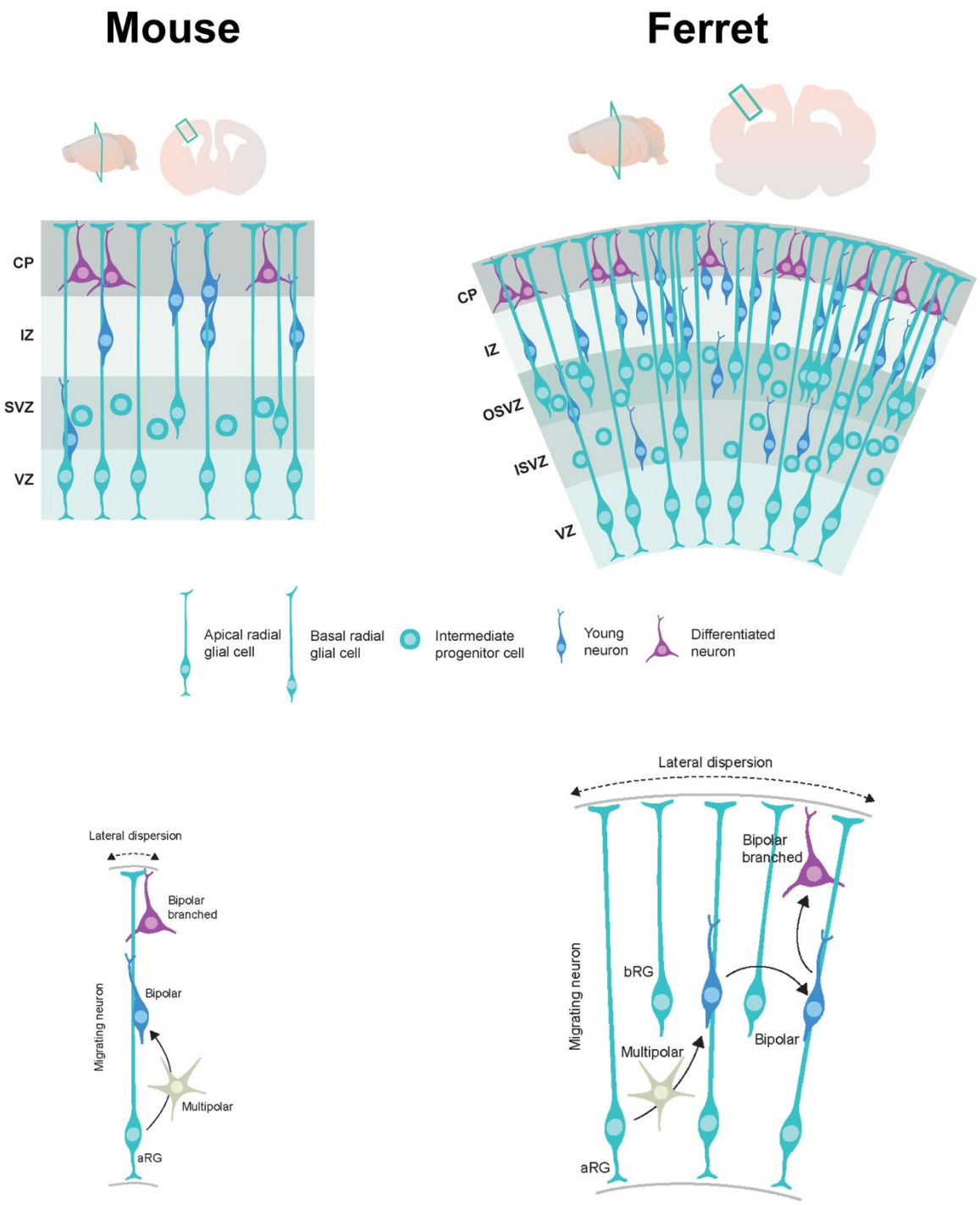

Figure 1.6.2 Cellular mechanisms of cortical expansion in folding

Different underlying mechanisms in lissencephalic species (e.g. mouse) and gyrencephalic species (e.g. ferret) during embryonic development. The first graphic illustration depicts the composition and organization of the embryonic cortex in mouse and ferret. The second schematic diagram depicts cortical migration in mouse (radial migration without lateral dispersion) and ferret

(enlarged trajectory of migration by lateral dispersion). MZ, marginal zone; VZ, ventricular zone; SVZ, subventricular zone; OSVZ, outer subventricular zone; ISVZ, inner subventricular zone; IZ, intermediate zone; CP, cortical plate; aRG; apical radial glia, bRG; basal radial glia (graphic adapted from Llinares-Benadero et al., 2019).

1.7 FLRT proteins and *Flrt1/3* DKO mice

The fibronectin leucine rich transmembrane proteins (FLRTs) were first identified in a screen for extracellular matrix proteins (Lacy et al., 1999). FLRTs are expressed in many tissues, but all FLRTs (FLRT1/2/3) are specifically exhibited in the brain (Lacy et al., 1999). In general, FLRTs are regulators of early embryonic, vascular, and neuronal development (Maretto et al., 2008; Müller et al., 2011; O'Sullivan et al., 2012). Importantly, FLRTs play a critical role in regulating cell migration during early embryonic development through their interactions with various proteins, such as Unc5D, Teneurin, and Latrophilin (Yamagashi et al., 2001; Karaulanov et al., 2009; Leyva-D´ıaz et al., 2014; Seiradake et al., 2014; Jackson et al.,2015; Del Toro et al., 2020). FLRTs also play a role in maintaining cell integrity during development (Haines et al., 2006; Muller et al., 2011).

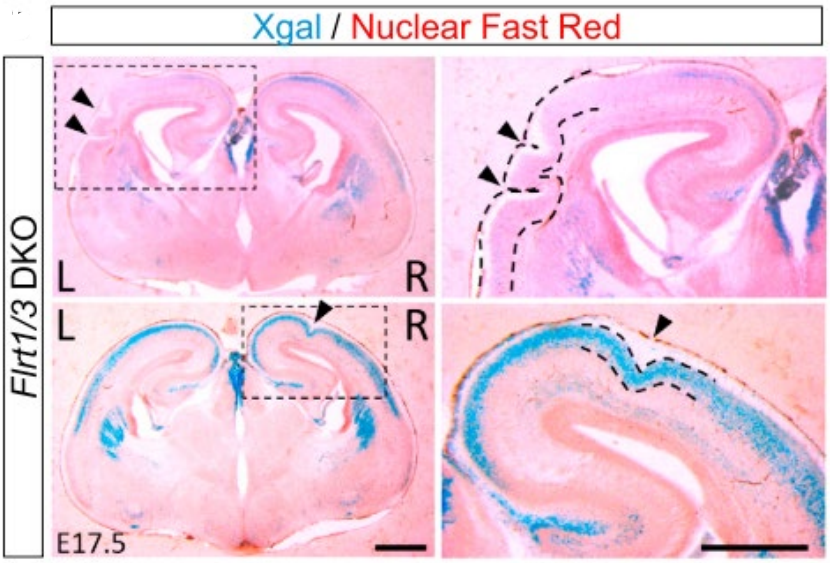

Figure 1.7 Cortical folding in E17.5 *Flrt1/3* double knockout (DKO) embryos

X-gal (blue) and Nuclear fast red (red) stained E17.5 brain sections of *Flrt1/3* DKO. Arrows indicate region showing cortical folding (marked by dash lines).

Interestingly, genetic deletion of FLRT1/3 in mice resulted in sulcus formation in the normally smooth mouse neocortex (Figure 1.7). In this mouse line, FLRT3 is conditionally deleted using Nestin-Cre, and FLRT1 is fully knocked out ($Flrt1^{-/-}$;$Flrt3^{lox/lacZ}$;Nestin-Cre mice; in short, *Flrt 1/3* DKO (Del Toro et al., 2017). Lack of FLRT1/3 reduced intercellular adhesion, enhanced neuron clustering along the tangential axis, and mildly accelerated radial migration, but there were no changes in cell proliferation that lead to an increase in neurons.

1.8 Cortical expansion and folding in *Cep83*cKO mice

To increase the progenitor cell population in the context of the Flrt 'cell migration' model, the *Cep83* cKO was chosen to improve our new model. Previous studies showed that centrosome proteins, which are localized to the mother centriole, play a role in influencing the stability of adherens junction complexes at the plasma membrane. Adherens junctions are especially crucial in the developing neocortical wall, as they are involved in distinguishing between different progenitor types. Apical progenitors (APs) are attached to the apical adherens junction belt, whereas basal progenitors (BPs) detach from the ventricular zone (VZ) after delaminating from the apical adherens junction belt. Integration of adherens junctions between two different the progenitor types has significant implications with regard to brain size (Rousso et al., 2012; Taverna et al., 2014; Stocker and Chenn, 2015; Wilsch-Bräuninger et al., 2016; Tavano et al., 2018, Wilsch-Bräuninger et al.,2021). The centrosome associated protein, AKNA (AT-hook transcription factor)

affects adherens junction stability. AKNA localizes to subdistal appendages on the mother centriole and is exclusively expressed in APs and BPs. It has the ability to directly bind to microtubules (MTs) and enhances MTOC (microtubule organizing center) activity at the centrosome, while also influencing MT stability. Knockdown of AKNA revealed stabilized junctions and blocked actin remodelling during delamination. In contrast, overexpression of AKNA induced faster delamination by loosening junctional complex. Overall, these findings suggest that AKNA is involved in the regulation of apical constriction and delamination of radial glia cells, which are crucial for neurogenesis. (Camargo Ortega et al., 2019). Talpid3, a centriolar protein, also plays a role in microtubule (MT) stability and adherens junctions. It localizes specifically to the distal end of centrioles (Yin et al., 2009; Kobayashi et al., 2014). Talpid3, along with Ninein, localizes to the mother centrioles and contributes to maintaining the integrity of adherens junctions by modulating MT stability (Wang et al.,2020). Knockdown of Talpid3 lead to delamination and ectopic divisions of progenitor cells in more basal regions (Wang et al.,2020), similar to the effects observed in overexpression of AKNA, ultimately resulting in reduced production of neurons. Similar to AKNA and Talpid3, Cep83 is known as an origin of the distal appendage (DAP) assembly pathway in mammalian cell cultures. The centrosome regulates the microtubule organizing center (MTOC) to promote mitotic spindle formation during cell division. (Tanos et al., 2013; Joo et al., 2013). Removing Cep83 causes dislocation of the basal bodies in the apical plasma membrane, while the centriole structure remains unaffected. Thus, it leads to an increased number of radial glia progenitor cells (RGPs) in the developing cortex, resulting in an enlarged cortex with folding in the cingulate cortex (medial cortex) (Figure 1.8). This result is mainly caused by disruption of distal appendages, affecting anchorage of the centrosome to the apical VZ. Thus, re-entry of RGPs into the cell cycle is accelerated and more neurons are produced in the developing cortex (Shao et al.,2020; Wilsch-Bräuninger et al., 2021).

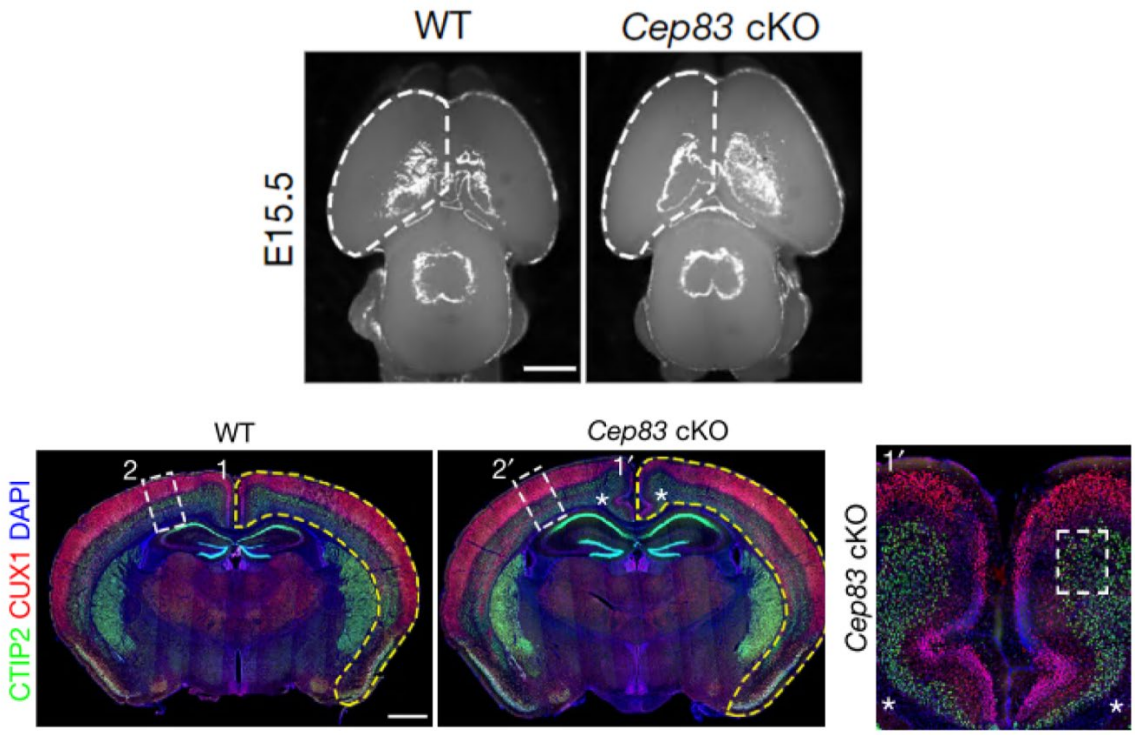

Figure 1.8 Embryonic and adult brains of WT and *Cep83*cKO mice

Increased cortical area and length of *Cep83*cKO in E15.5 and P21 mice. In P21, *Cep83*cKO exhibited cortical folding in the medial region (1') (Figure adapted from Shao et al., 2020).

1.9 Cortical expansion in *Fgf10* cKO mice

To increase the progenitor cell population in the context of the Flrt 'cell migration' model, the *Fgf10* cKO was chosen to improve our new model. Fibroblast growth factors (Fgfs) are signalling molecules that play diverse roles in the central nervous system (CNS), including the regulation of cortical size (Vaccarino et al., 1999; Shin et al., 2004) and cortical patterning (Fukuchi-Shimogori and Grove, 2001; O'Leary and Nakagawa, 2002; Garel et al., 2003; Hébert and Fishell, 2008). During early development, Fgf ligands, such as Fgf2, 3, 7, 8, 10, 15, 17, and 18 are expressed in the rostral telencephalic region and cortical primordium (Storm et al., 2003; Cholfin et al., 2007). Importantly, Fgfs have been shown to regulate neurogenesis (Raballo et al., 2000; Borello et al., 2008), and growth of

the cerebral cortex (Thomson et al., 2009; Kang et al., 2009; Stevens et al., 2010; Rash et al., 2011). Notably, Fgf10 signalling is known to be involved in the differentiation of NECs, a founder progenitor cell type, into RGCs (Yoon et al., 2004). Fgf10 receptors are expressed by cortical NEC transiently during the E9-E11. Ablation of Fgf10 delays radial glia differentiation, which occurs in the rostral cortex, and is accompanied by lengthening of symmetric NC divisions. This eventually leads to tangential expansion of frontal areas and increased laminar thickness (Figure 1.9) (Sahara et al., 2009). Based on this information, we chose to use the *Fgf10* cKO which is not published, but shows a similar phenotype (personal communication).

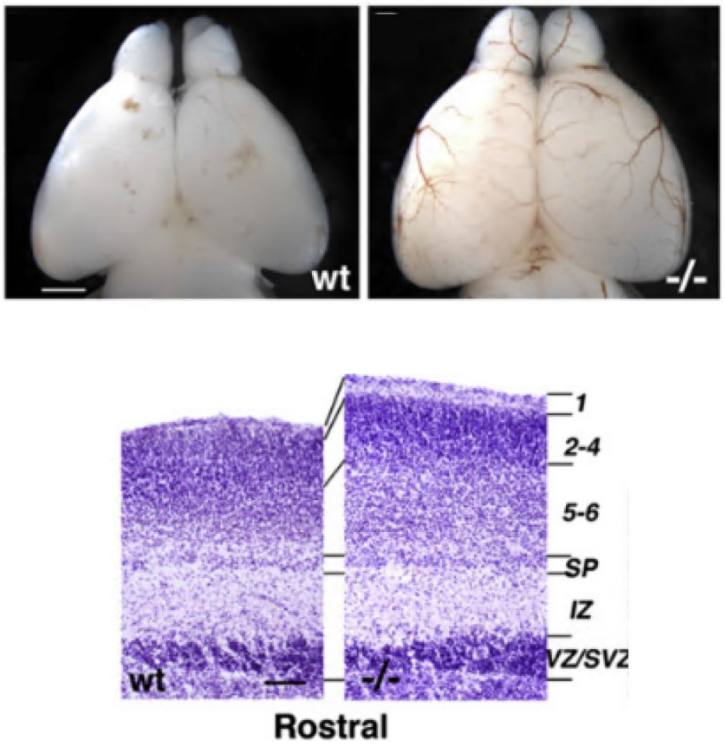

Figure 1.9 P0 brain of WT and Fgf10$^{-/-}$ mice

Increased cortical surface and laminar thickness in Nissl stained rostral cortex of Fgf10$^{-/-}$ mice compared to WT (Figure 1.9 adopted from Sahara et al., 2009).

1.10 Human brain malformations

The degree of cortical folding and brain size have a significant impact on brain functions, as changes in these factors can result in severe mental retardation (Guerriniet al, 2008; Barkovich et al., 2012). For example, microcephaly, polymicrogyria, and lissencephaly are cortical malformations highly correlated with brain size and cortical folding (Figure 1.10; Bilguvar et al, 2010; Adachi et al, 2011; Fernández et al., 2016). Microcephaly is a condition where the size of the brain is significantly decreased (Bond et al., 2002; Gilmore et al., 2013). This is mainly related to a decreased number of progenitors and affects cell cycle length (Boland et al., 2007; Desir et al., 2008; Passemard et al., 2009; Kumar et al., 2009;), mitotic spindle positioning, centrosome maturation (Feng et al.,2004; Bilguvar et al., 2010; Sakai et al., 2012; Poirier et al., 2013), and duplication and positioning of centrosome (Alkuraya et al., 2011; Bhat et al., 2011; Marthiens et al., 2013; Mirzaa et al., 2014). Thus, it affects balancing between differentiation and self-amplification of progenitors, which results in increased progenitor cell death (Jayaraman et al., 2018; Subramanian et al., 2020). Polymicrogyria is a condition where the cortex has an abnormally increased number of small gyri that are separated by small sulci. Previously, cytoskeleton regulation genes such as TUBB2B, TUBB3, TUBA1A, TUBAS were identified as associated genes that cause an ectopic folding phenotype and change in the control of cell adhesion (Roll et al., 2006; Abdollahi et al 2009; Jaglin et al., 2009; Poirier et al., 2013). Furthermore, their patients suffer severe cognitive defects caused by an abnormal thickness of the cortex (Pang et al., 2018). Lissencephaly is a condition where the cortex becomes smooth or cortical folding is simplified. Notably, type1 lissencephaly is caused by mutations in genes related to the cytoskeleton and cell migration, such as LIS1 (Marcorelles et al., 2010), DCX (Gleeson et al.,1998), RELN (Dulabon et al., 2000; Hong et al., 2000; Rice et al., 2001; Lee et al, 2016), and Cdk5 (Shinmyo et al, 2017); while type 2 lissencephlay is caused by alterations in the interaction between radial glia and the pial surface, resulting in the disruption of the cortical surface and the excess of neurons above

the meninges (Yamamoto et al., 2004; Luo et al., 2011). POMT1, POMT2, POMGNT1 genes were found to be highly related to type2 lissencephaly (Bouchet et al., 2006 and 2007)

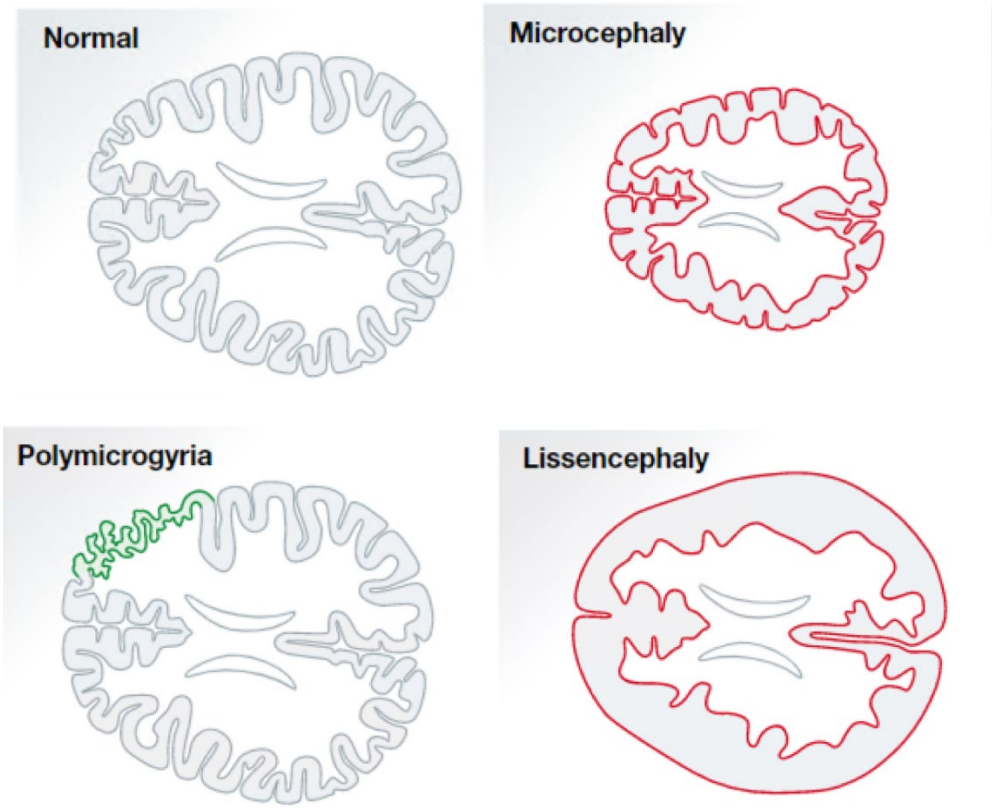

Figure 1.10 Human brain malformations

Schematic illustration depicting normal brains and phenotypic brains in each malformation

.

2. MATERIALS AND METHODS

2.1 Mouse lines

All animal experiments were approved by the Government of Upper Bavaria and carried out in accordance with German guidelines for animal welfare. All mice (C57BL/6 and 129/SvJ mixed background) were housed with 12:12h light/dark cycle and food/water available *ad libitum* in the facilities of the Max Planck Institute of Biological Intelligence. With regard to embryonic stage, the midday of vaginal plug formation was regarded as embryonic day 0.5 (E0.5). All mouse lines used are detailed in Table 2.1

Table 2.1 Mouse lines

Mouse lines	Official name	Source
FLRT1 null	Flrt1tm1.1Kln	Yamagishi et al., 2011
FLRT3 lox	Flrt3tm2Kln	Yamagishi et al., 2011
FLRT3 lacZ	Flrt3tm1Kln	Egea et al., 2008
Cep83 lox	Cep83tm1M	Shao et al., 2020
Fgf10 lox	B6;129-Fgf10<tm1.2Sms>/J	The Jackson Laboratory Urness et al., 2010
Emx1-Cre	B6.Cg-Emx1tm1(cre)Kr	Gorski et al., 2002
Foxg1-Cre	B6.129T(SJL)-Foxg1tm1.1(cre)Ddmo/J	The Jackson Laboratory Kawaguchi D., et al.2016
Ai9	B6.Cg-Gt(ROSA)26 Sortm9(CAG-tdTomato)Hze/J	The Jackson Laboratory Madisen L., et al.2010

2.2 Genotyping

For genotyping, DNA was extracted from tail biopsies of mice. Briefly, tails were boiled at 95°C for 45 min with 100 µl of 50 µM of NaOH. Then, 1.5 M Tris (pH 8.8) buffer was added to neutralize the pH for the polymerase chain reaction (PCR). Table 2.2 shows the primers used for genotyping, Table 2.3 the PCR programs, and Table 2.4 the buffers used.

Table 2.2 Genotyping primers

Name	Sequence (5'->3')
Cre forward	GCC TGC ATT ACC GGT CGA TGC AAC GA
Cre reverse	GTG GCA GAT GGC GCG GCA ACA CCA TT
FLRT1WT forward	CAG CGA GAT GGA TGA GTG CTT TGA
FLRT1WT reverse	GCC AGC ATT CTG TTC CTG GTT GA
FLRT1KO forward	TAG AGG ATC AGC TTG GGC TGC AGG TCG AGG
FLRT1KO reverse	TGA GAT CCA CAG CGA ACA GCA GGC ATT AGC
FLRT3 Lox forward	GAT ATT TGC CAA AGG AGA CAG AAA ATA
FLRT3 Lox reverse	CTG GGT TCA TTG CTG TCT ACC AAC AAG CAC
LacZ forward	CCA GCT GGC GTA ATA GCG AA
LacZ reverse	CGC CCG TTG CAC CAC AGA TG
CEP83 Lox forward	AGT GGG CTG TGA ATG TAG TCT T
CEP83 Lox reverse	AGC CAA CCA ATA ATA CAG AAA ACA
FGF10 Lox forward	GCC TTG GGT AGA CTG ATT AGT GTT AAG
FGF10 Lox reverse	ATA TCC TTG GGA GGC AGG A

Table 2.3 PCR programs

PCR	Denaturation	Denaturation	Annealing	Extension	# cycles	Extension
Cre	92°C	92°C	58°C	68°C	50	68°C
	10 min	10 sec	15 sec	1 min		5 min
FLRT1WT	94°C	94°C	60°C	72°C	29	72°C
	3 min	1 min	1 min	1 min		5 min
FLRT1KO	95°C	94°C	65°C	72°C	29	72°C
	3 min	1 min	1 min	1 min		5 min
FLRT3Lox	94°C	94°C	62°C	72°C	34	72°C
	3 min	1 min	1 min	1 min		20 min
LacZ	95°C	95°C	58°C	72°C	50	72°C
	5 min	30 sec	30 sec	30 sec		5 min
Cep83 Lox	94°C	95°C	60°C	68°C	30	68°C
	2 min	15 sec	15 sec	15 sec		5 min
Fgf10 Lox	94°C	95°C	60°C	68°C	30	68°C
	2 min	15 sec	15 sec	15 sec		5 min
Tomato	95°C	95°C	61°C	68°C	39	68°C
	3 min	1 min	1 min	1 min		2 min

2.3 Agarose gel electrophoresis

Agarose gels of final concentrations of 1.5%-3% were prepared in Tris-acetate-EDTA (TAE) buffer. Gels were pre-stained with Ethidium bromide (Carl Roth). Electrophoresis was performed in TAE buffer at a voltage of 100-180V for 25-30 mins. DNA gels were imaged using the Molecular Imager Gel Doc XR+ machine (Biorad).

Table 2.4 Genotyping buffers

Solution	Compounds	Amount
Master mix of genotyping	H_2O	41.6 µl
	2x Primer (50 pmol)	2x 0.5 µl
	Thermo Pol Reaction buffer 10x (NEB)	5 µl
	dNTPs-mix (25 mM each, Fermentas)	0.4 µl
	Taq Polymerase (NEB)	0.5 µl
Gel loading buffer, 50 ml	H_2O	24 ml
	Glycerol	25 ml
	TAE 50x	1 ml
	Orange G	0.1 g
50x TRIS-acetate buffer (TAE)	Tris acetate	2 M
	EDTA	50 mM

2.4 Immunohistochemistry

For tissue preparation, the whole head from E11.5, E13.5 mice and whole brain from E15,5, E17,5 mice was dissected. The dissected embryonic brains were fixed in 4% PFA in PBS at 4 °C overnight and stored in PBS. To obtain coronal brain sections, tissue was embedded in 4% agarose in PBS. Serial 100 µm (E15.5 and E17.5) and 80 µm (E11.5 and E13.5) thick sections were cut in PBS with a Leica VT1000 S vibratome. For CEP83 antibody staining, embryonic brains were fixed in 4% PFA in PBS at 4 °C overnight and placed in 30% sucrose/PBS (weight/volume) until the tissue sank (12-16hrs). After cryopreservation, brains were embedded in O.C.T. Compound (Sakura Finetek), frozen on dry ice, and stored at -80°C. Then, coronal brain sections (14 µm) were cut using a Leica CM3050S cryostat, mounted onto Superforst Ultra Plus slides (Thermo Scientific), and stored at -20°C. Frozen sections were air-dried for approximately 30 min. Dried sections were washed three times with Tris-buffered saline containing 0.1% Triton X-100 (TBST)

for 5 min. The sections were incubated with primary antibodies diluted with 0.2% BSA/0.5%Triton/5% donkey serum in PBS, including rabbit anti-SATB2 (1:500, Abcam), rat anti-Ctip2 (1:500, Abcam), goat anti-SOX2 (1:1000, R&D Systems), rat anti-Histone H3(1:500, Abcam), rabbit anti-Tbr2/Eomes (1:200, Abcam), rat anti-BrdU(1:100, Abacm), and rabbit anti Ki67 (1:200, Abcam). Secondary antibodies were diluted at 1:500 0.2% BSA/0.5%Triton/5% donkey serum in PBS and incubated for 2 hr at room temperature. The secondary antibodies used were Cy3-conjugated donkey anti-rat IgG, Cy3-conjugated donkey anti-rabbit IgG, Alexa 488-conjugated donkey anti-rabbit IgG, Alexa 488-conjugated donkey anti-rat IgG, and Alexa 674-conjugated donkey anti-goat IgG (Jackson Immunoresearch Laboratories). Cell nuclei were counterstained with 4',6-Diamidino-2-phenylindole dihydrochloride (DAPI)/PBS (1:1000; Invitrogen). For observation, sections were mounted with DAKO mounting medium, and sealed with cover slides by Menzel-Gläser (Menzel GmbH & CO). Images were visualized using a Leica SP8 confocal microscope.

Table 2.5 Primary antibodies used for immunostaining

Antibody	Reference	Dilution
Rabbit Anti-SATB2	Abcam, ab34735	1:500
Rat Anti-Ctip2	Abcam, ab18465	1:500
Goat Anti-SOX2	R&D Systems, AF2018	1:1000
Rat Anti-Histone H3	Abcam, ab10543	1:500
Rabbit Anti-Tbr2/Eomes	Abcam, ab183991	1:200
Rabbit Anti-Ki67	Abcam, ab15580	1:200
Rat Anti-BrdU	Abcam, ab6326	1:100
Rabbit Anti-CEP83	Sigma-Aldrich, HPA038161	1:200
DAPI	Invitrogen, D1306	1:1000

Table 2.6 Immunohistochemistry staining buffers

Solution	Compounds	Concentration
Blocking solution	PBS	
	Donkey serum	5%
	Bovine serum albumin	0.2%
	Triton X – 100	0.5%
Washing buffer (PBST)	PBS	
	Triton X – 100	0.1%

2.5 BrdU analysis

A single injection of BrdU dissolved in PBS, 0.15-0.2 ml at a concentration of 10 mg/ml 5-bromo-20-deoxyuridine (BrdU, Sigma-Aldrich) was administrated to pregnant females at E13.5 and E15.5 intraperitoneally for a short BrdU pulse analysis, to give a final concentration of 50 mg per g of mouse weight. Pregnant females were then sacrificed after 30 mins. Brains were collected and fixed overnight with 4% PFA and stored in PBS. For staining with the BrdU antibody, sections were pre-treated with 2N HCl for 30 min at RT and washed with $Na_2B_4O_7$ (pH 8.5) twice for 15 min.

Table 2.7 BrdU staining buffers

Solution	Compounds	Amount
2N HCl	37.5% HCl	16.35 ml
	H_2O	83.65 ml
$Na_2B_4O_7$ (pH 8.5)	Boric acid	6.185 g
	Sodium Chloride	4.385 g
	Sodium tetraborate	5.031 g
	H_2O	1000 ml

2.6 *In utero* electroporation

In utero electroporation was performed as described previously with minor modifications (Saito and Nakatsuji, 2001, Sato et al., 2013). Timed pregnant mutant mice at E13.5 were anesthetized with isoflurane (CP-pharma) using a Fluovac 34-0387 (Harvard Apparatus) and Vevo Compact Anesthesia System (VisualSonic). For surgery, the uterus of the mouse was exposed after making an approximately 3 cm incision in the middle abdominal region. Then, both sides of uterine horns were pulled out, and approximately 1-2 µl of a mixture containing 1 µg/µl pCAG-GFP plasmid (Addgene, Cat #11150) and 1% Fast Green (Sigma, final concentration 0.2%) in PBS was injected into the lateral ventricle of embryos with a mouth-controlled glass capillary pipette. Immediately, square pulses (30 V, 50 ms, six times at 1 s intervals) were delivered into embryos with an electroporator (ECM 830, BTX) and a forcep-type electrode (CUY650P5, NepaGene). After the electroporation, the uterus was returned back inside the abdomen using ring forceps and the incision was sutured with PERMA-HAND Seide (9.3 mm diameter curved needle, 45 cm of thread, Ethicon). After surgery, mice were placed on a 37°C heating pad for recovery and kept until the desired embryonic stage.

2.7 Time-lapse movies

Embryo cortices were electroporated at E13.5 with pCAG-GFP (Addgene Cat #11150). After 2 days, E15.5 of embryonic brains were isolated in an ice cold sterile filtered and aerated (95% O_2/5% CO_2) dissection medium (15.6 g/l DMEM/F12 (Sigma), 1.2g/l $NaHCO_3$, 2.9 g/l glucose (Sigma), 1% (v/v) penicillin streptomycin (GIBCO)). Using 4% low melting agarose (Biozym), brains were embedded for cutting into 300 mm thick sections using a vibratome (Leica, VT1200S). Sections were immersed in a collagen mix

(64% (v/v) cell matrix type I-A (Nitta Gelatin), 24% (v/v) 5x DMEM/F12, 12% (v/v) reconstitution buffer (200 mM HEPES, 50mM NaOH, 260mM $NaHCO_3$) and transferred onto a cell culture insert (Millicell, PICMORG50). Sections were then incubated at 37°C for 10 min to solidify the collagen mixture. 1.5 mL slice medium (88% (v/v) dissection medium, 5% (v/v) horse serum, 5% (v/v) fetal calf serum, 2% (v/v) B27 supplement (GIBCO), 1% (v/v) N2 supplement (GIBCO)) was added to the dish surrounding the culture insert and incubated for minimum 30 min at 37°C. Before imaging, culture medium was added to the top of the sections to allow objective immersion. Imaging was performed using a 20x water immersion objective on a Leica SP8 confocal microscope system equipped with a temperature-controlled carbon dioxide incubation chamber set to 37°C, 95% humidity, and 5% CO_2. Sequential images were acquired every 15 min for 24-48 hr. After imaging, slices were genotyped to identify triple knock outs and littermate controls. The neuronal movement was tracked using the software Fiji with plugin 'Manual Tracking.' Only neurons entering the CP were tracked. Single cell track analysis and plotting was carried out using homemade python scripts.

2.8 Fluorescence *in situ* hybridization

Embryonic brains (E11.5 and E15.5) were fixed in 4% PFA in PBS at 4°C overnight and placed in 30% sucrose/PBS (weight/volume) until the tissue sank (12 h-16hrs). After cryopreservation, the brains were embedded in O.C.T. Compound (Sakura Finetek), frozen on dry ice, and stored at -80°C. Coronal brain sections (14 µm) were cut using a Leica CM3050S cryostat, mounted onto Superfrost Ultra Plus slides (Thermo Scientific), and stored at -20°C. Frozen sections were air-dried for approximately 30 min. For FISH analysis, RNAscope Fluorescent Multiplex Assays (ACD, 320850, 322000, and 322340) were conducted according to the manufacturer's instructions (ACD, 320293-USM and 320535-TN) with RNAscope Probes directed against Fgf10 (ACD, 446371), Flrt1 (ACD,

555481) and Flrt3 (ACD, 490301). Immunostaining against CEP83 protein was performed prior to counterstaining with DAPI for *Cep83*^{TKO} embryos.

2.9 3DiSCO tissue clearing

A modified clearing protocol was used based on Belle et al., 2017. Briefly, E17.5 embryo brains were fixed in 4% PFA overnight at 4ºC and stored in PBS. First, whole brain immunostaining was performed before tissue clearing. Brains were incubated in blocking buffer for 24h at RT on a horizontal shaker. Then brains were stained with primary antibodies, rabbit anti-SATB2 (1:1000, Abcam) and rat anti-Ctip2 (1:1000, Abcam) over 7 days with blocking buffer containing saponin at 37ºC on a shaker. Next, brains were washed for 1 hour 6 times in 15 ml falcon tubes containing blocking buffer. Then, brains were incubated at 37ºC on the horizontal shaker over 2 days with secondary antibodies Alexa Fluor 647 and 594 (1:500, Jackson Immunoresearch Laboratories), which had been filtered with a 0.20 mm filter and diluted in blocking buffer with saponin 0.1%. The brains were washed for 1 hour 6 times in 15 ml falcon tubes filled with blocking buffer. Then, tissue clearing was performed. Briefly, the whole stained brains were immersed in 50% tetrahydrofurane (THF, Carl Roth) overnight, in 80% THF for 1 h, in 100% THF for 1 h, then in fresh 100% THF for another hr, then in 100% dichloromethane (DCM, Carl Roth) until the brains sank, and finally in 100% dibenzylether (DBE, Sigma), followed by another step of fresh 100% DBE. Then, cleared brains were imaged with a 4× objective lens (Olympus XLFLUOR 340) equipped with an immersion-corrected dipping cap mounted on a LaVision UltraII microscope coupled to a white-light laser module (NKT SuperK Extreme EXW-12). Images were taken with 16-bit depth and at a nominal resolution of 1.625 µm per voxel on the *x* and *y* axes. Brain structures were visualized with Alexa Fluor 594 (using a 580/25 nm excitation filter and a 625/30 nm emission filter) and Alexa Fluor 647 fluorescent dye (using a 640/40 nm excitation filter and a 690/50 nm emission filter)

in sequential order. Laser power was set for each channel so as not to exceed the dynamic range of the Neo 5.5 sCMOS camera (Andor). For 12× imaging, we used a LaVision objective (12×/0.53 NA MI PLAN with an immersion-corrected dipping cap). Camera exposure time was set to 105 ms and 90 ms for the 4× and 12× imaging respectively. In the *z* dimension, images were taken in 5 µm and 2 µm steps, while using left- and right-sided illumination for the 4× and 12× imaging, respectively. Our nominal resolution was 1.625 µm × 1.625 µm × 5 µm and 0.602 µm × 1.602 µm × 2 µm for the *x*, *y* and *z* axes, with 4× and 12× objectives. The thinnest point of the light sheet was 28 µm and 9 µm.

Table 2.8 Whole brain staining buffers

Solution	Compounds	Amount
Blocking buffer	PBS	
	Gelatin	0.2%
	Triton X-100	0.5%
	Sodium azide	0.01%
Secondary antibody incubation buffer	PBS	
	Gelatin	0.2%
	Triton X-100	0.5%
	Sodium azide	0.01%
	Saponin	0.1%

2.10 Data analysis

Images were processed with the open-source image analysis software Fiji. Automatic cell counting analysis was performed using open-source CellProfiler 4.2.5. Kernel Density Estimation (Heat Map) analysis was performed using Rstudio version 2021.09.0. Statistical analysis was conducted with GraphPad Prism 9.2.0 (GraphPad Software).

3. RESULTS

3.1 Cre lines used for manipulation of cortical neurons during embryonic development

Since the original *Flrt1/3*DKO model was created using Nestin-Cre (Del Toro et al., 2017), and both the *Cep83*^{TKO} and *Fgf10*^{TKO} models were made using Emx1-Cre and Foxg1-Cre, respectively, these new lines needed to be validated. The major differences among the Cre lines are the regions and starting points of expression. Nestin-Cre begins to be expressed at E11.5 in all CNS region (data not shown). To obtain the time and location of expression in each Cre lines, we crossed each Cre line with the Ai9 mouse line.

According to the original reference, Foxg1-Cre starts to be expressed around E8.5 (Kawaguchi D et al, 2016), and at E10.5-E11.5, tdTomato expression area was highly concentrated in the dorsal telencephalon (Figure 3.1 A',B). Given that *Fgf10* is expressed very early during cortical development (E9.5), we decided to use the Foxg1-Cre to delete its expression (Sahara et al, 2009).

Emx1-Cre was used for generating *Cep83/Flrt1/3*TKO mice (*Cep83*^{TKO}). tdTomato expression was mainly observed in dorsal telencephalon from E10.5, then it was continuously expressed more widely throughout the whole cortex and hippocampus (Figure 3.1 C',D) (Gorski et al., 2002). We chose Emx1-Cre to generate the *Cep83*^{TKO} mice because the *Cep83*cKO was also created using Emx1-Cre (Shao et al, 2020), and it is highly expressed in the lateral side of cortex, the region where we mostly see the folding phenotype.

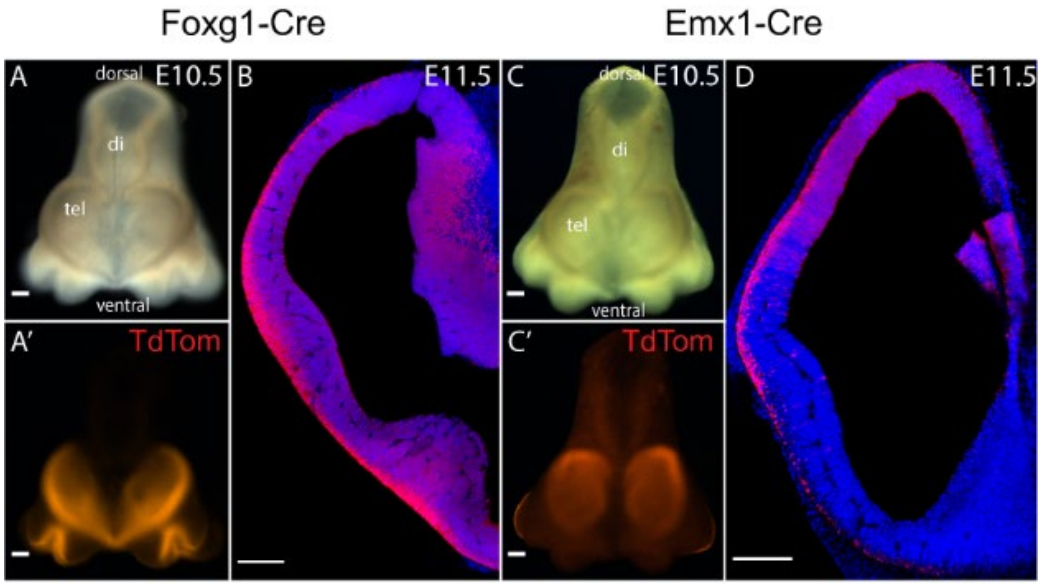

Figure 3.1 tdTomato expression in Foxg1-Cre and Emx1-Cre mice at E10.5 and E11.5

(A) Macroscopic image of E10.5 Foxg1-Cre embryo, head only. Telencephalon (tel), diencephlon (di). Scale bar 20 µm.

(A') tdTomato expression of Foxg1-Cre in embryo brain A. Scale bar 20 µm.

(B) tdTomato expression with 4',6-diamidino-2-phenylindole (DAPI) in E11.5 Foxg1-Cre, coronal view of cortex. Scale bar 100 µm

(C) Macroscopic image of E10.5 of Emx1-Cre embryo, head only. Scale bar 20 µm.

(C') tdTomato expression of Emx1-Cre in embryo brain C. Scale bar 20 µm

(D) tdTomato expression with DAPI in E11.5 Foxg1-Cre, coronal view of cortex. Scale bar 100 µm.

3.2 Validation of Emx1-Cre driver for the generation of *Cep83*^{TKO} mice

To increase the IP cell population in the *Flrt1/3* DKO 'cell migration' model, we decided to combine the *Emx1-Cre;Cep83*$^{lx/lx}$ *mice* with the *Flrt1*$^{-/-}$*;Flrt3*$^{lx/lacZ}$ mice. Thus, Emx1-cre was validated in *Cep83*cKO and *Flrt1/3* DKO mice. With this combination, the expectation was that the cortical areas of *Cep83*cKO mice would be significantly larger than those of WT littermate CTL mice at E17.5. Conversely, the cortical areas of *Emx1-Cre;Flrt1*$^{-/-}$*;Flrt3*$^{lx/lacZ}$ mice were expected to be normal because expansion of cell proliferation was absent (Del Toro et al., 2017). Indeed, I found that the cortical area in *Cep83*cKO mice was enlarged by approximately 10 percent, while that of *Emx1-Cre;Flrt1*$^{-/-}$*;Flrt3*$^{lx/lacZ}$ mice was unaltered compered to controls (Figure 3.2 A,B). To assess whether there was a direct correlation between brain size and cortical folding, we tracked the brains that exhibited folding, and saw that there was a trend that bigger brains showed folding. We also observed a mild phenotype of folding with lower penetrance in WT littermate CTLs (Figure 3.2 B).

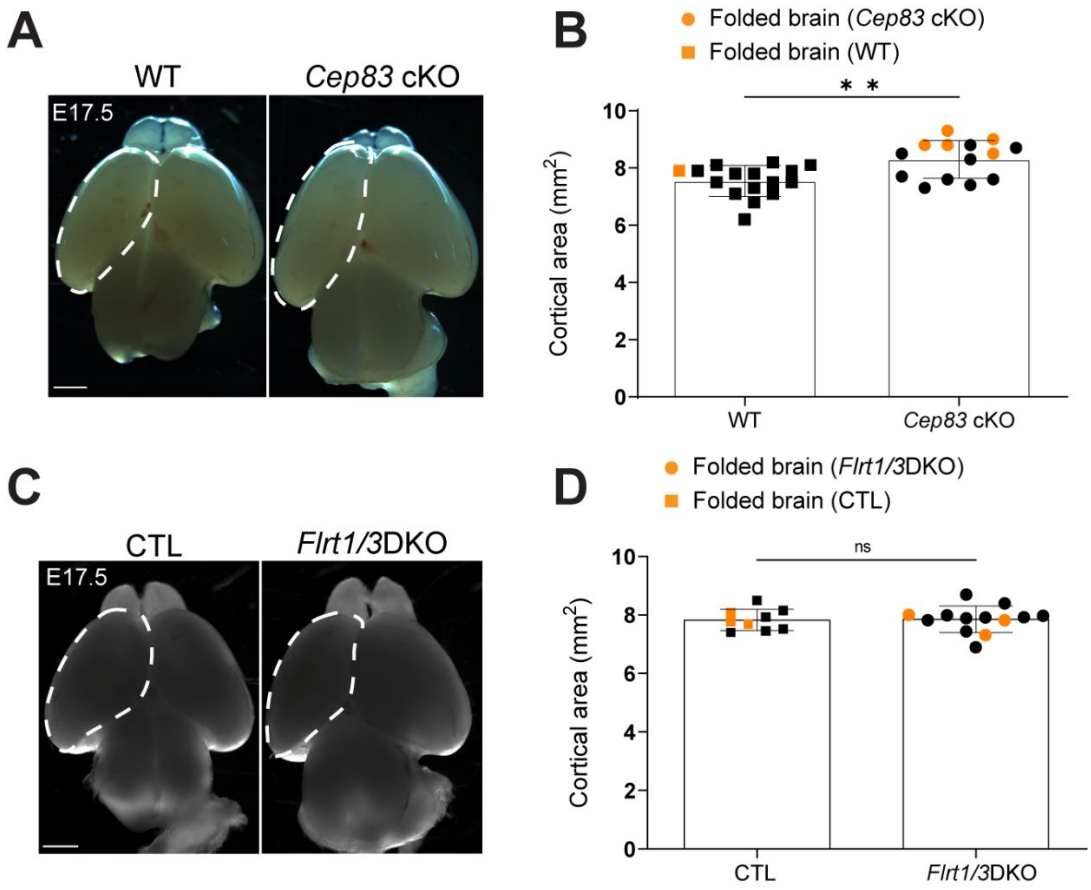

Figure 3.2 Cortical area of *Cep83*cKO and *Emx1-Cre*; *Flrt1/3*DKO mice

(A) Representative whole-mount images of E17.5 wild-type (WT) and *Cep83*cKO brains. Scale bar 1 mm.

(B) Quantification of the cortical areas (WT, n=14; *Cep83*cKO, n=16). Orange dot indicated folded brains in genotypes. Data are shown as mean ± SEM; **p<0.01, unpaired Student's t-test.

(C) Representative whole-mount images of E17.5 *Flrt1*KO*Flrt3*het (littermate control, CTL) and *Flrt1/3*DKO brains. Scale bar 1 mm.

(D) Quantification of the cortical areas (CTL, n=9; *Flrt1/3*DKO, n=13). Orange dot indicated folded brains in genotypes. Data are shown as mean ± SEM; no significant changes between groups, unpaired Student's t-test.

3.3 Characterization of *Cep83*^{TKO} mice

To generate *Emx1-Cre;Cep83*$^{lx/lx}$*;Flrt1*$^{-/-}$*;Flrt3*$^{lx/lacZ}$ *mice* (*Cep83*^{TKO} mice), we crossed *Flrt1*$^{-/-}$*; Flrt3*$^{lx/lacZ}$ mice (Yamagishi et al., 2011; Egea et al., 2008) with *Cep83*$^{lx/lx}$ mice (Shao et al., 2020), leading to *Flrt1*$^{-/-}$*; Flrt3*$^{lx/lacZ}$;*Cep83*$^{lx/lx}$ mice. These animals were further crossed with Emx1-Cre to remove the floxed alleles for Cep83 and FLRT3. To validate our mouse models, we performed RNAscope expression analysis for FLRTs coupled with antibody staining of Cep83. CTL littermates were *Flrt1*$^{-/-}$*Flrt3*$^{lacZ/+}$ mice lacking Cre expression. At E15.5, Cep83 antibody staining in littermate CTLs showed expression all over the cortical primordium, especially from the VZ to the SVZ and in CP layers as compared to the IZ. As expected, Cep83 there was no immunoreactivity in *Cep83*^{TKO} mice (Figure 3.3). Likewise, Flrt3 mRNA expression was removed from *Cep83*^{TKO} mice, whereas littermate CTLs exhibited intense Flrt3 expression in the IZ and CP. Flrt1 mRNA expression was undetectable in both genotypes (Figure 3.3).

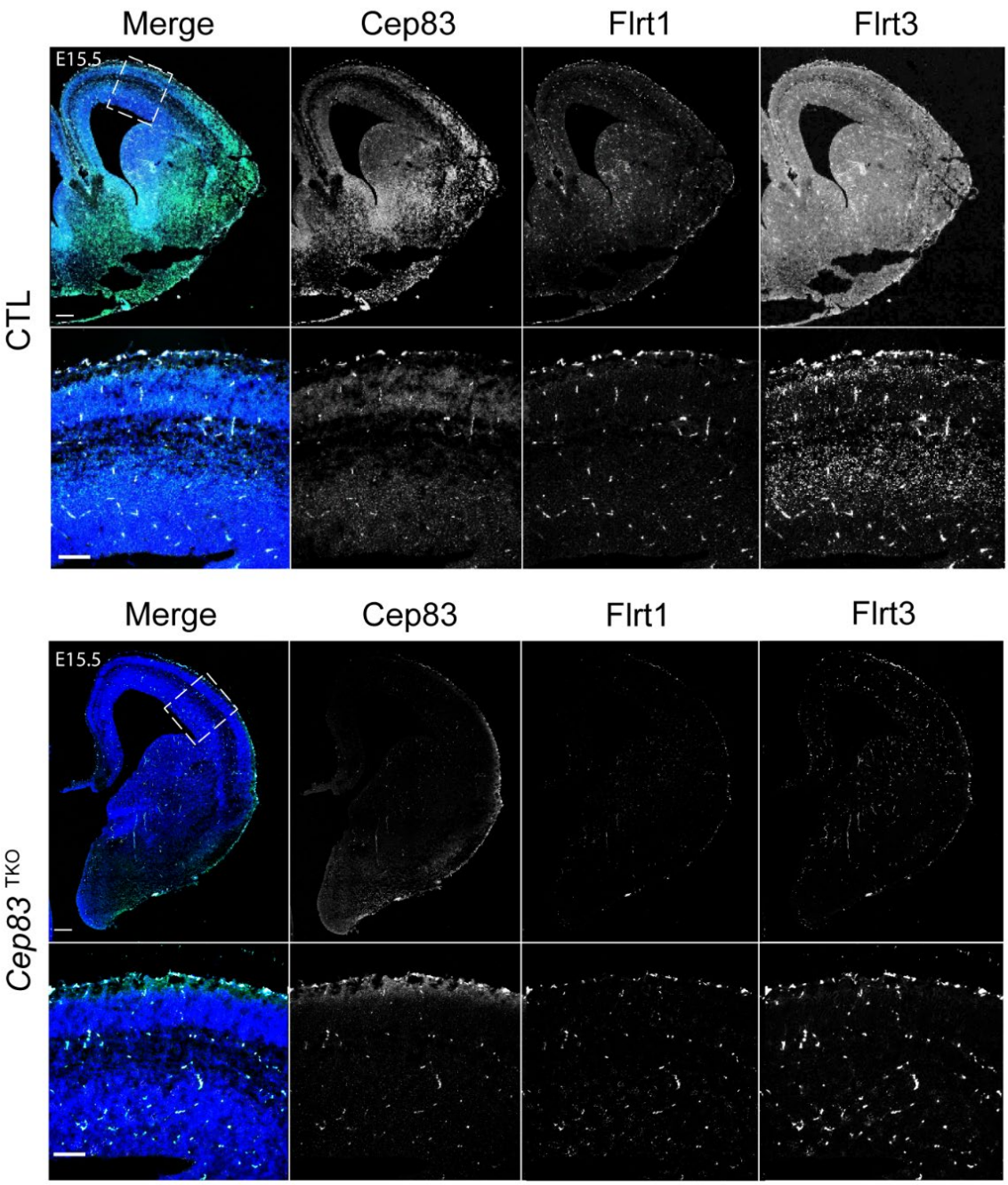

Figure 3.3 Expression of Cep83 and Flrt1/3 in *Cep83*^{TKO} and CTL mice

Double *in situ* hybridization (ISH) for Flrt1 and Flrt3 combined with Cep83 antibody staining in coronal sections of E15.5 cortex. Scale bars, 100 mm and 50 mm

3.4 *Cep83*^{TKO} mice show enhanced sulcus-like cortical folding

Cep83^{TKO} mice were born at the expected mendelian ratios, suggesting that this combination of loss-of-function alleles did not compromise normal embryonic development. Since cortical folding of *Flrt1/3*DKO mice was previously analyzed at E17.5, we also chose this time point for our analysis. To examine possible folding phenotypes, the neocortex was immunostained with the upper layer markers Satb2 and Ctip2. Freshly isolated *Cep83*^{TKO} brains exhibited superficial cortical folds under the dissection microscope (Figure 3.4 A). Cortical folds were detected after tissue clearing, and immunostaining, in 3D whole brain imaging (Figure 3.4 B) and in coronal sections (Figure 3.4 C), using a light-sheet microscope. This was in contrast to the smooth surface of the normal WT mouse cortex. Whenever Satb2 and Ctip2 immunostaining revealed deep invaginations resembling a sulcus, the apical surface of VZ remained smooth, indicating a *bona fide* cortical folding phenotype (Figure 3.4 C). Overall, the folding phenotype varied between individual brains from a single sulcus to multiple sulci and gyri. The penetrance of the phenotype increased to above 80% in *Cep83*^{TKO} and *Cep83/Flrt1*^{DKO}*Flrt3*^{het} mice, in short *Cep83*^{DKO}mice suggesting synergistic effects between the mutant alleles. Most of the brains showed sulcus-like folding. A small fraction (11%) of the brains displayed gyri, but only in the context of multiple sulci and gyri. The folding penetrance of control groups ranged between 10 and approximately 40% (Figure 3.4 and Table 3.1).

Unlike in the previous *Flrt1/3*DKO or *Cep83*cKO models where folds were only seen in the cingulate cortex, in the new *Cep83*^{TKO} model, the spatial location of folds in the cortex were seen either in the lateral side of the cortex, and in some mice, in both hemispheres (Figure 3.4 D). The majority of brains from *Cep83*^{TKO} and *Cep83*^{DKO} mice exhibited a mixture of folds in the cingulate and lateral side of cortex, indicative of a combination of the *Cep83*cKO and *Flrt1/3*DKO phenotypes. To quantify the folding phenotype, we calculated the gyrification index (GI), which is the ratio of the length of the

cortical surface (folded or unfolded) over the hypothetical minimal length of the cortical surface (Figure 3.4 E). The GI was obtained from three different groups, *Cep83*^{TKO}, *Flrt1/3*DKO, and *Cep83*cKO across rostro-medial-caudal cortical areas (Figure 3.4 F). While the control groups exhibited a GI value of nearly 1.0 and 1.01, indicated relatively mild phenotypes, the *Cep83*^{TKO} group reached a GI value of nearly 1.03 in the rostral cortical area (Figure 3.4 F). In summary, these results indicate that *Cep83*^{TKO} mice exhibit enhanced cortical folding, both in terms of degree of folding and penetrance.

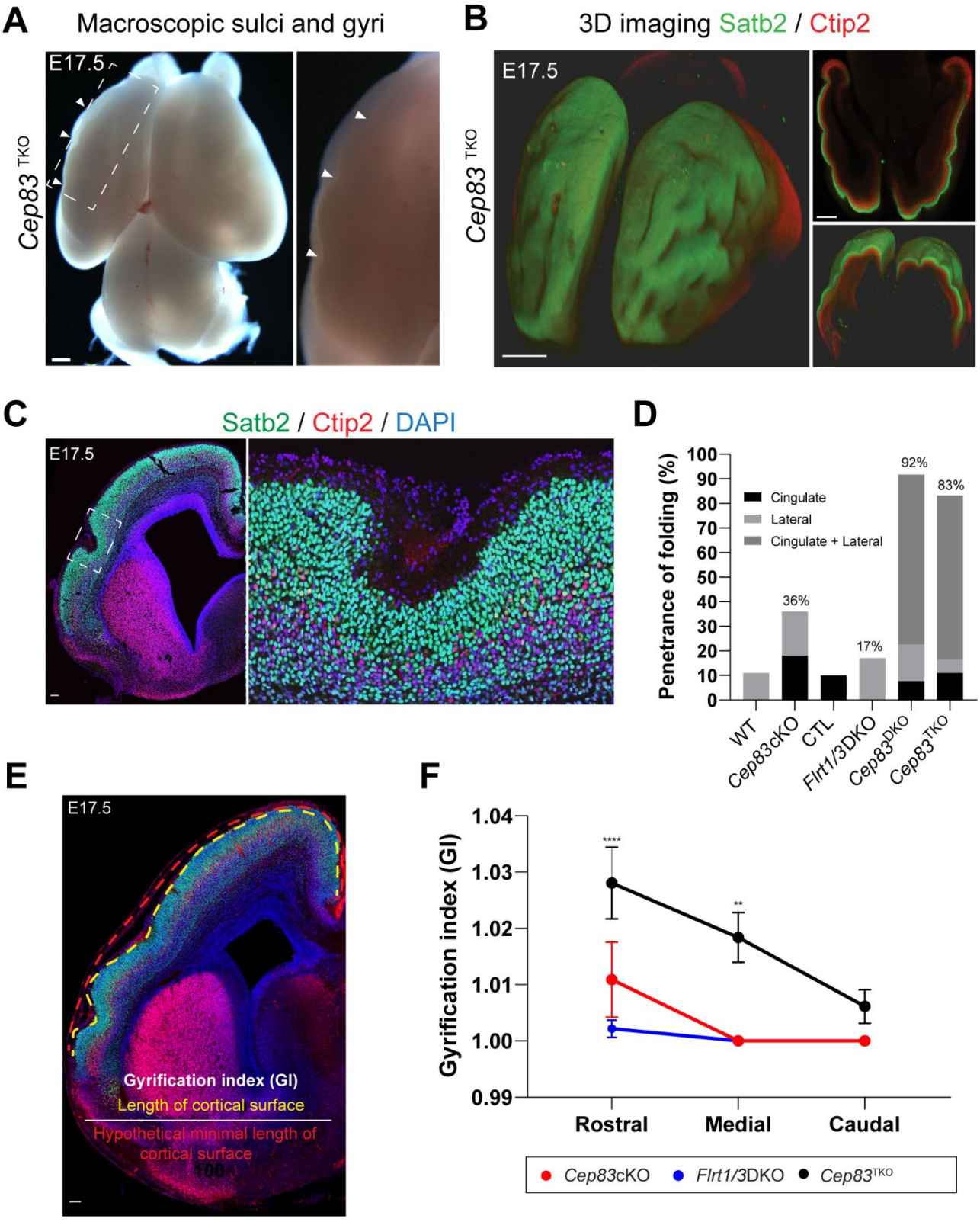
A
Macroscopic sulci and gyri
E17.5
Cep83 TKO
B
3D imaging Satb2 / Ctip2
E17.5
Cep83 TKO
C
Satb2 / Ctip2 / DAPI
E17.5
D
Penetrance of folding (%)
Cingulate
Lateral
Cingulate + Lateral
36%
17%
92%
83%
WT
Cep83cKO
CTL
Flrt1/3DKO
Cep83DKO
Cep83TKO
E
E17.5
Gyrification index (GI)
Length of cortical surface
Hypothetical minimal length of cortical surface
F
Gyrification index (GI)
Rostral
Medial
Caudal
Cep83cKO
Flrt1/3DKO
Cep83TKO

Figure 3.4 *Cep83*^{TKO} mice develop cortical sulci

(A) Macroscopic sulci and gyri in an E17.5 *Cep83*^{TKO} embryo. The area in the dashed rectangle is shown with higher magnification on the right, sulci and gyri are indicated by arrowhead. Scale bar 500 μm.

(B) 3D imaging of E17.5 *Cep83*^{TKO} embryo in (A). 3D whole brain, XY plane and YZ plane images are shown. Scale bars 300 μm (3D whole brain), 400 μm (XY,YZ plane).

(C) E17.5 *Cep83*^{TKO} brain section stained with Satb2, Ctip2, and DAPI. Area in dashed rectangle is shown with higher magnification on the right. Scale bar 100 μm

(D) Folding penetrance of WT (littermate CTL of *Cep83*cKO), *Cep83*cKO, CTL (littermate control of *Cep83*^{TKO}), *Flrt1/3*DKO, *Cep83*^{DKO}, and *Cep83*^{TKO}. Color code: Cingulate cortex (black), lateral side of cortex (light grey), and both (dark grey) indicates location of cortical folding in E17.5.

(E) Representative images of Gyrification Index (GI) value in *Cep83*^{TKO}. Yellow line indicates the *de facto* length of the cortical surface, red line indicates the hypothetical minimal length of the cortical surface. Scale bar 100 μm.

(F) Quantification of GI values in E17.5. n=11 *Cep83*cKO (red), n=13 *Flrt1/3*DKO (blue) and n=31 *Cep83*^{TKO} (black) at three positions: rostral, medial, and caudal. Data are shown as mean ± SEM; ***P< 0.001, ****P< 0.0001, two-way ANOVA with Tukey's post hoc analysis.

Table 3.1 Cortical folding penetrance at E17.5 of the indicated genotypes. Brains were analyzed for the presence of one or multiple sulci/gyri as shown in Figure 3.4

Genotype	N analyzed	N with folding	Penetrance
WT	9	1	11%
Emx1-Cre;Cep83 cKO	11	4	36.4%
Emx1-Cre;Flrt1$^{-/-}$*Flrt3*^{het} (CTL)	9	4	44%
*Emx1-Cre;Flrt1/3*DKO	14	2	30%
Cep83$^{+/+}$*;Flrt1*$^{-/-}$*Flrt3*^{het} (CTL)	11	1	9%
Emx1-Cre;Cep83/Flrt1^{DKO}*Flrt3*^{het} (*Cep83*^{DKO})	13	12	92%
Emx1-Cre;Cep83/Flrt1/3^{TKO} (*Cep83*^{TKO})	18	15	83%

3.5 Cortical expansion in *Cep83* ^{TKO} correlates with increased numbers of IPs and bRGs

The cortex of *Cep83*^{TKO} mice appeared significantly larger than that of CTL embryo at E17.5. In addition, *Cep83*^{DKO} brains exhibited increase cortical size (Figure 3.5.1 A,B), suggesting ablation of *Cep83/Flrt1/3* increase neuronal pool. To assess whether there is a direct correlation between brain size and cortical folding, we tracked the brains that exhibited folding and found there was a trend that bigger brains seem to have folding (Figure 3.5.1 B). In *Cep83*^{TKO} and *Cep83*^{DKO}, the location of folding was diverse, and could be seen in both the lateral and cingulate cortex when compared to the CTL group, suggesting synergistic effects in *Cep83* cKO and *Flrt1/3* DKO.

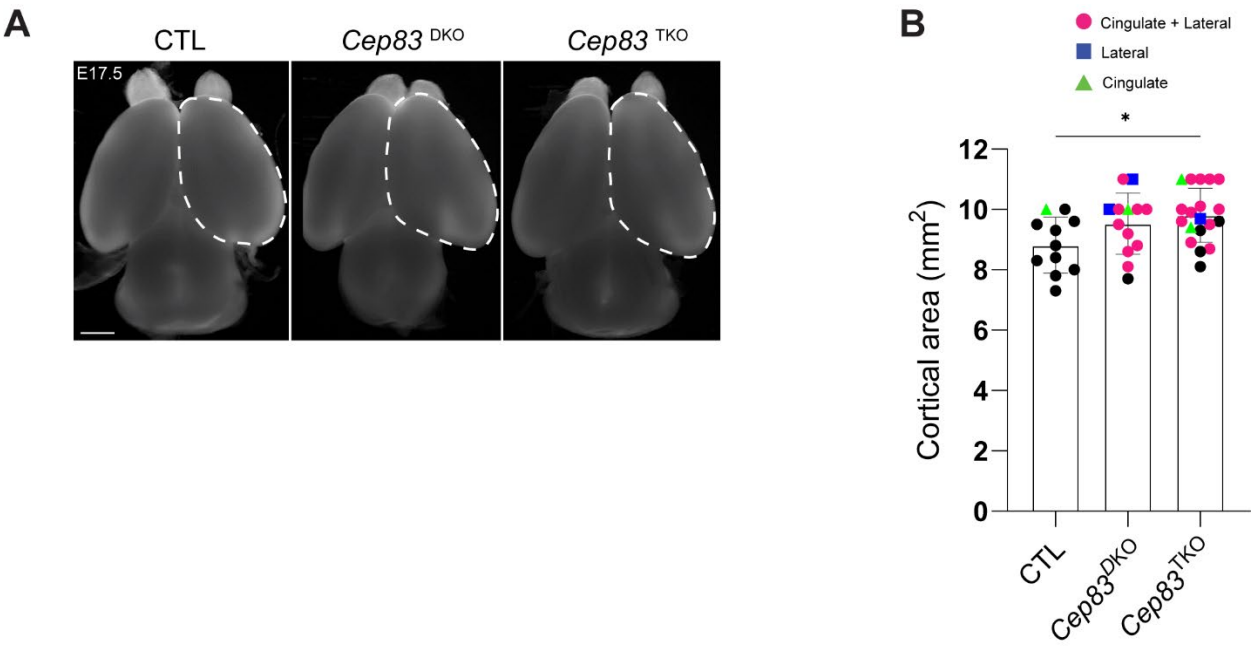

Figure 3.5.1 Cortical area of *Cep83/Flrt1/3* mutant embryos at E17.5

(A) Representative whole-mount images of E17.5 CTL, *Cep83*^{DKO}het, and *Cep83*^{TKO} brains. Scale bar 1 mm.

(B) Quantification of the cortical areas. Color and shape of dot indicates folded brains and location of folds (Pink circle, cingulate cortex and lateral side of cortex; Blue rectangle, lateral side of

cortex only; Green triangle, cingulate cortex only). Data are shown as mean ± SEM, *P< 0.05, two-way ANOVA with Tukey's post hoc analysis.

To investigate whether cell proliferation was mechanistically enhanced in triple mutant mice, we analyzed cell proliferation in rostral and medial neocortex sections at E13.5 by quantifying the number of apical progenitor (Sox2+), intermediate progenitor (Tbr2+), and dividing RGCs and mitotic dividing cells (pH3+) (Figure 3.5.1 A, A'). Moreover, the neuronal population that co-expressed Sox2 and Tbr2 was quantified to obtain bRGs, which is a key cell type that induces tangential growth of the brain resulting in an enlarged cortex with a folded structure in gyrenchepalic species (Figure 3.5.1 A). Further, to examine tangential expansion in the proliferative area, an area mainly composed of RGCs, the total length of the Sox2+ domain was measured (Figure 3.5.2 A,D,D'). In rostro-medial regions, we observed significantly increased IPs (Tbr2+) in triple mutant embryos, whereas apical progenitors, mitotic dividing cells, and RGCs were unchanged (Figure 3.5.2 B,B'). The proportion of mitotic cells in the apical versus basal layer was also not altered in triple mutants (Figure 3.6.1 C, C'). Interestingly, bRGs and the length of the Sox2+ domain in the rostral/medial region were significantly increased (Figure 3.5.2 D, D'). Collectively, these results suggest that deletion of *Cep83/Flrt1/3* cause a dramatic increase in the total number of IPs and bRGs, and consequently a tangential expansion of the neocortex.

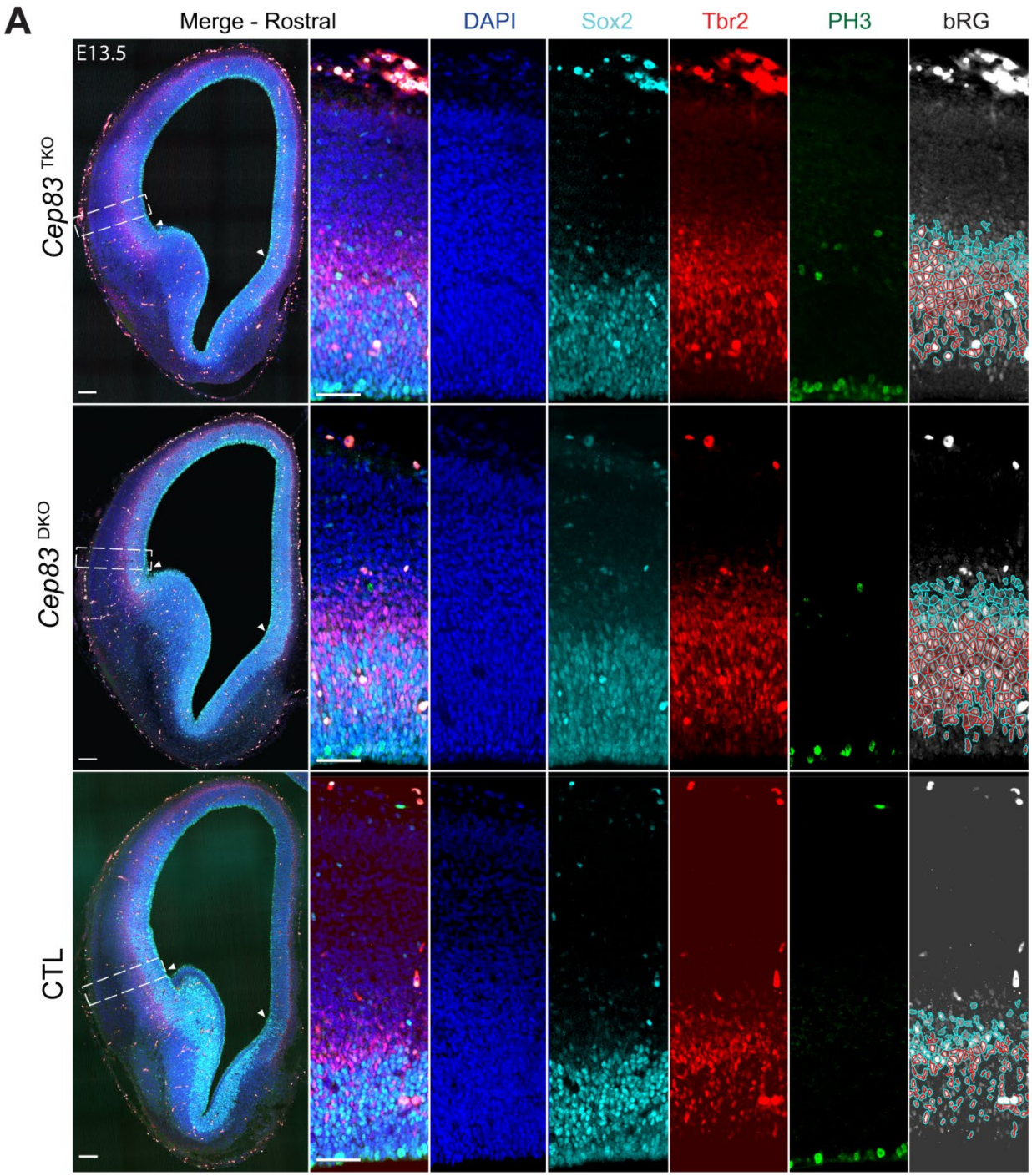
A
Merge - Rostral
DAPI
Sox2
Tbr2
PH3
bRG
E13.5
Cep83 TKO
Cep83 DKO
CTL

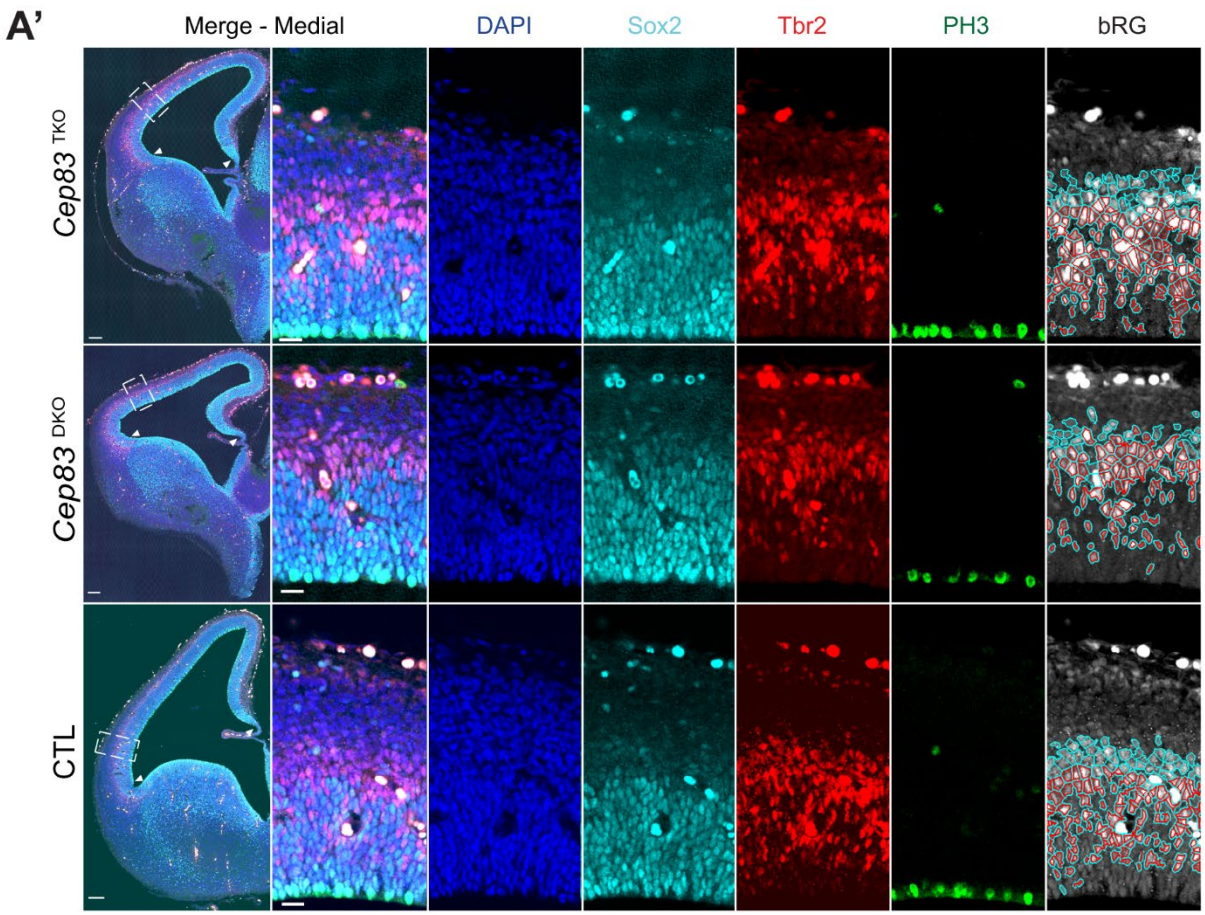
A'
Merge - Medial
DAPI
Sox2
Tbr2
PH3
bRG
Cep83 TKO
Cep83 DKO
CTL

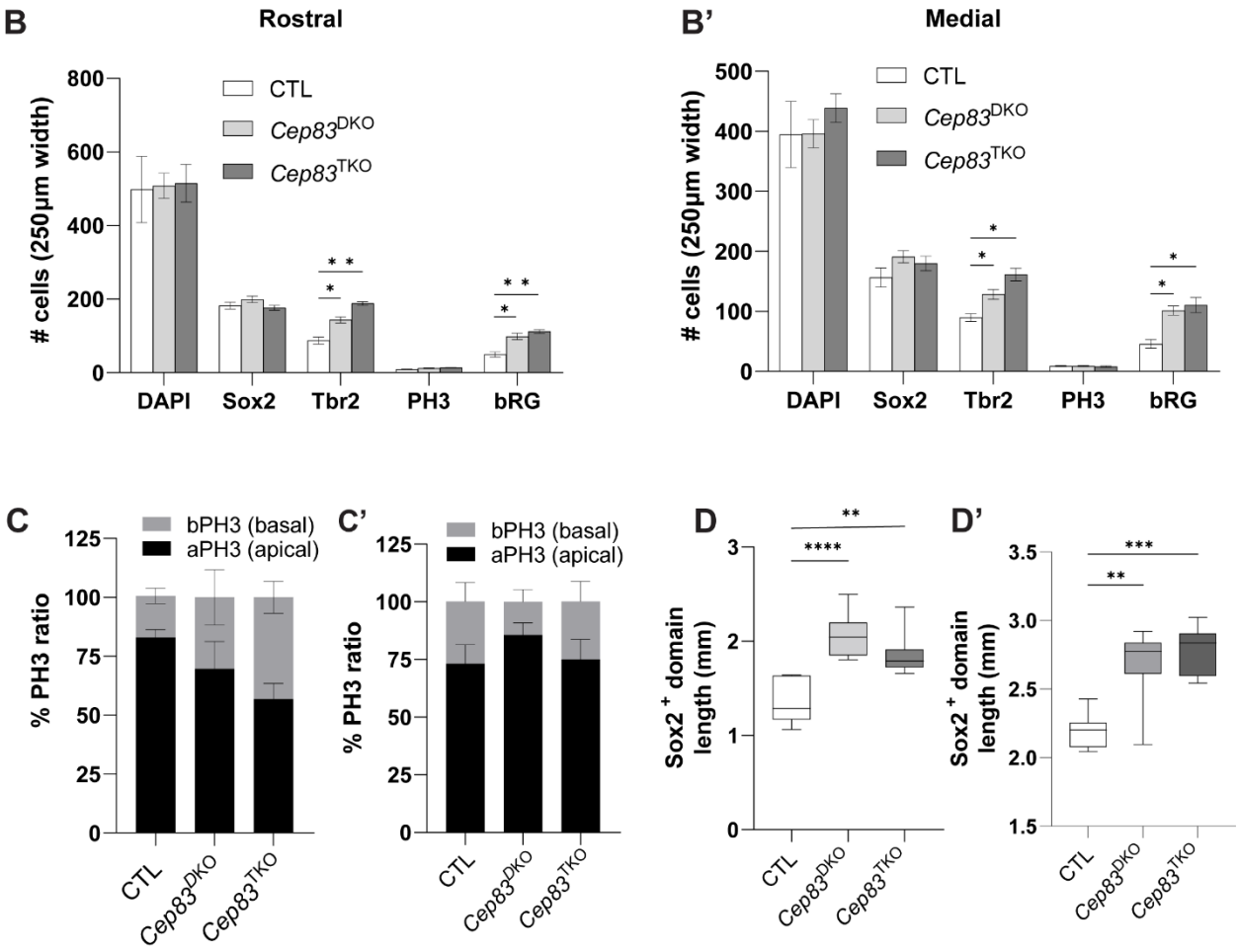

Figure 3.5.2 Alteration of cell proliferation in *Cep83*^{TKO} mice

(A) E13.5 rostral cortices of CTL, *Cep83*^{DKO}. and *Cep83*^{TKO} embryos were stained with DAPI (blue), early neuronal progenitors Sox2 (cyan), intermediate progenitors Tbr2 (red), and mitotic cells PH3 (green). Basal radial glia cells (bRGs) are seen as co-staining of Sox2/Tbr2. Areas in dashed rectangles in (A) are shown with higher magnification on the right. Arrowheads indicate boundaries of the Sox2+ domain. Scale bars 100 µm, 50 µm.

(A') E13.5 medial cortices of CTL, *Cep83*^{DKO}, and *Cep83*^{TKO} embryos were stained with DAPI (blue), early neuronal progenitors Sox2 (cyan), intermediate progenitors Tbr2 (red), and mitotic cells PH3 (green). Basal radial glia cells (bRGs) are seen as co-staining of Sox2/Tbr2 (Cell profiler). Areas in dashed rectangles in (A') are shown with higher magnification on the right. Arrowheads indicate boundaries of the Sox2+ domain. Scale bars 100 µm, 50 µm.

(B) Quantification of data shown in (A). (CTL n=5, *Cep83* ^{DKO} n=5, *Cep83* ^{TKO}, n=5) Data are shown as mean ± SEM; *P< 0.05, **P< 0.01, two-way ANOVA with Tukey's post hoc analysis.

(B') Quantification of data shown in (A'). (CTL *n*=5, *Cep83* ^{DKO} *n*=5, *Cep83* ^{TKO}, *n*=5) Data are shown as mean ± SEM; **P< 0.01, two-way ANOVA with Tukey's post hoc analysis.

(C) Proportion of apical/basal mitotic cells (PH3) in rostral region (CTL *n*=5, *Cep83* ^{DKO} *n*=5, *Cep83* ^{TKO}, *n*=5). Data are shown as mean ± SEM; no significant changes between groups, two-way ANOVA with Tukey's post hoc analysis.

(C') Proportion of apical/basal mitotic cells (PH3) in medial region (CTL *n*=5, *Cep83* ^{DKO} *n*=5, *Cep83* ^{TKO}, *n*=5). Data are shown as mean ± SEM; no significant changes between groups, two-way ANOVA with Tukey's post hoc analysis.

(D) Quantification of the length of the Sox2+ domain (CTL *n*=5, *Cep83* ^{DKO} *n*=5, *Cep83* ^{TKO}, *n*=5). Data are shown as mean value; **P< 0.01, ****P< 0.0001, two-way ANOVA with Tukey's post hoc analysis.

(D') Quantification of the length of the Sox2+ domain (CTL *n*=5, *Cep83* ^{DKO} *n*=5, *Cep83* ^{TKO}, *n*=5). Data are shown as mean value; **P< 0.01, ***P< 0.001, two-way ANOVA with Tukey's post hoc analysis.

To further define cell cycle progression of the increased bRGs and IPs in triple mutant mice, we administered a single dose of 5-bromo-2′-deoxyuridine (BrdU, a thymidine analogue) to the pregnant mice for checking embryo at E13.5. After 30 min, the neocortex was collected for immunostaining analysis with the proliferative marker Ki67, and DAPI (Figure 3.5.3 A). We observed that both BrdU+ and Ki67+ were significantly increased in the triple mutant neocortex as compared to littermate CTLs (Figure 3.5.3 B), suggesting that increased cell proliferation in the *Cep83* ^{DKO} and *Cep83* ^{TKO} mutant cortex is due to lengthening of the S phase in the cell cycle. Altogether, these results suggest that cortical expansion in *Cep83* ^{TKO} mice during embryonic development is caused by an increased cell cycle progression of S phase with an increased number of IPs and bRG, which leads to expansion of neuronal pool.

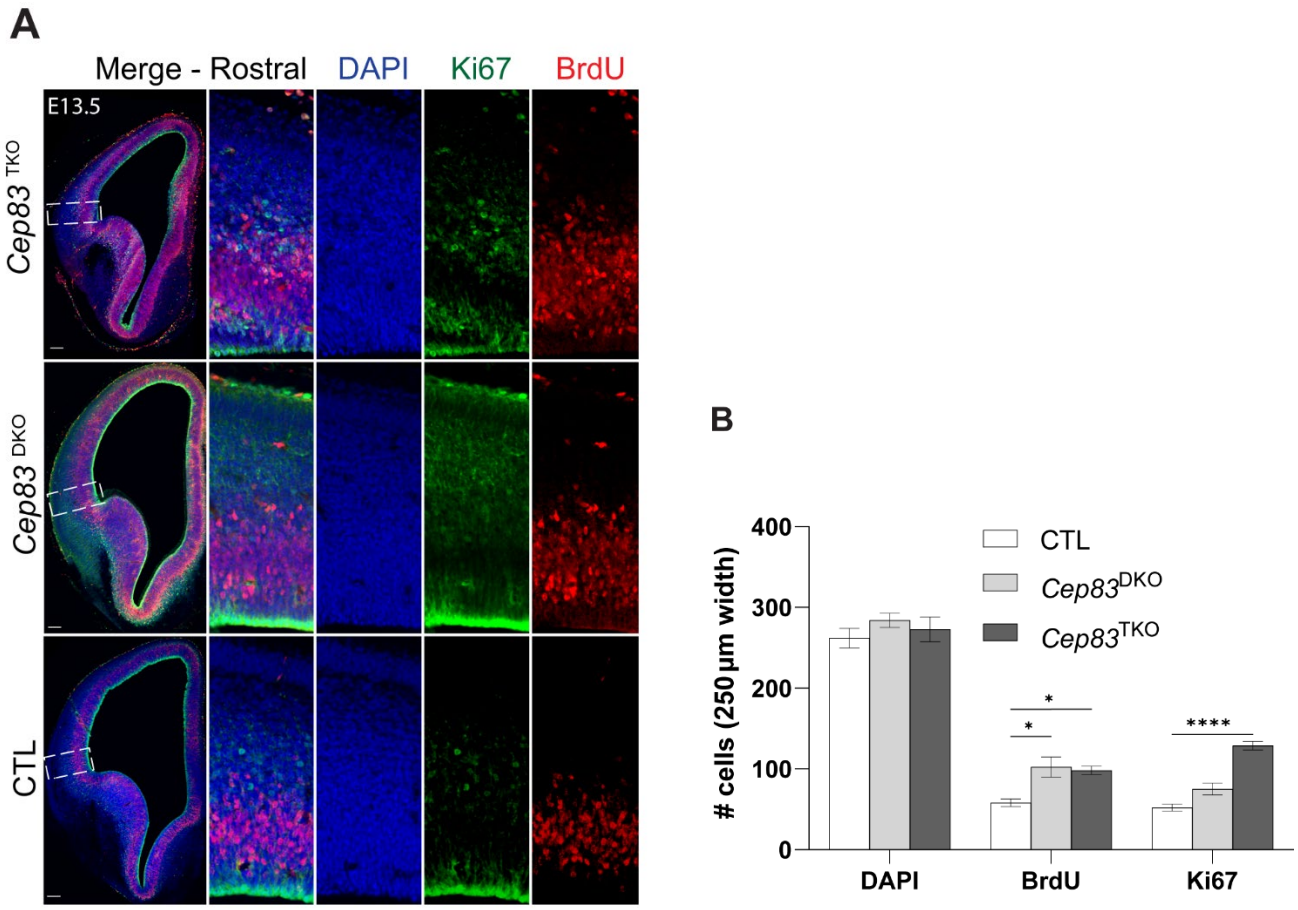

Figure 3.5.3 Increased cell proliferation in *Cep83*^{TKO} mice seen in BrdU analysis

(A) CTL, *Cep83* ^{DKO}, and *Cep83* ^{TKO} E13.5 cortices labeled with a short pulse (30 min) of BrdU (red) were counterstained with 4′,6-diamidino-2-phenylindole (DAPI, blue) and the cell proliferation marker Ki67 (green). Areas in dashed rectangles in (A) are shown with higher magnification on the right. Scale bar 100 µm.

(B) Quantification of data shown in (A). (*n*=4 mice per groups) Data are shown as mean ± SEM; *p<0.05, ****p<0.0001, two-way ANOVA with Tukey's post hoc analysis.

3.6 Increased number of CP neurons in *Cep83*^{TKO} mice

Given the alteration in the number of IPs in triple mutant mice, we next investigated distribution and migration of cortical neurons in the CP layer where cortical folds were seen. The cortical layer remained normal in the sulcus area of triple mutants (Figure 3.6.1 C). In addition, the density of Satb2+ neurons in the sulcus was also analyzed. In both control and *Cep83/Flrt1/3* deficient mice, Satb2+ neurons were homogeneously distributed over all regions, including the sulcus area (Figure 3.6.1 A,A'B). Notably, the proportion of Satb2+ neurons in the upper versus lower CP was significantly higher in the sulcus and adjacent area of the sulcus as compared to CTL mice (Figure 3.6.1 D). Similar results were obtained after BrdU labeling at E13.5 and analyzing those neuronal distributions in the CP at E16.5 (Figure 3.6.2 A,C). The proportion of *Cep83/Flrt1/3* ablated BrdU+ neurons were divided into lower/middle/upper parts of the CP (Figure 3.6.2 A). There seemed to be more BrdU+ neurons in the upper CP layer and less in the lower CP layer in triple mutant mice as compared to CTL mice (Figure 3.6.2 B). Subsequently, we further subdivided the CP into uCP and lCP, based on Tbr1+ layer (Figure 3.6.2 C). The proportion of BrdU+ neurons in the uCP was significantly increased and in the lCP was remarkably decreased as compared to the CTL (Figure 3.6.2 D). These results suggested that *Cep83/Flrt1/3* deficient cortical neurons migrated faster through the CP, which led to a higher proportion of cells in the upper CP. This notion was further supported after we obtained direct evidence of the migration speed of cortical neurons using live imaging of embryonic cortices *ex vivo* (Figure 3.6.2 F,F'). Neurons from triple mutant mice showed an increasing trend of average of speed in the CP layer (Figure 3.6.2 G).

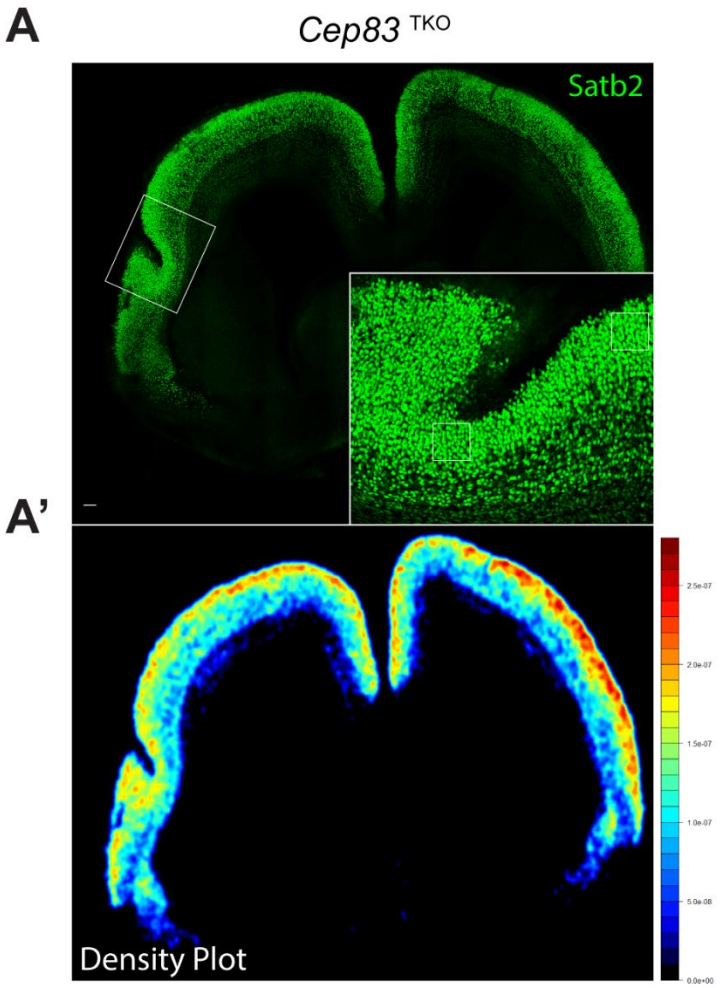
A
Cep83 TKO
Satb2
A'
Density Plot

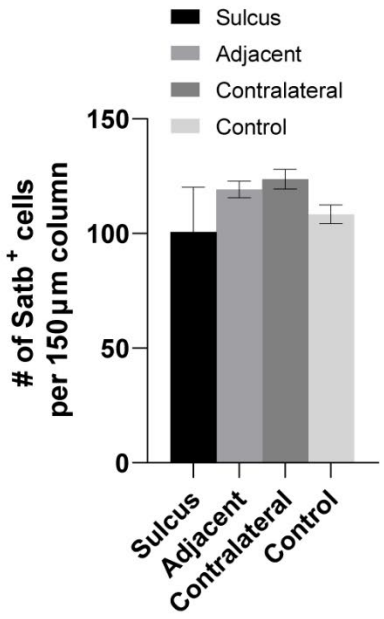
B
Sulcus
Adjacent
Contralateral
Control
# of Satb+ cells per 150 µm column
150
100
50
0
Sulcus
Adjacent
Contralateral
Control

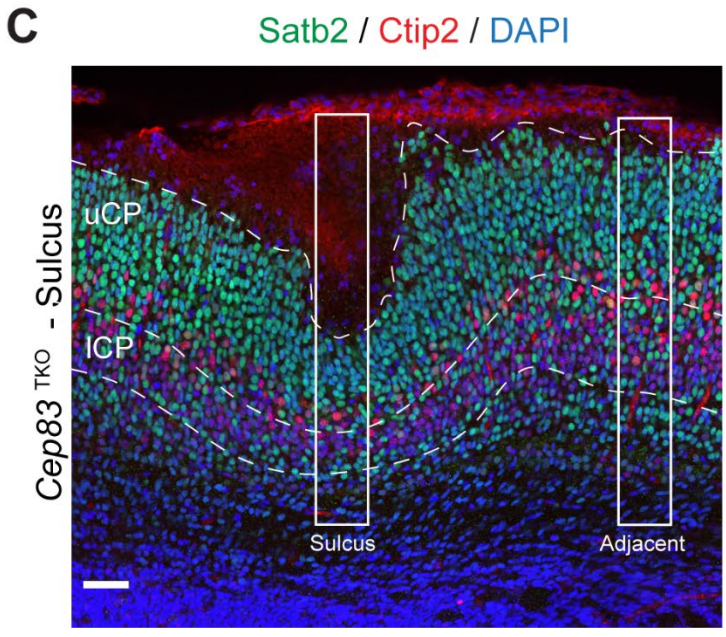
C
Satb2 / Ctip2 / DAPI
Cep83 TKO - Sulcus
uCP
lCP
Sulcus
Adjacent

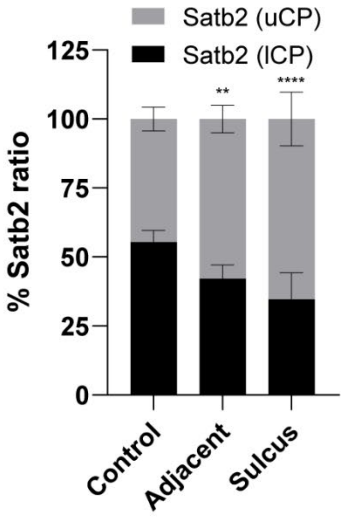
D
Satb2 (uCP)
Satb2 (lCP)
% Satb2 ratio
125
100
75
50
25
0
**
****
Control
Adjacent
Sulcus

Figure 3.6.1 Distribution of CP neurons in the sulcus area of *Cep83*^{TKO} mice

(A) Coronal brain sections of *Cep83*^{TKO} at E17.5 immunostained with Satb2, a CP neuronal marker. Area in dashed rectangles in (A) are shown with higher magnification on the right. Scale bar 100 μm.

(A') Satb2+ cell distribution in A. The color bar indicates a higher (red) or lower (blue) density of Satb+ cells.

(B) Quantification of data shown in (A). Satb2+ cells were counted in sulci and adjacent and contralateral side of cortices and littermate controls. (sulcus, contralateral, control cortices, n=6; adjacent cortices, *n*=5). Data are shown as mean ± SEM; no significant changes between groups, one-way ANOVA with Tukey's post hoc analysis.

(C) Sulcus and adjacent region from an E17.5 *Cep83*^{TKO} section immunostained with Satb2 (green) and Ctip2 (red), DAPI (blue). Scale bar 50 μm

(D) Quantification of data shown in (C). The CP was subdivided into upper and lower CP. Proportion of Satb2+cells in the upper and lowerCP, versus areas adjacent to the sulcus, and the sulcus in mutant mice and CTL mice (*n*=6 mice per groups). Data are shown as mean ± SEM; **p<0.01, ****p<0.0001, two-way ANOVA with Tukey's post hoc analysis.

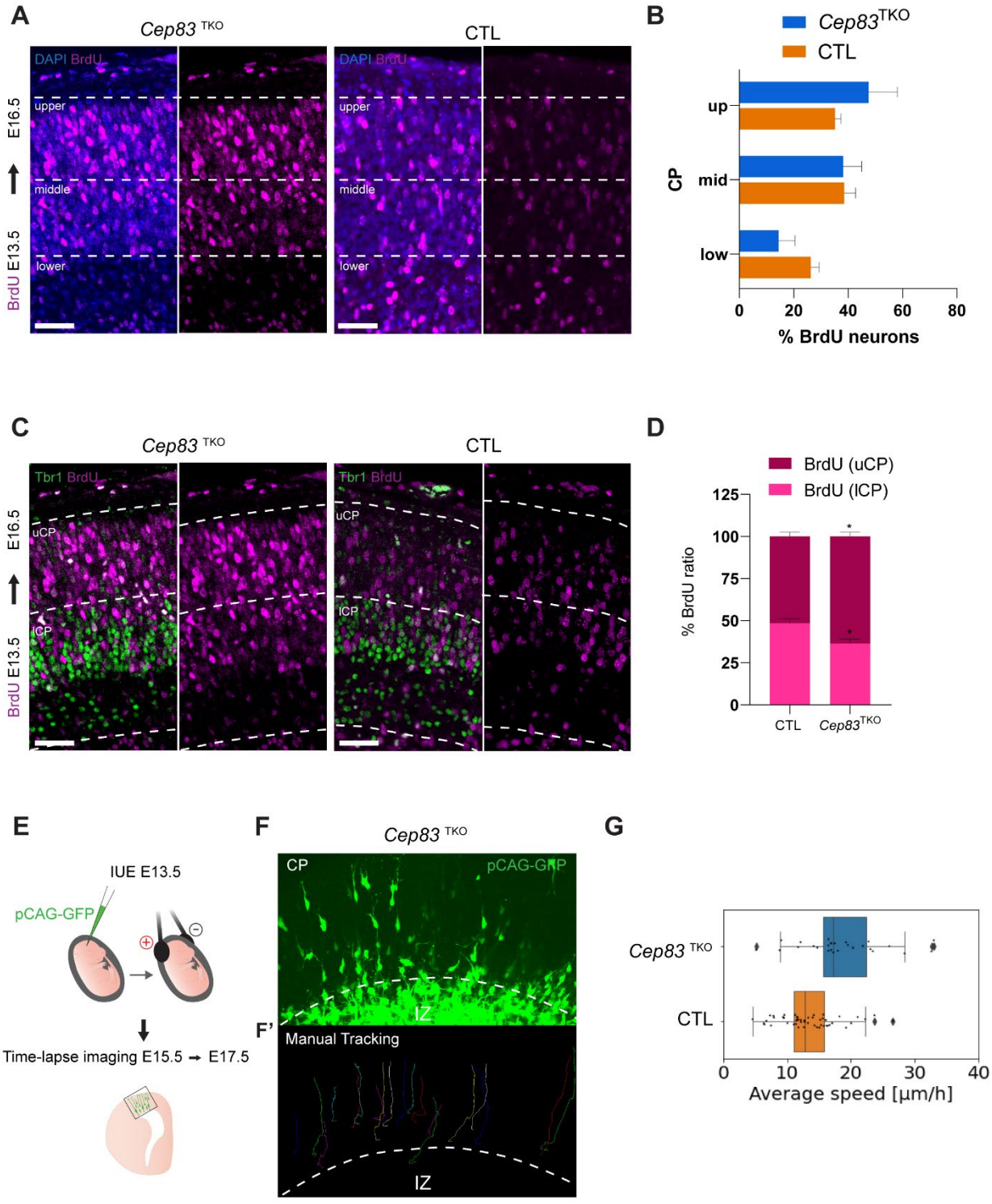
A
Cep83 TKO
CTL
DAPI BrdU
E16.5
BrdU E13.5
upper
middle
lower
B
Cep83TKO
CTL
up
mid
low
CP
0
20
40
60
80
% BrdU neurons
C
Cep83 TKO
CTL
Tbr1 BrdU
uCP
lCP
D
BrdU (uCP)
BrdU (lCP)
% BrdU ratio
125
100
75
50
25
0
CTL
Cep83TKO
E
IUE E13.5
pCAG-GFP
Time-lapse imaging E15.5 → E17.5
F
Cep83 TKO
CP
pCAG-GFP
IZ
F'
Manual Tracking
IZ
G
Cep83 TKO
CTL
0
10
20
30
40
Average speed [μm/h]

Figure 3.6.2 Neuronal migration in *Cep83*^{TKO} and CTL mice

(A) BrdU injection was performed at E13.5 and analyzed at E16.5. BrdU expression was confirmed by immunostaining coronal sections with BrdU (magenta). The CP was subdivided into 3 bins (upper, middle, and lower), and the number of BrdU+ neurons in each bin was quantified. Scale bar 50 μm

(B) Quantification of the data shown (B). n=4, Data are shown as mean ± SEM; no significant changes between groups, two-way ANOVA with Tukey's post hoc analysis.

(C) BrdU injection was performed at E13.5 and analyzed at E16.5. BrdU expression was confirmed by immunostaining coronal sections with BrdU (magenta). The CP was subdivided into uCP and lCP using Tbr1, and the number of BrdU+ neurons in each layer was quantified. Scale bar 50 μm

(D) Quantification of the data shown (C). n=4, Data are shown as mean ± SEM; *$p<0.05$, two-way ANOVA with Tukey's post hoc analysis.

(E) Schematic of *in utero* electroporation (IUE) performed at E13.5 and time-lapse imaging at E15.5 over 48 hours.

(F) Migrating GFP labelled neurons by IUE was tracked in the CP

(F') Progression lines of tracked migrating neurons in (F)

(G) Quantification of the data shown (F). The average speed of tracked neurons is shown as a whisker plot; *Cep83*^{TKO} n=3 CTL n=2. Data are shown as mean ± SEM.

3.7 Validation of the Foxg1-Cre driver for the generation of *Fgf10*^{TKO}

To increase the early progenitors, RGC and NECS, cell population in the *Flrt1/3* DKO 'cell migration' model, we decided to combine the *Foxg1-Cre;Fgf10*$^{lx/lx}$ *mice* with the *Flrt1*$^{-/-}$*;Flrt3*$^{lx/lacZ}$ mice. Thus, Foxg1-Cre driver was validate in *Fgf10*cKO and *Flt1/3*DKO mice. The cortical area of *Fgf10*cKO mice were not altered as compared to WT mice at E17.5 (Figure 3.7 A,B). To further identify whether there is a direct correlation between brain size and cortical folding, we tracked the brains that exhibit folding using color dots. Similar to *Cep83*cKO, we found that bigger brains tend to show more cortical folding (Figure 3.7 B). Unexpectedly, we also observed a mild folding phenotype in WT mice (Figure 3.7 B). *Flrt1/3* DKO with the Foxg1-Cre line was also investigated with regard to size of cortical area, however we did not see any alteration of brain size between *Flrt1/3* DKO and CTL mice (Figure 3.7 C,D), suggesting there is no alteration of neuronal production. This corresponds with findings which were already reported in the *Flrt1/3*DKO using Nestin-Cre (Del Toro et al, 2017).

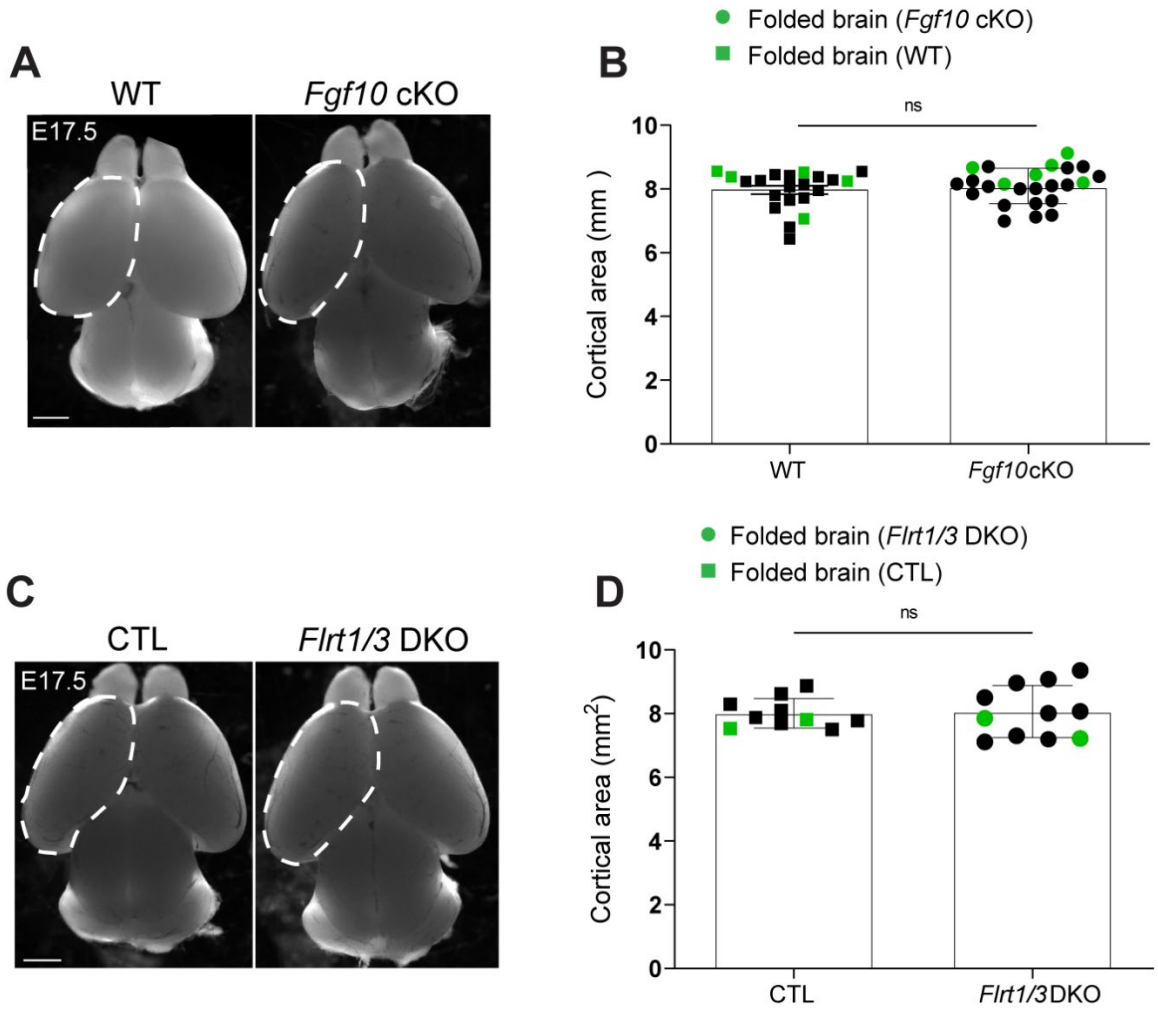

Figure 3.7 Cortical area of *Fgf10*cKO and Foxg1-Cre;*Flrt1/3*DKO mice

(A) Representative whole-mount images of E17.5 wild-type (WT) and *Fg*f10cKO brains. Scale bar 1 mm.

(B) Quantification of the cortical areas (WT *n*=21, *Fgf10*cKO *n*=24). Green dots indicate folded brains. Data are shown as mean ± SEM; no significant changes between groups, unpaired Student's t-test.

(C) Representative whole-mount images of E17.5 CTL and *Flrt1/3*DKO brains. Scale bar 1 mm.

(D) Quantification of the cortical areas (CTL *n*=10, *Flrt1/3*DKO *n*=11). Green dots indicate folded brains. Data are shown as mean ± SEM; no significant changes between groups, unpaired Student's t-test.

3.8 Characterization of *Fgf10*^{TKO} mice

To generate *Foxg1-Cre;Fgf10*$^{lx/lx}$*;Flrt1*$^{-/-}$*;Flrt3*$^{lacZ/lx}$ *mice* (*Fgf10*^{TKO} mice), we crossed *Flrt1*$^{-/-}$*; Flrt3*$^{lx/lacZ}$ mice (Yamagishi et al., 2011; Egea et al., 2008) with *Fgf10* $^{lx/lx}$ mice (Urness et al., 2010) leading to *Flrt1*$^{-/-}$*; Flrt3*$^{lx/lacZ}$;*Fgf10*$^{lx/lx}$ mice. These animals were further crossed with Foxg1-Cre to remove the floxed alleles for Fgf10 and FLRT3. To validate our mouse models, we performed RNAscope analysis of Fgf10. Our littermate CTL was *Flrt1*$^{-/-}$*Flrt3*$^{lacZ/+}$, and showed no Cre expression. At E11.5, Fgf10 RNA levels in CTL mice showed signal mainly in the VZ, whereas in *Fgf10*^{TKO} mice, the Fgf10 signal was reduced (Figure 3.8).

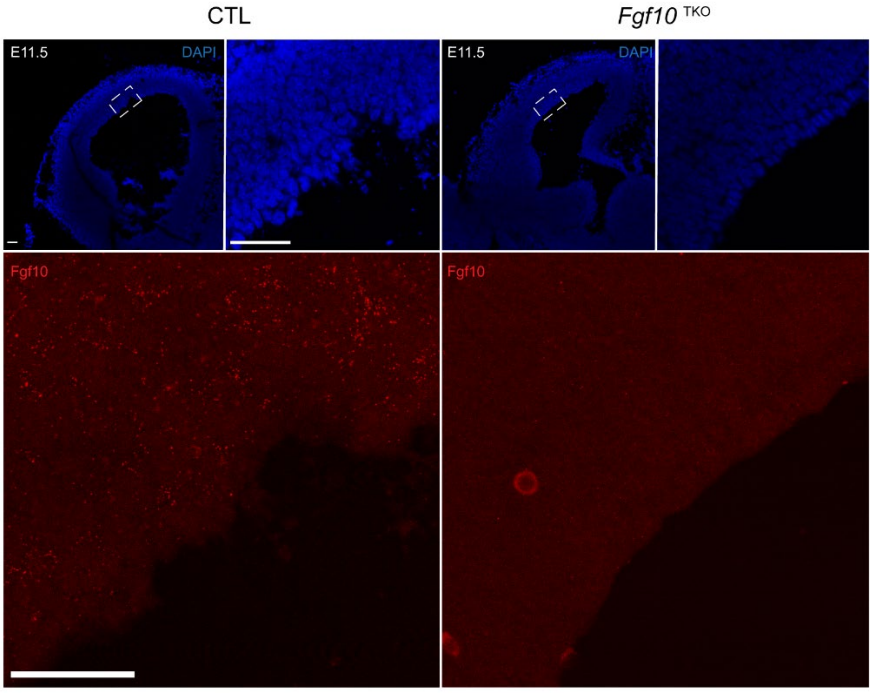

Figure 3.8 Expression of Fgf10 in *Fgf10*^{TKO} and CTL mice

ISH for Fgf10 in coronal sections of E11.5 cortex. Scale bars 50 µm. Fgf10 expression is shown in higher magnification in the VZ.

3.9 *Fgf10*^{TKO} mice shows stronger gyrus formation

To analyze folding phenotypes, the upper layer markers, Satb2 and Ctip2 were applied to the E17.5 neocortex. The *Fgf10*^{TKO} mice exhibited cortical folds in microscopic images (Figure 3.9 A), 3D whole brain images (Figure 3.9 B), and coronal sections (Figure 3.9 C). Satb2 and Ctip2 staining revealed protrusions in the lateral side of the cortical area, while the cortical layering and apical surface of the VZ remain unaltered, indicating a *bona fide* cortical folding phenotype (Figure 3.9 C). Overall, the phenotype revealed varies from a single gyrus to multiple sulci and gyri. Strikingly, 93% of the neocortex exhibited a gyrus phenotype in only the rostral cortical area of *Fgf10*^{TKO} and *Fgf10/Flrt1*^{DKO}*Flrt3*^{het} mice, in short *Fgf10*^{DKO}. Seven percent of the neocortices showed a sulci phenotype, but only when folding emerged simultaneously with multiple sulci and gyri across the rostro-caudal cortical area. Compared to ablation of *Flrt1/3*DKO (14%) or *Fgf10*cKO (22%), the mouse models where three genes were deleted, regardless of whether it was one or two Flrt3 alleles; showed increased penetrance, where up to 90% of mice showed an improved folding phenotype (Figure 3.9 D and Table 3.2).

To quantify the folding phenotype, GI, which is the ratio of the length of the cortical surface (folded or unfolded) over the hypothetical minimal length of the cortical surface (Figure 3.9 E), was obtained from three different groups: the first where *Fgf10/Flrt1/3* were all ablated, the second where *Flrt1/3* were both ablated, and the third where *Fgf10* was ablated. Overall, the GI value was measured only in rostral cortical region. In the group where *Flrt1/3* were ablated and in the *Fgf10*cKO, the neocortex exhibited a GI value of nearly 1.01-1.02, which indicated a relatively smooth or mild phenotype. In contrast, in the group where *Fgf10/Flrt1/3* were all ablated, the neocortex reached a GI value of above 1.03. Strikingly, the group where all three genes were deleted showed the significantly highest GI value among the other groups, indicating an enhanced cortical folding

phenotype in the mouse model where the *Fgf10/Flrt1/3* genes were all deleted compared to *Flrt1/3* and *Fgf10c*KO (Figure 3.9 F).

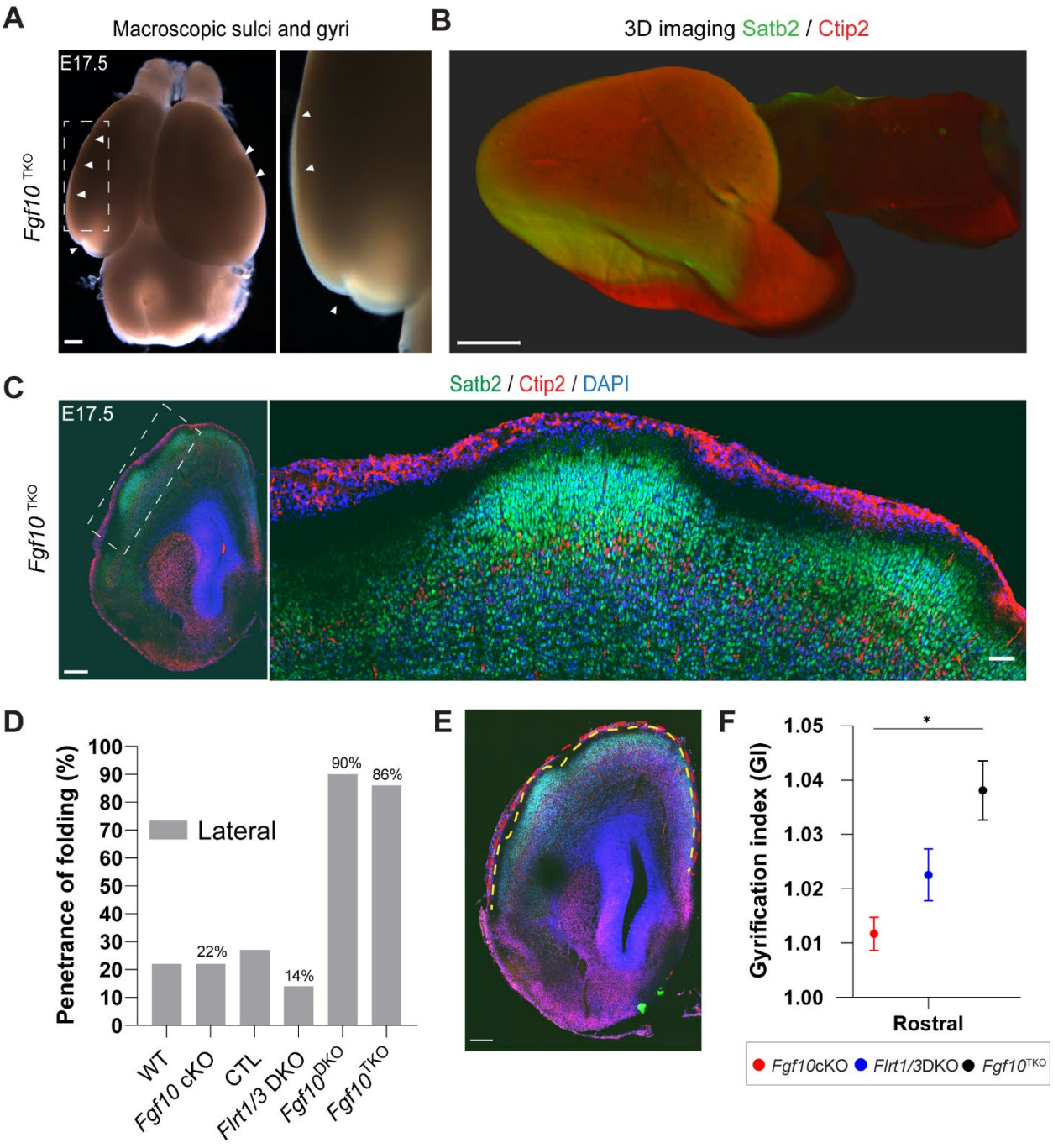

Figure 3.9 *Fgf10*^{TKO} mice develop cortical gyri

(A) Macroscopic sulci and gyri in E17.5 *Fgf10*^{TKO} embryo. The area in the dashed rectangle is shown with higher magnification on the right, sulci and gyri are indicated by arrowheads. Scale bars 500 μm.

(B) 3D imaging of the E17.5 *Fgf10*^{TKO} embryo in (A). Scale bar 500 μm.

(C) E17.5 *Fgf10*^{TKO} brain section stained with Satb2, Ctip2, and DAPI. Area in dashed rectangle is shown with higher magnification on the right. Scale bar 1000 μm

(D) Folding penetrance of WT, *Fgf10*cKO, CTL, *Flrt1/3*DKO, *Fgf10*^{DKO}, and *Fgf10*^{TKO}. All folding phenotypes were seen only in the lateral side of cortex at E17.5

(E) Representative images of GI measurement in *Fgf10*^{TKO}. Yellow line indicates the *de facto* length of the cortical surface; red line indicates the hypothetical minimal length of the cortical surface. Scale bar 100 μm.

(F) Quantification of GI values in E17.5 embryos. n= 6 *Fgf10*cKO (red), n= 4 *Flrt1/3*DKO (blue) and n=15 *Fgf10*^{TKO} (black) at rostral region of brain. Data are shown as mean ± SEM; **P*< 0.05, two-way ANOVA with Tukey's post hoc analysis.

Table 3.2Cortical folding penetrance at E17.5 of the indicated genotypes. Brains were analyzed for the presence of one or multiple sulci/gyri as shown in Figure 3.9

Genotype	N analyzed	N with foldings	Penetrance
WT	23	5	22%
Foxg1-Cre;Fgf10 cKO	27	6	22%
Foxg1-Cre;Flrt1$^{-/-}$*Flrt3*^{het} (CTL)	11	3	27%
*Foxg1-Cre;Flrt1/3*DKO	14	2	14%
Fgf10$^{+/+}$*;Flrt1*$^{-/-}$*Flrt3*^{het} (CTL)	8	1	12.5%
Foxg1-Cre;Fgf10/Flrt1^{DKO}*Flrt3*^{het} (*Fgf10*^{DKO})	21	19	90%
Foxg1-Cre;Fgf10/Flrt1/3^{TKO} (*Fgf10*^{TKO})	14	13	86%

3.10 Cortical expansion in *Fgf10*^{TKO} mice correlates with increased early progenitors, NECs & aRGCs

Analysis of the cortical area of *Fgf10*^{TKO} and *Fgf10*^{DKO} mice revealed a significant increase in size as compares to CTL embryos at E17.5 (Figure 3.10.1 A,B), suggesting an increase in the neuronal population in those brains. To identify whether there is a direct correlation between brain size and cortical folding, we tracked the brains that exhibited folding. There was a trend that bigger brains seem to have folding. (Figure 3.10.1 B).

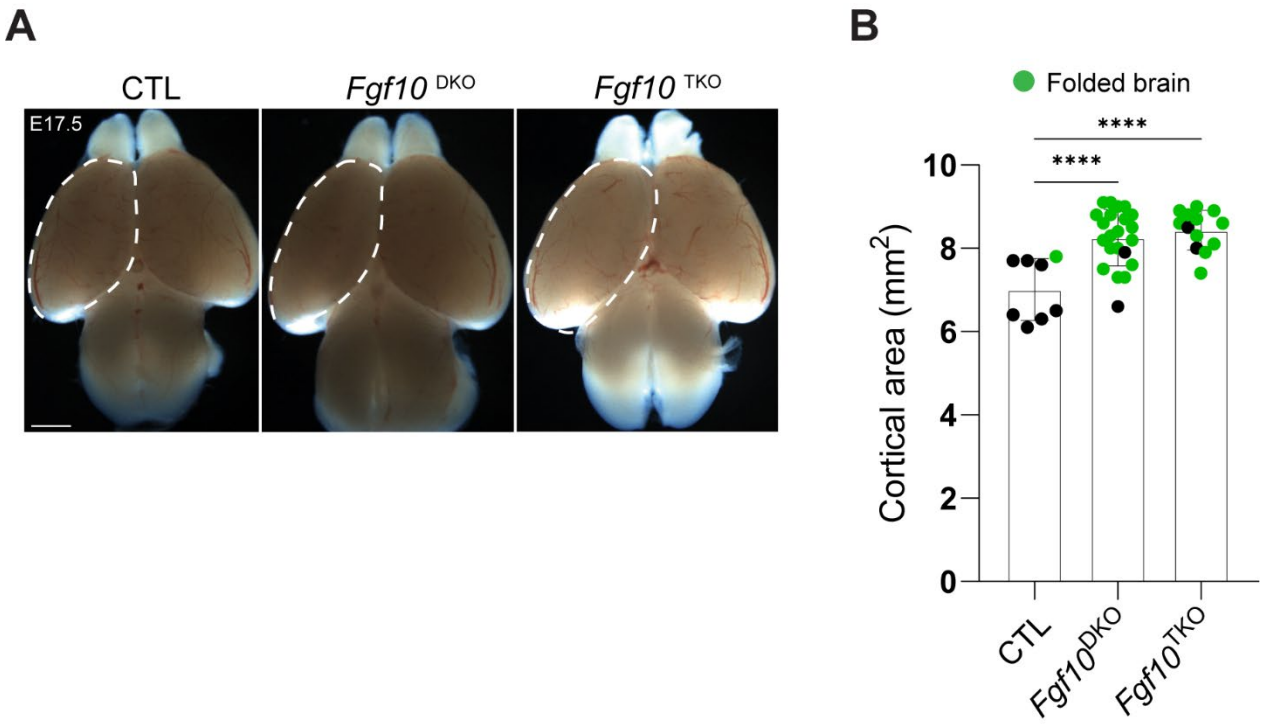

Figure 3.10.1 Cortical area of *Fgf10/Flrt1/3* mutant embryos at E17.5

(A) Representative whole-mount images of E17.5 CTL, *Fgf10*^{DKO} and *Fgf10*^{TKO} brains. Scale bar 1 mm.

(B) Quantification of the cortical areas. Green dots indicate folded brains. Data are shown as mean ± SEM; ****P< 0.0001, Two-way ANOVA, Tukey Post hoc test.

To investigate whether cell proliferation was mechanistically enhanced in triple mutant mice, we analyzed cell proliferation in rostral neocortex sections at E11.5 by quantifying the number of apical progenitor (Sox2+), intermediate progenitor (Tbr2+), and dividing RGCs and mitotic dividing cells (pH3+). Further, the neuronal population that co-expressed Sox2 and Tbr2 was quantified to obtain bRGs. To examine tangential expansion in the proliferative area, which is composed of mainly RGCs, the total length of the Sox2+ domain was measured (Figure 3.10.2 A). In rostral regions, we observed a significant increase in early progenitors (Sox2+ cells) in triple mutant embryos, whereas IPs, mitotic dividing cells, and RGCs remained unchanged (Figure 3.10.2 A, B). Interestingly, the proportion of mitotic cells (pH3+) in the apical versus basal layer exhibited a significant increase in triple mutants (Figure 3.10.2 C), suggesting an increase in dividing NECs and aRGCs. However, the total length of the Sox2+ domain was unchanged, even though there was a trend of increasing length in the Sox2+ domain in triple mutants compared to littermate CTLs (Figure 3.10.2 D). Collectively, these results suggest that deletion of *Fgf10/Flrt1/3* substantially increases division of early apical progenitors, NECs, and aRGCs, an observation which further is supported by an increase in mitotic division in the apical VZ.

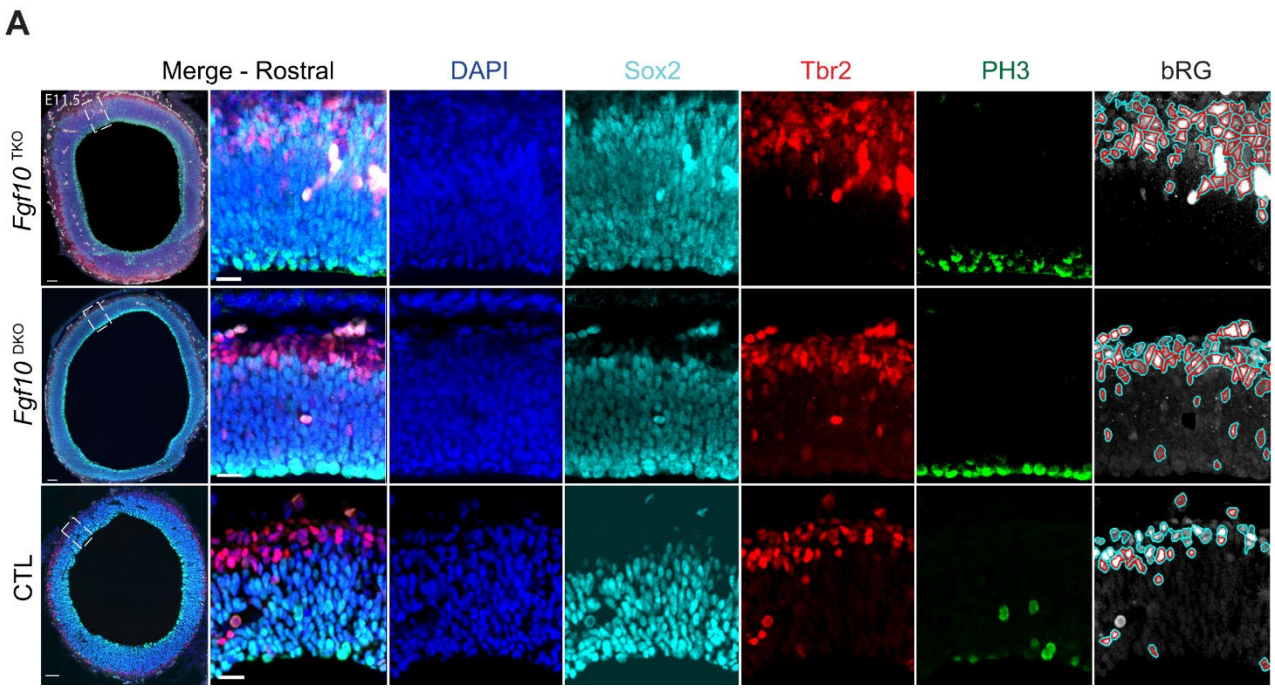
A
Merge - Rostral
DAPI
Sox2
Tbr2
PH3
bRG
Fgf10 TKO
Fgf10 DKO
CTL
E11.5

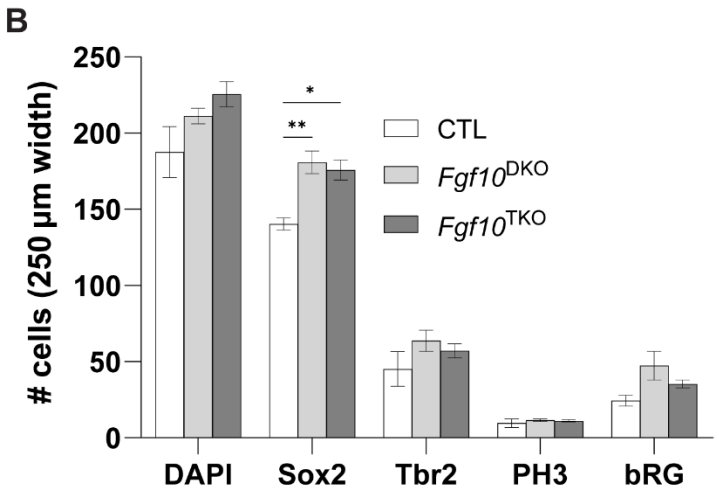
B
cells (250 µm width)
250
200
150
100
50
0
*
**
CTL
Fgf10DKO
Fgf10TKO
DAPI
Sox2
Tbr2
PH3
bRG

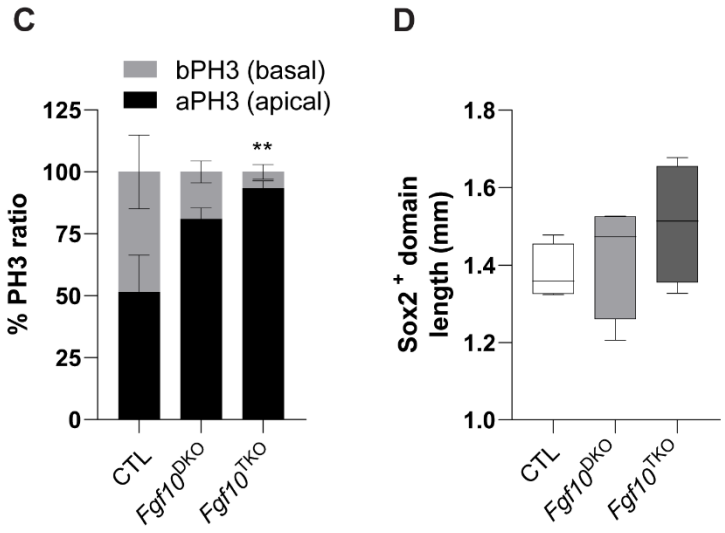

Figure 3.10.2 Cell proliferation in *Fgf10*^{TKO} mice

(A) E11.5 rostral cortices of CTL, *Fgf10*^{DKO} and *Fgf10*^{TKO} embryos were stained with DAPI (blue), early neuronal progenitors Sox2 (cyan), intermediate progenitors Tbr2 (red), and mitotic cells PH3 (green). Basal radial glia cells (bRGs) are seen as co-staining of Sox2/Tbr2 (Cell profiler).. Areas in dashed rectangles in (A) are shown with higher magnification on the right. The Sox2+ domain was obtained from entire cortex. Scale bar 100 μm.

(B) Quantification of the data shown in (A). (CTL *n*=5, *Fgf10*^{DKO} *n*=5, *Fgf10*^{TKO} *n*=5) Data are shown as mean ± SEM; no significant changes between groups two-way ANOVA with Tukey's post hoc analysis.

(C) Proportion of apical/basal mitotic cells (PH3) in rostral region (CTL *n*=5, *Fgf10*^{DKO} *n*=5, *Fgf10*^{TKO} *n*=5. Data are shown as mean ± SEM; *p<0.05, two-way ANOVA with Tukey's post hoc analysis.

(D) Quantification of the length of the Sox2+ domain (CTL *n*=3, *Fgf10*^{DKO} *n*=3, *Fgf10*^{TKO} *n*=3). Data are shown as mean value; no significant changes between groups, two-way ANOVA with Tukey's post hoc analysis.

To further define cell cycle progression of the increased early progenitors, we administered a single dose of 5-bromo-2′-deoxyuridine (BrdU, a thymidine analogue) at E13.5. After 30 min, the neocortex was collected for immunostaining analysis using proliferative markers, Ki67, and DAPI (Figure 3.10.3 A). We observed an increasing trend

in BrdU+ in *Fgf10*^{TKO} neocortex compared to CTL (Figure 3.10.3 B), suggesting an increase in cell proliferation in the *Fgf10/Flrt1/3* mutant cortex, compare to CTL groups (n=1). Taken together, these results suggest an increase in cell cycle progression in *Fgf10*^{TKO} mice, and thus an increase in early apical progenitors with mitotic division in the apical VZ, leads to cortical expansion with gyrus folding during cortical development.

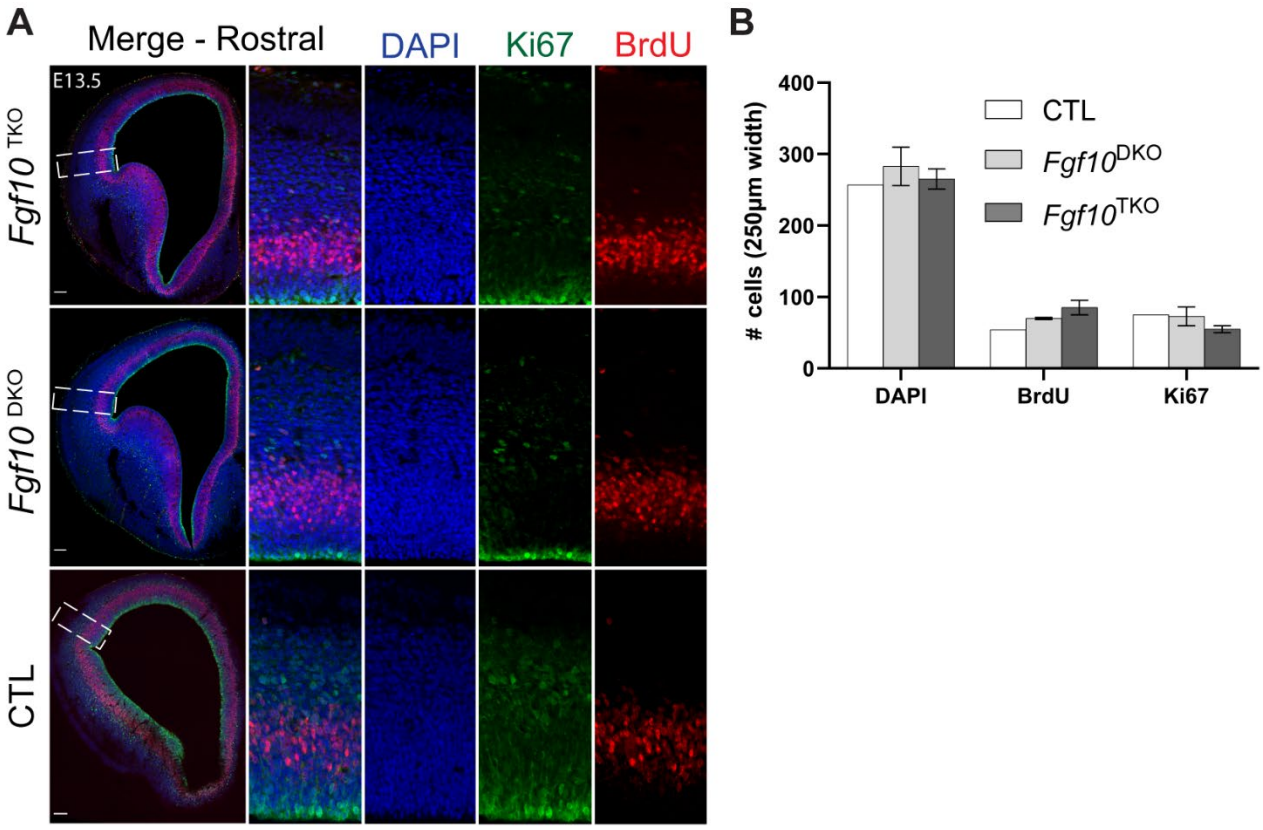

Figure 3.10.3 Increased cell proliferation in *Fgf10*^{TKO} seen in BrdU analysis

(A) CTL, *Fgf10*^{DKO}, and *Fgf10*^{TKO} E13.5 cortices labeled with a short pulse (30 min) of BrdU (red) were counterstained with DAPI (blue) and the cell proliferation marker, Ki67 (green). Areas in dashed rectangles in (A) are shown with higher magnification on the right. Scale bar 100 µm.

(B) Quantification of data shown in (A). *Fgf10*^{DKO} and *Fgf10*^{TKO} *n*=4, CTL n=1) Data are shown as mean ± SEM.

3.11 Increased number of CP neurons in *Fgf10*^{TKO} mice

Given the increase in early progenitors and apical mitotic divisions in triple mutant mice, we next investigated the distribution and migration of cortical neurons in the CP layer where cortical folds were seen. The cortical layer remained normal in the gyrus area of triple mutant mice (Figure 3.11.1 C). Interestingly, in *Fgf10/Flrt1/3* deficient mutant, Satb2+ neurons were much more dense in the gyrus area, especially in protrusion regions, which is further supported by the density plot (Figure 3.11.1 A,A',B). Notably, the proportion of Satb2+ neurons in the upper versus lower CP was significantly higher in the gyrus than in the area adjacent to the gyrus as compared to CTLs (Figure 3.11.1 D). Similar results were obtained after BrdU labeling at E13.5 and analyzing that neuronal distribution in the CP at E16.5 (Figure 3.11.2 A, C). The proportion of *Fgf10/Flrt1/3* ablated BrdU+ neurons were divided into lower/middle/upper part of the CP (Figure 3.11.2 A). In triple mutant mice, BrdU+ neurons at E16.5 seemed more in the upper CP layer and less in the lower CP layer as compared to CTLs (Figure 3.11.2 B). Subsequently, we further analyzed the CP and subdivided it into uCP and lCP areas, based on Tbr1^{+} layer (Figure 3.11.2 C). There was an increasing trend with regard to the proportion of BrdU+ neurons in the uCP, whereas, in the lCP less neurons were observed compared to littermate CTLs (Figure 3.11.2 D). These results suggested that *Fgf10/Flrt1/3* deficient cortical neurons migrated faster through the CP, which led to a higher proportion of cells in the upper CP (Figure 3.11.1 D). This was further supported after we obtained direct evidence of the migration speeds of cortical neurons using live imaging of embryonic cortices *ex vivo* (Figure 3.11.2 F,F'). Neurons from triple mutant mice showed a trend of increasing average of speed in CP layer (Figure 3.11.2 G).

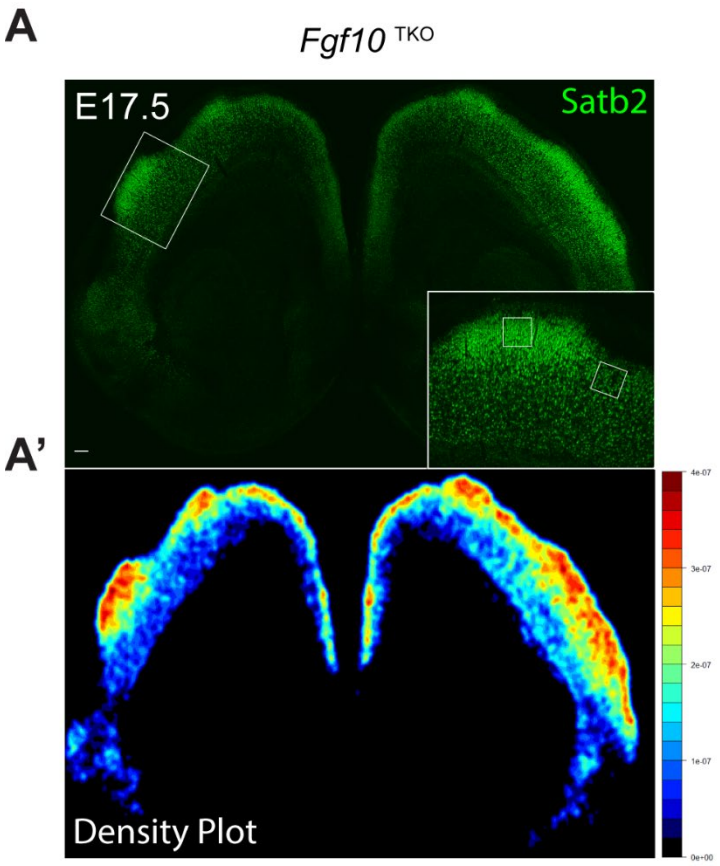
A
Fgf10 TKO
E17.5
Satb2
A'
Density Plot

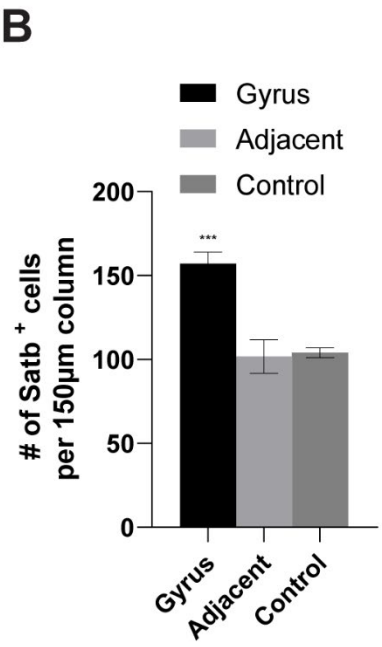
B
Gyrus
Adjacent
Control
# of Satb+ cells per 150µm column
200
150
100
50
0
***
Gyrus
Adjacent
Control

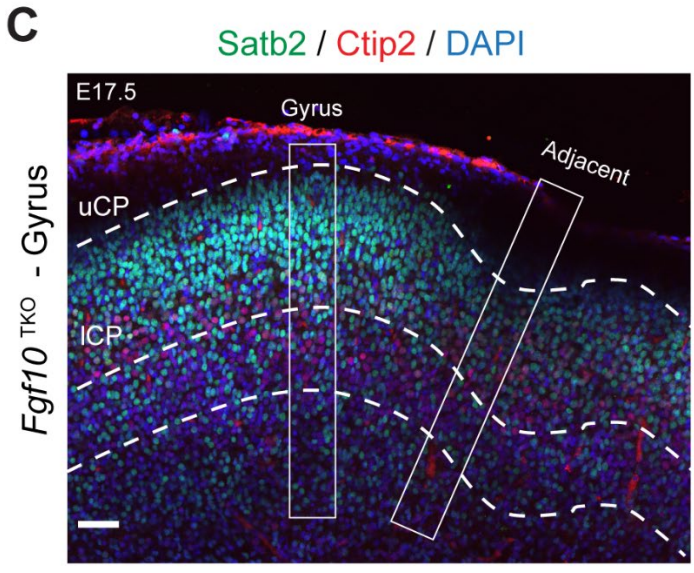
C
Satb2 / Ctip2 / DAPI
E17.5
Gyrus
Adjacent
uCP
lCP
Fgf10 TKO - Gyrus

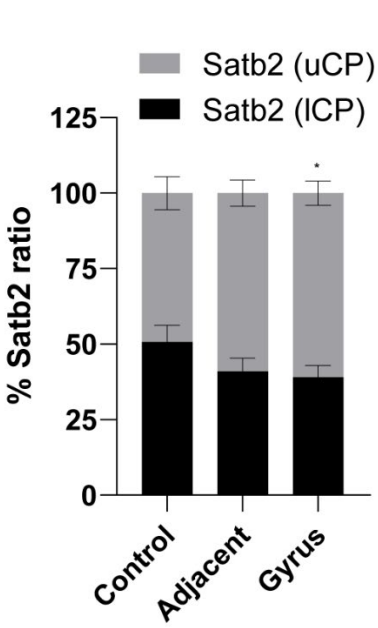
D
Satb2 (uCP)
Satb2 (lCP)
% Satb2 ratio
125
100
75
50
25
0
*
Control
Adjacent
Gyrus

Figure 3.11.1 Distribution of CP neurons in the gyrus area of *Fgf10*^{TKO} mice

(A) Coronal brain sections of *Fgf10*^{TKO} at E17.5, immunostained with Satb2, CP neuronal markers. Area in dashed rectangles in (A) are shown with higher magnification on the right. Scale bar 100 μm.

(A') Satb2+ cells distribution in A. The color bar indicates a higher (red) or lower (blue) density of Satb+ cells.

(B) Quantification of data shown in (A). Satb2+ cells were counted in sulci and adjacent and contralateral side of cortices and in littermate controls (gyrus, contralateral, control cortices n=6, adjacent cortices *n*=6). Data are shown as mean ± SEM; ***$P< 0.001$, one-way ANOVA with Tukey's post hoc analysis.

(C) Gyrus and adjacent region from an E17.5 *Fgf10*^{TKO} section immunostained with Satb2 (green), Ctip2 (red), and DAPI (blue). Scale bar 50 μm

(D) Quantification of data shown in (C). The CP was subdivided into upper and lower CP. Proportion of Satb2+cells in the upper and lowerCP, versus areas adjacent to the gyrus, and the gyrus in mutant mice and CTL (*n*=6 mice per groups). Data are shown as mean ± SEM; *$p<0.05$, two-way ANOVA with Tukey's post hoc analysis.

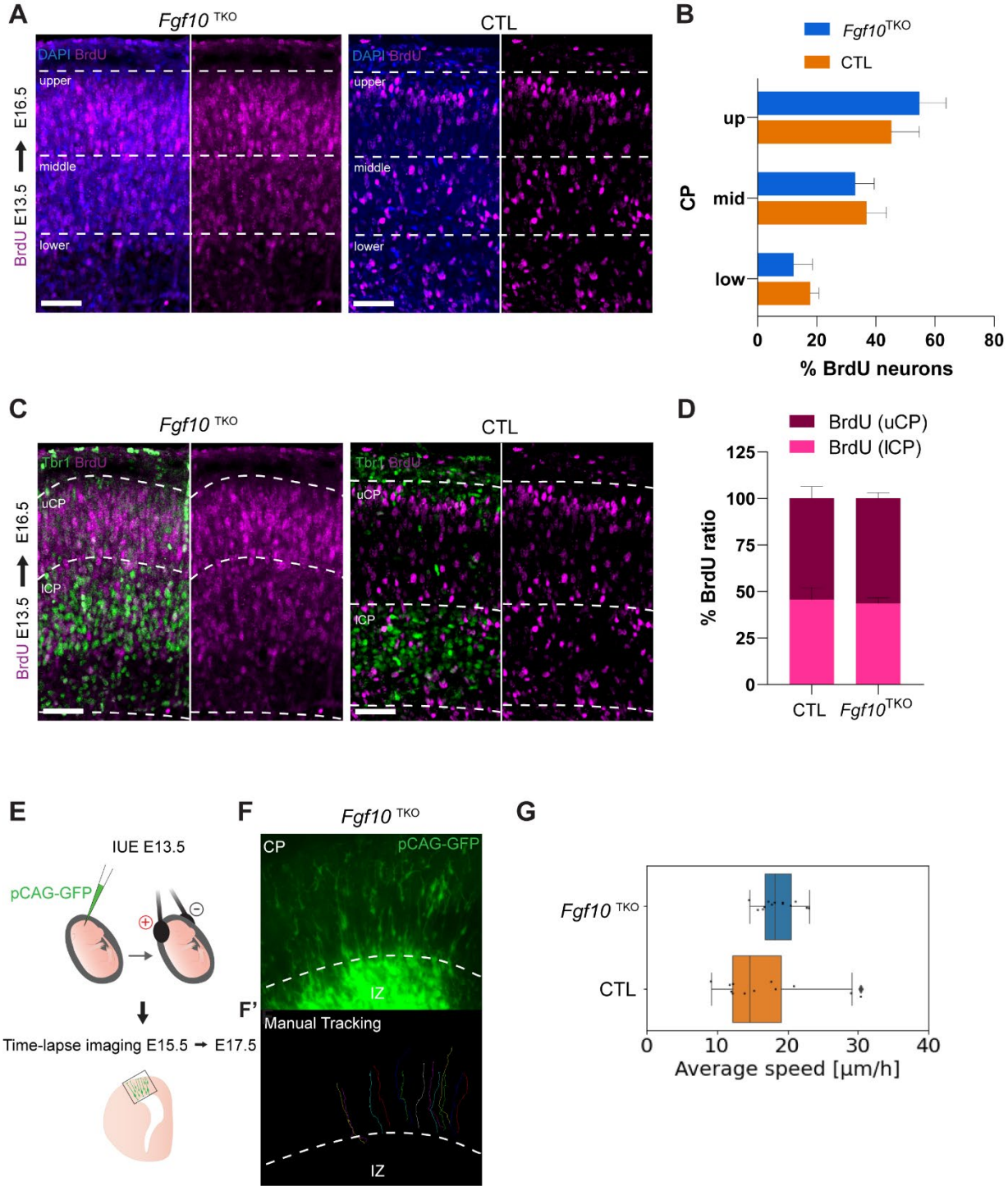
A
Fgf10 TKO
CTL
DAPI BrdU
upper
middle
lower
BrdU E13.5
E16.5
B
Fgf10TKO
CTL
up
mid
low
CP
0
20
40
60
80
% BrdU neurons
C
Fgf10 TKO
CTL
Tbr1 BrdU
uCP
lCP
D
BrdU (uCP)
BrdU (lCP)
% BrdU ratio
125
100
75
50
25
0
CTL
Fgf10TKO
E
IUE E13.5
pCAG-GFP
Time-lapse imaging E15.5 → E17.5
F
Fgf10 TKO
CP
pCAG-GFP
IZ
F'
Manual Tracking
IZ
G
Fgf10 TKO
CTL
0
10
20
30
40
Average speed [μm/h]

Figure 3.11.2 Neuronal migration in *Fgf10* ^{TKO} and CTL mice

(A) BrdU injection was performed at E13.5 and analyzed in coronal sections at E16.5. BrdU expression was confirmed by immunostaining with BrdU (magenta). The CP was subdivided into 3 bins (upper, middle, and lower), and the number of BrdU+ neurons in each bin was quantified. Scale bar 50 μm

(B) Quantification of the data shown in (B). n=3, Data are shown as mean ± SEM; no significant changes between groups, two-way ANOVA with Tukey's post hoc analysis.

(C) BrdU injection was performed at E13.5 and analyzed in coronal sections at E16.5. BrdU expression was confirmed by immunostaining with BrdU (magenta). The CP was subdivided into uCP and lCP using Tbr1, and the number of BrdU+ neurons in each layer was quantified. Scale bar 50 μm

(D) Quantification of the data shown in (C). n=3, Data are shown as mean ± SEM; no significant changes between groups, two-way ANOVA with Tukey's post hoc analysis.

(E) Schematic of *in utero* electroporation (IUE) performed at E13.5 and time-lapse imaging at E15.5 over 48 hours.

(F) Migrating GFP labelled neurons by IUE was tracked in CP

(F') Progression lines of tracked migrating neurons in (F)

(G) Quantification of the data shown in (F). The average speed of tracked neurons is shown as a whisker plot; *Fgf10*^{TKO}, n=1, CTL n=1. Data are shown as mean ± SEM.

4. DISCUSSION

In this study, we show two novel genetic mouse models that allow the study of the relative contribution of proliferation and cell migration to cortex folding. Interestingly, we discovered that different sub-types of progenitor cells induce anatomically different folding, namely sulci and gyri. Genetic ablation of *Cep83*, *Flrt1*, and *Flrt3* (referred to as *Cep83*^{TKO}) in mice favored the formation of cortical sulci. These structural changes correlated with promoting proliferation of the IP cell type, with an acceleration of migration speed of cortical neurons via divergent radial migration. Genetic ablation of *Fgf10*, *Flrt1*, and *Flrt3* (referred to as *Fgf10*^{TKO}) in mice resulted in the formation of cortical gyri, induced by promoting proliferation of early progenitor cell types, NECs and aRGCs, with faster migration of cortical neurons via radial movement.

4.1 Mechanisms of folding in *Cep83*^{TKO} mice

Cep83^{TKO} mice are a newly generated genetic mouse model that combined two essential mechanisms of cortical folding. The synergistic effects of cell proliferation and faster migration resulted in an enhanced sulci type of cortical folding in the lissencephalic mouse. The development of cortical sulci is achieved by robust formation of IPs (Tbr2+) and bRGs (Sox2+/Tbr2+) in the SVZ (Figure 3.5.2). An increased bRG population has been reported to be a key factor in the expansion of the neocortex in gyrencephalic species, both as progenitors induce abundant neurons, and as a scaffolding element leading radially migration neurons into lateral expansion (Lui et al., 2011; Borrell et al, 2012; Kelava et al., 2013; Wang et al.,2011). Moreover, in *Cep83*^{TKO} mice, an increase in number of BrdU and Ki67, while PH3 and Cyclin D1 remained unchanged (Figure 3.5.3, Cyclin D1 data not shown). These results indicate an increase in cell cycle progression in the S phase, but no

change in the G2/M phase of the cell cycle. Duration of S phase is a major target of cell cycle in neuronal progenitors of gyrencephalic ferret neocortex (Turrero García et al.,2016). In addition, cortical expansion in *Cep83*cKO mice suggests that asymmetric centrosome inheritance may affect the balance between symmetric and asymmetric division of apical progenitors as a result of an increase in the proliferative area (Pax6+ domain) as well as an increase in BrdU+ cells, indicating increased cell proliferation (Shao et al, 2020). Together, these observations support the hypothesis that increased proliferation is caused by increased IPs, bRGs, and the VZ, proliferative domain of the cortex labelled by Sox2 (Figure 3.5.2 D, D'), resulting in expansion of the proliferation in *Cep83*^{TKO} mice. IPs, also known as BPs, play a key role in generating cortical neurons (Sun et al.,2014). A higher proportion of cells in the S phase then leads to a more abundant neuronal population at a later time point in the CP (Figure 3.6.1 D and Figure 3.6.2 B,D). Further, Satb2+ neurons in the CP were increased in the sulcus area of *Cep83*^{TKO} mice (Figure 3.6.1 D). Consequently *Cep83*^{TKO} mice exhibited an enlarged cortical size (Figure 3.5.1).

Favoring the idea of neurogenesis resulting from bRGs, abundant proliferation of bRGs provides more radial fibers for the scaffold in a basally enlarged fan-like manner, thus inducing divergence of cortical radial migration, which leads to the tangential growth of the cortical surface and thus, folding (Stahl et al., 2013). Accordingly, cortical neurons ablated in *Cep83*^{TKO} mice migrate toward the uCP faster (Figure 3.6.2 B,D), in a similar manner to *Flrt1/3*DKO mice. This is caused by a lower intercellular adhesion between radial fibers and cortical neurons (Del Toro et al., 2017), resulting in homogeneously distributed CP neurons in the sulcus (Figure 3.6.1 A,A',B). Notably, reducing the speed of uCP neurons makes the sulcus shallower in ferrets (Shinmyo et al, 2017), further supporting our result that faster migration of cortical neurons drives enhanced sulci folding in *Cep83*^{TKO}. These significant findings strongly suggest that ablation of *Cep83* results in the expansion of cortical progenitors leading to an increased number of bRGs and upper cortical neurons. Given that these neurons lack *Flrt1* and *Flrt3*, their average speed is increased due to reduced adhesion, which also favors their tangential distribution across

the radial fibers or bRGs. This results in a larger proportion of neurons populating the uCP, favoring the formation of sulci.

4.2 Mechanisms of folding in *Fgf10*^{TKO} mice

In *Fgf10*^{TKO} mice, we showed that combining two essential mechanisms of cortical folding, cell proliferation and faster migration, induced synergistic effects that led to an enhanced gyri type of cortical folding in the lissencephalic mouse. The development of cortical gyri was driven by an increase in early progenitors, namely NECs and aRGCs, accompanied by apical mitotic division in the apical VZ (Figure 3.10.2 A,B, C). Ablation of *Fgf10* delayed RG differentiation, initially increasing self-amplifying NECs, followed by a diminished neuronal population and BPs. However, eventually the abundant NECs differentiate into RG cells, resulting in an overproduction of neurons and BPs, which leads to tangential growth of frontal areas (Sahara et al., 2009). Moreover, there is a trend of increased BrdU+ and VZ, proliferative domain of the cortex labelled by Sox2 in *Fgf10*^{TKO} mice as compared to CTLs, suggesting an increase in cell proliferation (Figure 3.10.2 B,D and Figure 3.10.3), with a resulting increase in cortical size (Figure 3.10.1 B) and in the CP neuronal pool at a later time point (Figure 3.11.1).

Intriguingly, mice with triple ablation of *Fgf10/Flrt1/3* exhibit gyri type folding in the rostral region (Figure 3.9 C and Figure 3.11.1 C). This result strongly supports the previously described transient expression of Fgf10 in the rostral cortex (Sahara et al., 2009). Distinct time (E8.5-E11.5) and localization (apical VZ) of the expression pattern of Fgf10 strongly suggests that the dramatic effect of removal of Fgf10 could be due to its early expression during neurogenesis. Therefore, aRGCs or the NEC marker, Sox2+ was markedly increased in E11.5, but at later time points, E13.5 and E15.5, it remained unchanged in the neocortex between triple ablation of *Fgf10/Flrt1/3* and littermate CTLs (data not shown). Thus, subsequent BrdU short pulse analysis of cell cycle progression in

E9.5 or E10.5 would be critical to have more direct evidence of progenitor expansion in the *Fgf10*^{TKO} mice.

In favor of increased neurogenesis by apical mitotic event regulated by NECs and aRGCs, I found a notably dense populated Satb2+ CP neurons in gyri, or the protrusion area (Figure 3.11.1 A,A',D). This result suggests that regulation of differentiation of NECs, a founder progenitor, induces massive generation of the neuronal pool among progenitors. This dramatic increases in cortical neurons in *Fgf10*^{TKO} mice migrates toward uCP faster (Figure 3.11.2), suggesting their underlying migration mechanism is affected by removal of *Flrt1/3*, reducing intercellular adhesion between radial fibers and migrating neurons (del Toro et al., 2017). However, unaltered bRGs in the *Fgf10*^{TKO} mice (Figure 3.10.2 B) indicate that their migratory trajectory has a rather rigid movement compared to the *Cep83*^{TKO} mice. In addition, the gradient expression pattern of Flrt3 along the rostro-caudal axis of the neocortex is low-rostral/high-caudal (see 4.7 graphical summary), suggesting less impact of Flrt3 in neuronal migration in *Fgf10*^{TKO} mice, resulting in highly dense CP neurons in the rostral region only. Therefore, reduced levels of Flrt3 may cause migrating neurons to be, by default, less keen to switch to different radial fibers during movement, which can lead to a relatively narrow migratory path. Their migration path is rather narrow, meaning a massive number of neurons are driven by early apical progenitors that would concentrate in a rather limited area causing the formation of gyri. Together, our findings suggest that the formation of gyri in the rostral region of *Fgf10*^{TKO} mice occurs in dual modes that is causally linked by two essential mechanisms: neurogenesis regulated by early progenitor subtypes, NECs and aRGCs; and the rather narrow fan-like radial trajectory of neuronal migration coupled with faster speed of migration.

In *Fgf10*^{TKO} mice, although gyri formation is induced by the early apical progenitors, NECs and aRGs, it has been previously shown in the gyrencephalic ferret that cortical regions with abundant BPs are more likely to develop into a gyrus than regions with fewer BPs (de Juan Romero et al., 2015, Reillo et al., 2011). Ectopic expansion of the BP pool in the ferret generates additional gyri (Masuda et al., 2015, Nonaka-Kinoshita et al., 2013),

and its reduction has a stronger effect on cortical layering of gyri than sulci (Toda et al., 2016). In addition, in *SmoM2* mice mutant, increased number of IPs and bRGs induces sulci formation and cortex folding in the cingulate cortex (Wang et al., 2016). This suggests that different animal models exhibit distinct folding patterns, whether characterized by sulci or gyri, which are initially associated with increased proliferation. Additionally, these models require enhanced migration rates to promote the occurrence of folding within the CP layer. Similarly, in mice where Trnp1 is knocked out using short hairpin RNA (shRNA), cortical folds are observed, although the specific distinction between sulci and gyri in their phenotype was not made (Stahl et al., 2013). This study indicated that both increased proliferation and migration speed are crucial factors for inducing cortical folds *in vivo*, emphasizing the significance of the interplay between progenitor expansion and migration in the process.

4.3 Variability of the folding phenotype

Cortical folding is based on a three-dimensional structure, and cortical folding patterns vary across individuals and species, resulting in a unique arrangement of gyri and sulci. Therefore, analyzing folds requires several different kinds of method, such as measuring the degree of folds (GI values), and visualization of cortical folding, all of which were used in this study. In particular, 3D imaging of TKO brains gave a valuable insight to be able to visualize and understand *Cep38*^{TKO} and *Fgf10*^{TKO} brains with regard to many factors, including the degree of waviness in sulci and gyri, the location of folds, and cortical layering information with whole brain staining method. However, the process of 3D imaging is time-consuming, and acquiring a sufficient sample size for each analysis presents practical challenges. Therefore, in addition to 3D visualization, most of the analyses in this study were conducted on 2D coronal sections of each TKO cortex. These

2D sections enable the study of neuronal progenitor cell growth, organization, and neuronal movements.

Furthermore, it is worth noting that the penetrance of folding varied among different genotypes within the control group. In the case of both the *Cep83*cKO and *Fgf10*cKO, I observed a lower penetrance of folding and minimal waviness (GI value close to 1.00) in the wild-type (WT) control group. The WT control group consists of littermates that do not express the Cre recombinase, serving as a control for the cKO lines. The breeding strategy for the cKO lines involved ensuring that one parent carries both the Cre and lox alleles on one side, increased the chance of obtaining the desired genotypes in the embryos. Therefore, possibly germ line recombination occurs, thus it affected to penetrance of folding in WT control. Moreover, I observed varying penetrance of the phenotype in *Flrt1/3*DKO and *Cep83*^{TKO} mice, depending on their different genetic backgrounds. Initially, when the *Flrt1/3*DKO mice were generated, they were bred in a mixed BL6-SVJ129 background. However, over time, the genetic background of these mice shifted to a BL6 background, which is the in-breeding mouse background used in our institution's animal facility. This change in genetic background can also be observed through differences in fur color, as the mice that were originally maintained using mainly agouti (brown-colored) mice now predominantly exhibit black fur, indicating a shift in genetic background. Remarkably, the black fur mice, which represent the altered genetic background, exhibit a lower penetrance of folding in both *Flrt1/3* DKO and *Cep83*^{TKO} mice, accompanied by smaller folds (data not shown). The influence of genetic background on a variety of phenotypes in genetically engineered mice has been reported previously in several studies (Doetschman 2009; Linder 2006; Xavier 2000).

Moreover, the variation in penetrance and phenotype of cortical folding in *Flrt1/3*DKO mice and *Cep83*^{TKO} mice can be attributed to the use of different Cre lines, as each Cre line has different activation times and affects different locations. Originally, *Flrt1/3*DKO mice were generated using Nestin-Cre, which resulted in approximately 30% penetrance of folding, with varying degrees of folds in one hemisphere of the brain.

However, it was necessary to cross the *Flrt1/3*DKO mice with Emx1-Cre and Foxg1-Cre, respectively, to achieve the optimal combination for removing the three genes (*Flrt1/3* and *Cep83* or *Fgf10*) and inducing folding. Interestingly, in *Flrt1/3*DKO mice, earlier activation of Cre and a more locally concentrated activation area of Cre in the cortex or frontal cortex (such as with Emx1-Cre and Foxg1-Cre) resulted in a lower penetrance of folding (around 15-20%), with relatively smaller folds compared to Nestin-Cre;*Flrt1/3*DKO mice. This suggests that different Cre activation timings may influence cortical fold development in terms of penetrance and phenotype. It is possible that the differences observed in cortical folds between *Cep83*^{TKO} and *Fgf10*^{TKO} mice may also be influenced by different Cre activations. To observe the confounding factor of Cre activation, future studies could involve characterizing the Foxg1-Cre;*Cep83*^{TKO} line and comparing it to the Emx1-Cre;Cep83^{TKO} line to determine the sole effect of the genetic manipulation of *Cep83* with different Cre activation on the folding phenotype and penetrance.

4.4 FLRT interaction with Cep83 and Fgf10

The FLRT family of proteins, characterized by leucine-rich repeat (LRR) motifs, has been implicated in various biological processes such as FGF signaling, early embryonic development, and neurite outgrowth. Experimental evidence suggests that FLRT proteins can undergo physical interactions, as demonstrated by the observation that FLRT-transfected cells in culture exhibit a distinct sorting behavior from non-transfected cells, indicating changes in adhesive properties (Karaulanov et al., 2006). A similar sorting effect has also been observed in Xenopus embryos and tissue aggregates (Böttcher et al., 2004). However, it is important to note that Xenopus lack a cortex, and there have been no studies demonstrating the physical interaction between FLRTs and FGFs *in vivo.* Furthermore, no evidence has been found to support an interaction between Cep83 and the FLRT family. Their distinct subcellular localizations make it highly unlikely for a physical interaction to

occur. Cep83 is primarily expressed in the centrosome, while FLRTs are localized on the cell surface membrane (Haines et al., 2006). To investigate whether FLRTs interact with Cep83 or Fgf10 proteins, immunostaining techniques using specific antibodies, as well as ISH, would need to be conducted. These methods would enable the visualization of any potential physical interaction between FLRTs and Cep83 or Fgf10 proteins *in vivo*.

4.5 Divergent cell migration in *Cep83* ^{TKO} and *Fgf10* ^{TKO} mice

To investigate the migration of cortical neurons in *Cep83*^{TKO} and *Fgf10*^{TKO} mice, two different methods, BrdU labeling and time-lapse imaging, were used. However, our data thus far have provided only partial success in obtaining a conclusive interpretation.

Initially, we aimed to discover direct evidence of neuronal speed and movement by conducting time-lapse imaging movies. However, we encountered technical challenges and limitations with this approach. To perform time-lapse imaging experiments, we first performed IUE in the specific region of the TKO cortex. However, since the genotype of the embryos was not known at the time of surgery and sectioning of these IUE embryos, the brain slices that were cultured for imaging had to be transferred and kept in a restricted area on a filter in a petri dish. Genotypes were only determined after all steps in the experiment were completed, including imaging, which necessitated re-collection of brain tissues from the slices for PCR analysis.

Moreover, the confocal microscope used for imaging is an inverted microscope, which allowed imaging in a small-sized petri dish. If the microscope lens had been located below the stage, a multi-well plate could have been used for imaging, enabling the imaging of multiple sections simultaneously. Additionally, during the two-day imaging process, tissue outgrowth caused changes in the microscope's focus. Unfortunately, the microscope

lacked an auto-focusing function, resulting in videos often going out of focus. Consequently, the combination of these limitations and challenges resulted in a low sample size for speed analysis, and I was unable to obtain high-quality videos that accurately captured neuronal movements.

Therefore, to obtain more indirect evidence of neuronal movement and speed, I administered BrdU to *Cep83*^{TKO} and *Fgf10*^{TKO} at E13 and collected their brains at E16. This approach allowed for the indirect assessment of neuronal speed by indicating possible variations in the number of neurons in different CP locations, such as the upper/middle/lower CP.

4.6 Mechanical aspects of cortical folding

There are currently multiple theories regarding the formation of cortical folds, ranging from mechanical to genetic explanations (Kroenke and Bayly, 2018). Folding of the human neocortex is believed to be governed by a complex interplay of genetic and mechanical factors, where both aspects interact and modulate each other. Therefore, many genetic studies, including our mice models, have showed that manipulating individual genes, such as Trnp1 and Arhgap11, can induce folding in mice (Stahl et al., 2013; Florio et al., 2015). However, in our models, the mechanical aspect of cortical folds were not fully considered as a modulator that can affect our folding phenotype. From a mechanical perspective, non-uniform tangential basal expansion during neocortical development has been proposed as a mechanism for folding (Tallinen et al., 2016; Florio et al., 2015). Further, regulation of the extracellular matrix (ECM), which causes changes in ECM stiffness has been found to induce and modify the initial folding stage. Previously, it has been reported that the young's modulus (elastic modulus) was significantly higher in the apical membrane in the cortex of *Cep83*cKO mice than in WT mice. This indicates stiffness of cortex tissue may have a role in cortical expansion and folding (Shao et al., 2020).

Furthermore, in human embryo slices, sulci are softer which can be link where reduced intracellular adhesion between neurons lead to sulcus formation in *Flrt1/3*DKO mice (Long et al., 2018; Del Toro et al., 2017). In addition, their gyrus area are stiffer which becomes more evident in later stages. This is in line with the finding that increased density of Satb2+ cells in the CP which I saw in *Fgf10*^{TKO} mice (Figure 3.11.1) (Long et al., 2018).

4.7 Graphical summary: mechanism of folding in *Cep83* ^{TKO} and *Fgf10* ^{TKO} mice

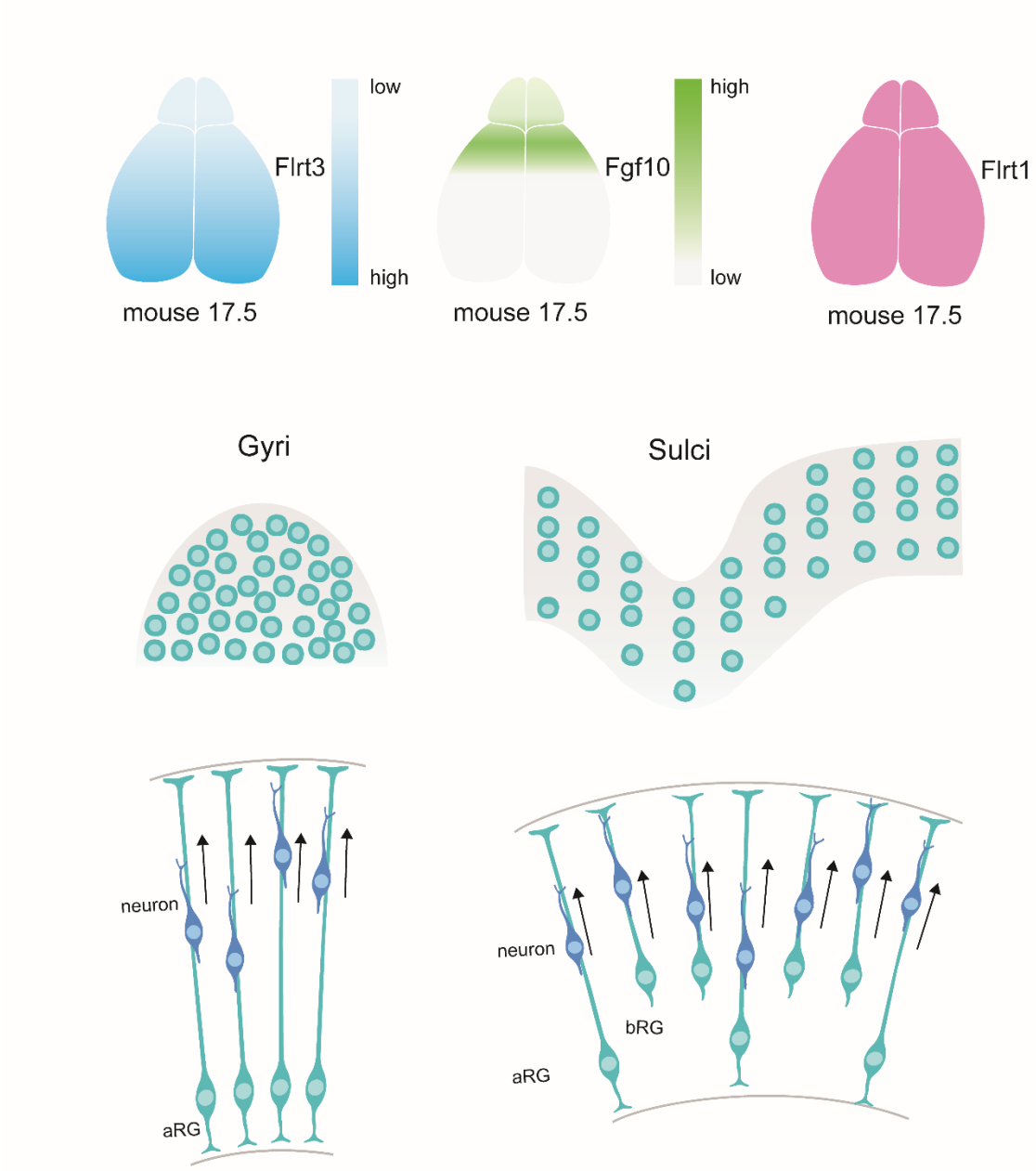

4.8 Future directions

Cortical folding occurs at multiple scales, from molecular and cellular processes to tissue mechanics, and brain-scale dynamics. Future studies could include developing multi-scale computational models that integrate data from various levels, such as molecular signaling pathways, cellular behaviors, and tissue mechanics to gain a more comprehensive understanding of how these different levels interact and contribute to cortical folding. Therefore, it would be interesting if the creation of our two new biological mouse models, *Cep83*^{TKO} and *Fgf10*^{TKO} is recapitulated by computational modeling. This would provide an overall supportive insight into the underlying mechanisms of structurally different cortical folding in the two genetic mouse models. Moreover, cortical folding is not only a structural feature but also has functional implications. Future studies that aim to elucidate the relationship between cortical folding patterns and functional connectivity, and cognitive functions in the brain through animal behavior studies should be further investigated. These would explain the functional aspects of cortical folding in brain network organization, synaptic connectivity, and neuronal activity. Furthermore, transcriptomic studies would give an insight into comparison studies between species, mainly gyrencephalic and lissencephalic. By analyzing gene expression data across species, and identifying molecular features associated with the specific phenotype (sulci and gyri) of cortical folding, further information into the genetic and molecular mechanisms that underlie the unique cortical folding patterns in our mouse models would be revealed. It is intriguing to note that in the gyrencephalic marmoset, an evolutionary perspective reveals the presence of sulci in their cortex but the absence of proper gyri. This observation suggests that the mechanisms underlying gyrus and sulcus formation may differ. Thus, conducting transcriptomic studies comparing *Cep83*^{TKO} mice and *Fgf10*^{TKO} mice, or examining the differences between sulci and gyri in each mouse line, would provide valuable insights into the underlying mechanisms involved in the development of sulci and gyri.

REFERENCES

Abdollahi MR, Morrison E, Sirey T, Molnar Z, Hayward BE, Carr IM, Springell K, Woods CG, Ahmed M, Hattingh L, Corry P, Pilz DT, Stoodley N, Crow Y, Taylor GR, Bonthron DT, Sheridan E (2009) Mutation of the variant alpha-tubulin TUBA8 results in polymicrogyria with optic nerve hypoplasia. *Am J Hum Genet* 85: 737–744.

Adachi Y, Poduri A, Kawaguch A, Yoon G, Salih MA, Yamashita F, Walsh CA, Barkovich AJ (2011) Congenital microcephaly with a simplified gyral pattern: associated findings and their significance. *AJNR Am J Neuroradiol* 32: 1123–1129.

Agirman G, Broix L, Nguyen L. Cerebral cortex development: an outside-in perspective. *FEBS Lett.* 2017 Dec;591(24):3978-3992.

Albert M, Huttner WB. Clever space saving—how the cerebral cortex folds. *EMBO J*. 2015 Jul 14;34(14):1845-7.

Alkuraya FS, Cai X, Emery C, Mochida GH, Al-Dosari MS, Felie JM, Hill RS, Barry BJ, Partlow JN, Gascon GG, Kentab A, Jan M, Shaheen R, Feng Y, Walsh CA (2011) Human mutations in NDE1 cause extreme microcephaly with lissencephaly *Am J Hum Genet* 88: 536–547.

Arai Y, Taverna E. Neural Progenitor Cell Polarity and Cortical Development. Front Cell

Neurosci. 2017 Dec 5;11:384.

Attardo A, Calegari F, Haubensak W, Wilsch-Bräuninger M, Huttner WB. Live imaging at the onset of cortical neurogenesis reveals differential appearance of the neuronal phenotype in apical versus basal progenitor progeny. *PLoS One*. 2008 Jun 11;3(6):e2388.

Azzarelli R, Guillemot F, Pacary E. Function and regulation of Rnd proteins in cortical projection neuron migration. *Front Neurosci*. 2015 Feb 6;9:19.

Barkovich AJ, Guerrini R, Kuzniecky RI, Jackson GD, Dobyns WB. A developmental and genetic classification for malformations of cortical development: update 2012. *Brain*. 2012 May;135(Pt 5):1348-69.

Betizeau M, Cortay V, Patti D, Pfister S, Gautier E, Bellemin-Ménard A, Afanassieff M, Huissoud C, Douglas RJ, Kennedy H, Dehay C. Precursor diversity and complexity of lineage relationships in the outer subventricular zone of the primate. *Neuron*. 2013 Oct 16;80(2):442-57.

Bhat V, Girimaji SC, Mohan G, Arvinda HR, Singhmar P, Duvvari MR, Kumar A (2011) Mutations in WDR62, encoding a centrosomal and nuclear protein, in Indian primary microcephaly families with cortical malformations. *Clin Genet* 80: 532–540.

Bilguvar K, Ozturk AK, Louvi A, Kwan KY, Choi M, Tatli B, Yalnizoglu D, Tuysuz B, Caglayan AO, Gokben S, Kaymakcalan H, Barak T, Bakircioglu M, Yasuno K, Ho

W, Sanders S, Zhu Y, Yilmaz S, Dincer A, Johnson MH et al (2010) Whole-exome sequencing identifies recessive WDR62 mutations in severe brain malformations. *Nature* 467: 207–210.

Boland E, Clayton-Smith J, Woo VG, McKee S, Manson FD, Medne L, Zackai E, Swanson EA, Fitzpatrick D, Millen KJ, Sherr EH, Dobyns WB, Black GC (2007) Mapping of deletion and translocation breakpoints in 1q44 implicates the serine/threonine kinase AKT3 in postnatal microcephaly and agenesis of the corpus callosum. *Am J Hum Genet* 81: 292–303.

Bond J, Roberts E, Mochida GH, Hampshire DJ, Scott S, Askham JM, Springell K, Mahadevan M, Crow YJ, Markham AF, Walsh CA, Woods CG (2002) ASPM is a major determinant of cerebral cortical size. *Nat Genet* 32: 316–320.

Borello U, Cobos I, Long JE, McWhirter JR, Murre C, Rubenstein JL. FGF15 promotes neurogenesis and opposes FGF8 function during neocortical development. *Neural Dev*. 2008;3:17.

Borrell V, Reillo I. Emerging roles of neural stem cells in cerebral cortex development and evolution. *Dev Neurobiol*. 2012 Jul;72(7):955-71.

Borrell V. How Cells Fold the Cerebral Cortex. *J Neurosci*. 2018 Jan 24;38(4):776-783.

Borrell V, Götz M. Role of radial glial cells in cerebral cortex folding. *Curr Opin Neurobiol.* 2014 Aug;27:39-46.

Bottcher RT, Pollet N, Delius H, and Niehrs C. The transmembrane protein xflrt3

forms a complex with fgf receptors and promotes fgf signalling. *Nature cell biology*, 6(1):38, 2004.

Böttcher, R., Pollet, N., Delius, H. et al. The transmembrane protein XFLRT3 forms a complex with FGF receptors and promotes FGF signalling. *Nat Cell Biol* 6, 38–44 (2004).

Bouchet C, Vuillaumier-Barrot S, Gonzales M, Boukari S, Bizec CL, Fallet C, Delezoide AL, Moirot H, Laquerriere A, Encha-Razavi F, Durand G, Seta N. Detection of an Alu insertion in the POMT1 gene from three French Walker Warburg syndrome families. *Mol Genet Metab*. 2007 Jan;90(1):93-6.

Bouchet C, Gonzales M, Vuillaumier-Barrot S, Devisme L, Lebizec C, Alanio E, Bazin A, Bessières-Grattagliano B, Bigi N, Blanchet P, Bonneau D, Bonnières M, Carles D, Delahaye S, Fallet-Bianco C, Figarella-Branger D, Gaillard D, Gasser B, Guimiot F, Joubert M, Laurent N, Liprandi A, Loget P, Marcorelles P, Martinovic J, Menez F, Patrier S, Pelluard-Nehmé F, Perez MJ, Rouleau-Dubois C, Triau S, Laquerrière A, Encha-Razavi F, Seta N. Molecular heterogeneity in fetal forms of type II lissencephaly. *Hum Mutat*. 2007 Oct;28(10):1020-7.

Cadwell CR, Bhaduri A, Mostajo-Radji MA, Keefe MG, Nowakowski TJ. Development and Arealization of the Cerebral Cortex. *Neuron*. 2019 Sep 25;103(6):980-1004.

Camargo Ortega G, Falk S, Johansson PA, Peyre E, Broix L, Sahu SK, Hirst W, Schlichthaerle T, De Juan Romero C, Draganova K, Vinopal S, Chinnappa K, Gavranovic A, Karakaya T, Steininger T, Merl-Pham J, Feederle R, Shao W, Shi

SH, Hauck SM, Jungmann R, Bradke F, Borrell V, Geerlof A, Reber S, Tiwari VK, Huttner WB, Wilsch-Bräuninger M, Nguyen L, Götz M. The centrosome protein AKNA regulates neurogenesis via microtubule organization. *Nature*. 2019 Mar;567(7746):113-117.

Cárdenas A, Villalba A, de Juan Romero C, Picó E, Kyrousi C, Tzika AC, Tessier-Lavigne M, Ma L, Drukker M, Cappello S, Borrell V. Evolution of Cortical Neurogenesis in Amniotes Controlled by Robo Signaling Levels. *Cell*. 2018 Jul 26;174(3):590-606.e21.

Cholfin JA, Rubenstein JL. Patterning of frontal cortex subdivisions by Fgf17. *Proc Natl Acad Sci U S A*. 2007;104:7652–7657.

Cooper, J. A. (2013). Mechanisms of cell migration in the nervous system. *J. Cell Biol* . 202, 725–734.

De Juan Romero C, Borrell V. Coevolution of radial glial cells and the cerebral cortex. Glia. 2015 Aug;63(8):1303-19. doi: 10.1002/glia.22827. Epub 2015 Mar 23.

Del Toro D, Ruff T, Cederfjäll E, Villalba A, Seyit-Bremer G, Borrell V, Klein R. Regulation of Cerebral Cortex Folding by Controlling Neuronal Migration via FLRT Adhesion Molecules. *Cell*. 2017 May 4;169(4):621-635.e16.

Del Toro D, Carrasquero-Ordaz MA, Chu A, Ruff T, Shahin M, Jackson VA, Chavent M, Berbeira-Santana M, Seyit-Bremer G, Brignani S, Kaufmann R, Lowe E, Klein R, Seiradake E. Structural Basis of Teneurin-Latrophilin Interaction in Repulsive

Guidance of Migrating Neurons. *Cell.* 2020 Jan 23;180(2):323-339.

Desir J, Cassart M, David P, Van Bogaert P, Abramowicz M (2008) Primary microcephaly with ASPM mutation shows simplified cortical gyration with antero-posterior gradient pre- and post-natally. *Am J Med Genet* A 146A: 1439–1443.

Doetschman T. Influence of genetic background on genetically engineered mouse phenotypes. Methods Mol Biol. 2009;530:423-33.

Dulabon L, Olson EC, Taglienti MG, Eisenhuth S, McGrath B, Walsh CA, Kreidberg JA, Anton ES (2000) Reelin binds alpha3beta1 integrin and inhibits neuronal migration. *Neuron* 27: 33–44.

Egea J, Erlacher C, Montanez E, Burtscher I, Yamagishi S, Hess M, Hampel F, Sanchez R, Rodriguez-Manzaneque MT, Bösl MR, Fässler R, Lickert H, Klein R. Genetic ablation of FLRT3 reveals a novel morphogenetic function for the anterior visceral endoderm in suppressing mesoderm differentiation. *Genes Dev.* 2008 Dec. 1;22(23):3349-62

Farkas LM, Huttner WB. The cell biology of neural stem and progenitor cells and its significance for their proliferation versus differentiation during mammalian brain development. *Curr Opin Cell Biol*. 2008 Dec;20(6):707-15.

Feng Y, Walsh CA (2004) The many faces of filamin: a versatile molecular scaffold for cell motility and signalling. *Nat Cell Biol* 6: 1034–1038

Fernández V, Llinares-Benadero C, Borrell V, Cerebral cortex expansion and folding

: what have we learned? *The EMBO Journal* 35, 1021-1044 (2016).

Florio M, Albert M, Taverna E, Namba T, Brandl H, Lewitus E, Haffner C, Sykes A, Wong FK, Peters J, Guhr E, Klemroth S, Prüfer K, Kelso J, Naumann R, Nüsslein I, Dahl A, Lachmann R, Pääbo S, Huttner WB. Human-specific gene ARHGAP11B promotes basal progenitor amplification and neocortex expansion. *Science.* 2015 Mar 27;347(6229):1465-70.

Fukuchi-Shimogori T, Grove EA. Neocortex patterning by the secreted signaling molecule FGF8. *Science*. 2001;294:1071–1074.

Gao, P., Sultan, K. T., Zhang, X. J. & Shi, S. H. Lineage-dependent circuit assembly in the neocortex. *Development* 140, 2645–2655 (2013).

Garcia KE, Kroenke CD, Bayly PV. Mechanics of cortical folding: stress, growth and stability. *Philos Trans R Soc Lond B Biol Sci*. 2018 Sep 24;373(1759).

Garel S, Huffman KJ, Rubenstein JL. Molecular regionalization of the neocortex is disrupted in Fgf8 hypomorphic mutants. *Development*. 2003;130:1903–1914.

Gertz CC, Kriegstein AR. Neuronal Migration Dynamics in the Developing Ferret Cortex. *J Neurosci*. 2015 Oct 21;35(42):14307-15.Gilmore EC, Herrup K. Cortical development: layers of complexity. *Curr Biol*. 1997 Apr1;7(4):R231-4.

Gilmore EC, Walsh CA (2013) Genetic causes of microcephaly and lessons for neuronal d evelopment. *Wiley Interdiscip Rev Dev Biol* 2: 461–478.

Gleeson, J. G., Allen, K. M., Fox, J. W., Lamperti, E. D., Berkovic, S., Scheffer, I.,et al.

(1998). Doublecortin, a brain-specific gene mutated in human X-linkedlissencephaly and double cortex syndrome, encodes a putative signaling protein. *Cell* 92, 63–72.

Gorski JA, Talley T, Qiu M, Puelles L, Rubenstein JL, Jones KR. Cortical excitatory neurons and glia, but not GABAergic neurons, are produced in the Emx1-expressing lineage. *J Neurosci.* 2002 Aug 1;22(15):6309-14.

Götz M, Huttner WB, The cell biology of neurogenesis. *Nature Reviews Molecular Cell Biology* 6, 777 (2005).

Gressens P. Mechanisms and disturbances of neuronal migration. *Pediatr Res*. 2000 Dec;48(6):725-30.

Haines BP, Wheldon LM, Summerbell D, Heath JK, Rigby PW. Regulated expression of FLRT genes implies a functional role in the regulation of FGF signalling during mouse development. *Dev Biol.* 2006 Sep 1;297(1):14-25.

Hatanaka Y, Zhu Y, Torigoe M, Kita Y, Murakami F. From migration to settlement: the pathways, migration modes and dynamics of neurons in the developing brain. *Proc Jpn Acad Ser B Phys Biol Sci.* 2016;92(1):1-19.

Hébert JM, Fishell G. The genetics of early telencephalon patterning: some assembly required. *Nat Rev Neurosci*. 2008;9:678–685.

Homem CC, Knoblich JA. Drosophila neuroblasts: a model for stem cell biology. *Development*. 2012 Dec 1;139(23):4297-310.

Hong SE, Shugart YY, Huang DT, Shahwan SA, Grant PE, Hourihane JO, Martin ND,

Walsh CA (2000) Autosomal recessive lissencephaly with cerebellar hypoplasia is associated with human RELN mutations. *Nat Genet* 26: 93–96.

Ishikawa Y, Yamamoto N, Yoshimoto M, Ito H. The primary brain vesicles revisited: are the three primary vesicles (forebrain/midbrain/hindbrain) universal in vertebrates? *Brain Behav Evol.* 2012;79(2):75-83.

Itoh N and Ornitz DM. Fibroblast growth factors: from molecular evolution to roles in development, metabolism and disease. *The Journal of Biochemistry*, 149(2):121–130, 2011.

Jackson, V. A.; del Toro, D.; Carrasquero, M.; Roversi, P.; Harlos, K.; Klein, R.; Seiradake, E.: Structural basis of latrophilin-FLRT interaction. *Structure* 23 (4), pp. 774 - 781 (2015).

Jaglin XH, Chelly J (2009) Tubulin-related cortical dysgeneses: microtubule dysfunction underlying neuronal migration defects. *Trends Genet* 25: 555–566.

Jansen AC, Oostra A, Desprechins B, De Vlaeminck Y, Verhelst H, Regal L, Verloo P, Bockaert N, Keymolen K, Seneca S, De Meirleir L, Lissens W (2011) TUBA1A mutations: from isolated lissencephaly to familial polymicrogyria. *Neurology* 76: 988–992.

Jayaraman, D., Bae, B.-I., and Walsh, C. A. (2018). The genetics of primary microcephaly. Annu. Rev. *Genomics Hum. Genet*. 19, 177–200.

Joo K et al., CCDC41 is required for ciliary vesicle docking to the mother centriole. *Proc*

Natl Acad Sci U S A 110, 5987-5992 (2013).

Ju XC, Hou QQ, Sheng AL, Wu KY, Zhou Y, Jin Y, Wen T, Yang Z, Wang X, Luo ZG. The hominoid-specific gene TBC1D3 promotes generation of basal neural progenitors and induces cortical folding in mice. *Elife*. 2016 Aug 9;5:e18197.

Kang W, Wong LC, Shi SH, Hébert JM. The Transition from Radial Glial to Intermediate Progenitor Cell Is Inhibited by FGF Signaling during Corticogenesis. *J Neurosci*. 2009;29:14571–14580.

Karaulanov E., Böttcher R.T., Stannek P., Wu W., Rau M., Ogata S., Cho K.W.Y., Niehrs C. Unc5B interacts with FLRT3 and Rnd1 to modulate cell adhesion in Xenopus embryos. *PLoS ONE*. 2009;4:e5742.

Karaulanov E, Böttcher R.T, Niehrs C. A role for fibronectin-leucine-rich transmembrane cell-surface proteins in homotypic cell adhesion. *EMBO Rep*. 2006 Mar;7(3):283-90.

Kawaguchi D, Sahara S, Zembrzycki A, O'Leary DDM. Generation and analysis of an improved Foxg1-IRES-Cre driver mouse line. *Dev Biol*. 2016 Apr 1;412(1):139-147.

Kelava I, Lewitus E, Huttner WB. The secondary loss of gyrencephaly as an example of evolutionary phenotypical reversal. *Front Neuroanat*. 2013 Jun 26;7:16.

Kobayashi, T., Kim, S., Lin, Y. C., Inoue, T., and Dynlacht, B. D. (2014). The CP110-interacting proteins Talpid3 and Cep290 play overlapping and distinct roles in cilia assembly. *J. Cell. Biol.* 204, 215–229.

Kornack DR, Rakic P (1995) Radial and horizontal deployment of clonally related cells in the primate neocortex: relationship to distinct mitotic lineages. *Neuron* 15:311–321.

Kosodo Y, Suetsugu T, Suda M, Mimori-Kiyosue Y, Toida K, Baba SA, Kimura A, Matsuzaki F. Regulation of interkinetic nuclear migration by cell cycle-coupled active and passive mechanisms in the developing brain. *EMBO* J. 2011 May 4;30(9):1690-704.

Kowalczyk T, Pontious A, Englund C, Daza RA, Bedogni F, Hodge R, Attardo A, Bell C, Huttner WB, Hevner RF. Intermediate neuronal progenitors (basal progenitors) produce pyramidal-projection neurons for all layers of cerebral cortex. *Cereb Cortex.* 2009 Oct;19(10):2439-50.

Kriegstein A, Parnavelas JG. Changing concepts of cortical development. *Cereb Cortex*. 2003 Jun;13(6):541.

Kriegstein A, Noctor S, Martínez-Cerdeño V. Patterns of neural stem and progenitor cell division may underlie evolutionary cortical expansion. *Nat Rev Neurosci*. 2006 Nov;7(11):883-90.

Kroenke CD, Bayly PV How Forces Fold the Cerebral Cortex. *J Neurosci* 24 January 2018, 38 (4) 767-775

Kumar RA, Marshall CR, Badner JA, Babatz TD, Mukamel Z, Aldinger KA, Sudi J, Brune CW, Goh G, Karamohamed S, Sutcliffe JS, Cook EH, Geschwind DH, Dobyns WB, Scherer SW, Christian SL (2009) Association and mutation analyses of 16p11.2

autism candidate genes. *PLoS ONE* 4: e4582.

Lacy SE, Bönnemann CG, Buzney EA, Kunkel LM. Identification of FLRT1, FLRT2, and FLRT3: a novel family of transmembrane leucine-rich repeat proteins. *Genomics*. 1999 Dec 15;62(3):417-26.

Lambert de Rouvroit C, Goffinet AM. Neuronal migration. *Mech Dev*. 2001 Jul;105(1-2):47-56.

Lee, G. H., and D'Arcangelo, G. (2016). New insights into reelin-mediated signaling pathways. *Front. Cell. Neurosci*. 10:122.

Leventer RJ, Guerrini R, Dobyns WB. Malformations of cortical development and epilepsy. *Dialogues Clin Neurosci*. 2008;10(1):47-62.

Leyva-Díaz E, Del Toro D, Menal M. J,Cambray S, Susín R, Tessier-Lavigne M, Klein R, Egea J, and López-Bendito G. Flrt3 is a robo1-interacting protein that determines netrin-1 attraction in developing axons. *Current Biology*, 24(5):494–508, 2014.

Linder CC, Genetic Variables That Influence Phenotype. *ILAR Journal*, Volume 47, Issue 2, 2006, Pages 132–1

Llinares-Benadero, C. & Borrell, V. Deconstructing cortical folding: genetic, cellular and mechanical determinants. *Nat. Rev. Neurosci*. 20, 161–176 (2019).

Lohmann G, Von Cramon DY, and Colchester AC. Deep sulcal landmarks provide an organizing framework for human cortical folding. *CerebralCortex*,18(6):1415–

1420 2007.

Long KR, Newland B, Florio M, Kalebic N, Langen B, Kolterer A, Wimberger P, Huttner WB. Extracellular Matrix Components HAPLN1, Lumican, and Collagen I Cause Hyaluronic Acid-Dependent Folding of the Developing Human Neocortex. *Neuron*. 2018 Aug 22;99(4):702-719.e6.

Lui JH, Hansen DV, Kriegstein AR. Development and evolution of the human neocortex. *Cell*. 2011 Jul 8;146(1):18-36.

Luo R, Jeong SJ, Jin Z, Strokes N, Li S, Piao X (2011) G protein-coupled receptor 56 and collagen III, a receptor-ligand pair, regulates cortical development and lamination. *Proc Natl Acad Sci USA* 108: 12925–12930.

Madisen L, Zwingman TA, Sunkin SM, Oh SW, Zariwala HA, Gu H, Ng LL, Palmiter RD, Hawrylycz MJ, Jones AR, Lein ES, Zeng H. A robust and high-throughput Cre reporting and characterization system for the whole mouse brain. *Nat Neurosci.* 2010 Jan;13(1):133-40.

Marcorelles, P., Laquerrière, A., Adde-Michel, C., Marret, S., Saugier-Veber, P.,Beldjord, C., et al. (2010). Evidence for tangential migration disturbances in human lissencephaly resulting from a defect in LIS1, DCX and ARX genes. *Acta Neuropathol*. 120, 503–515.

Maretto S., Müller P.-S., Aricescu A.R., Cho K.W.Y., Bikoff E.K., Robertson E.J. Ventral closure, headfold fusion and definitive endoderm migration defects in mouse embryos lacking the fibronectin leucine-rich transmembrane protein FLRT3. *Dev.*

Biol. 2008;318:184–193.

Marthiens V, Rujano MA, Pennetier C, Tessier S, Paul-Gilloteaux P, Basto R (2013) Centrosome amplification causes microcephaly. *Nat Cell Biol* 15: 731–740.

Martínez-Cerdeño V, Noctor SC. Neural Progenitor Cell Terminology. *Front Neuroanat.* 2018 Dec 6;12:104.

Masuda K, Toda T, Shinmyo Y, Ebisu H, Hoshiba Y, Wakimoto M, Ichikawa Y, Kawasaki H. Pathophysiological analyses of cortical malformation using gyrencephalic mammals. *Scientific Reports*. 2015;5:15370.

Meyer G, Soria JM, Martínez-Galán JR, Martín-Clemente B, Fairén A. Different origins and developmental histories of transient neurons in the marginal zone of the fetal and neonatal rat cortex. *J Comp Neurol.*

Mirzaa GM, Enyedi L, Parsons G, Collins S, Medne L, Adams C, Ward T, Davitt B, Bicknese A, Zackai E, Toriello H, Dobyns WB, Christian S (2014) Congenital microcephaly and chorioretinopathy due to de novo heterozygous KIF11 mutations: five novel mutations and review of the literature. *Am J Med Genet A* 164A: 2879–2886.

Molnár Z, Clowry GJ, Šestan N, Alzu'bi A, Bakken T, Hevner RF, Hüppi PS, Kostović I, Rakic P, Anton ES, Edwards D, Garcez P, Hoerder-Suabedissen A, Kriegstein A. New insights into the development of the human cerebral cortex. *J Anat*. 2019 Sep;235(3):432-451.

Molyneaux BJ, Arlotta P, Menezes JR, Macklis JD. Neuronal subtype specification in the cerebral cortex. *Nat Rev Neurosci*. 2007 Jun;8(6):427-37.

Mukhtar T, Taylor V. Untangling Cortical Complexity During Development. *J Exp Neurosci.* 2018 Mar 1;12:

Müller P.-S., Schulz R., Maretto S., Costello I., Srinivas S., Bikoff E., Robertson E. The fibronectin leucine-rich repeat transmembrane protein Flrt2 is required in the epicardium to promote heart morphogenesis. *Development*. 2011;138:1297–1308.

Nonaka-Kinoshita M, Reillo I, Artegiani B, Martínez-Martínez MÁ, Nelson M, Borrell V, Calegari F. Regulation of cerebral cortex size and folding by expansion of basal progenitors. *EMBO J*. 2013 Jul 3;32(13):1817-28.

O'Leary DD, Nakagawa Y. Patterning centers, regulatory genes and extrinsic mechanisms controlling arealization of the neocortex. *Curr Opin Neurobiol*. 2002;12:14–25.

O'Sullivan M.L., de Wit J., Savas J.N., Comoletti D., Otto-Hitt S., Yates J.R., III, Ghosh A. FLRT proteins are endogenous latrophilin ligands and regulate excitatory synapse development. *Neuron*. 2012;73:903–910.

Pang T, Atefy R, and Sheen V. Malformations of cortical development. *Theneurologist,* 14(3):181, 2008.

Passemard S, Titomanlio L, Elmaleh M, Afenjar A, Alessandri JL, Andria G, de Villemeur TB, Boespflug-Tanguy O, Burglen L, Del Giudice E, Guimiot F, Hyon C, Isidor B, Megarbane A, Moog U, Odent S, Hernandez K, Pouvreau N, Scala I, Schaer M et

al (2009) Expanding the clinical and neuroradiologic phenotype of primary microcephaly due to ASPM mutations. *Neurology* 73: 962–969.

Poirier K, Lebrun N, Broix L, Tian G, Saillour Y, Boscheron C, Parrini E, Valence S, Pierre BS, Oger M, Lacombe D, Genevieve D, Fontana E, Darra F, Cances C, Barth M, Bonneau D, Bernadina BD, N'Guyen S, Gitiaux C et al (2013) Mutations in TUBG1, DYNC1H1, KIF5C and KIF2A cause malformations of cortical development and microcephaly. *Nat Genet* 45: 639–647.

Raballo R, Rhee J, Lyn-Cook R, Leckman JF, Schwartz ML, Vaccarino FM. Basic Fibroblast Growth Factor (Fgf2) is necessary for cell proliferation and neurogenesis in the developing cerebral cortex. *J Neurosci*. 2000;20:5012–5023.

Rahimi-Balaei M, Bergen H, Kong J, Marzban H. Neuronal Migration During Development of the Cerebellum. *Front Cell Neurosci*. 2018 Dec 17;12:484.

Rakic, P. & Sidman, R. L. Supravital DNA synthesis in the developing human and mouse brain. J. Neuropathol. *Exp. Neurol*. 27, 246–276 (1968).

Rakic P, Evolution of the neocortex: a perspective from developmental biology. *Nature Reviews Neuroscience* 10, 724 (2009).

Rash BG, Lim HD, Breunig JJ, Vaccarino FM. FGF signaling expands embryonic cortical surface area by regulating Notch-dependent neurogenesis. *J Neurosci*. 2011 Oct 26;31(43):15604-17.

Reillo I, de Juan Romero C, García-Cabezas MÁ, Borrell V. A role for intermediate radial

glia in the tangential expansion of the mammalian cerebral cortex. *Cereb Cortex*. 2011 Jul;21(7):1674-94.

Rice DS, Curran T (2001) Role of the reelin signaling pathway in central nervous system development. *Annu Rev Neurosci* 24: 1005–1039.

Roll P, Rudolf G, Pereira S, Royer B, Scheffer IE, Massacrier A, Valenti MP, Roeckel-Trevisiol N, Jamali S, Beclin C, Seegmuller C, Metz-Lutz MN, Lemainque A, Delepine M, Caloustian C, de Saint Martin A, Bruneau N, Depetris D, Mattei MG, Flori E et al (2006) SRPX2 mutations in disorders of language cortex and cognition. *Hum Mol Genet* 15: 1195–1207.

Rousso, D. L., Pearson, C. A., Gaber, Z. B., Miquelajauregui, A., Li, S., Portera-Cailliau, C., et al. (2012). Foxp-mediated suppression of N-cadherin regulates neuroepithelial character and progenitor maintenance in the CNS. *Neuron* 74, 314–330.

Rubio-Garrido P, Pérez-de-Manzo F, Porrero C, Galazo MJ, Clascá F. Thalamic input to distal apical dendrites in neocortical layer 1 is massive and highly convergent. *Cereb Cortex*. 2009 Oct;19(10):2380-95.

Sahara S, O'Leary DD. Fgf10 regulates transition period of cortical stem cell differentiation to radial glia controlling generation of neurons and basal progenitors. *Neuro*n 2009 Jul 16;63(1):48-62.

Sakai D, Dixon J, Dixon MJ, Trainor PA (2012) Mammalian neurogenesis requires Treacle-Plk1 for precise control of spindle orientation, mitotic progression, and

maintenance of neural progenitor cells. *PLoS Genet* 8: e1002566.

Sauer ME, Walker BE. Radioautographic study of interkinetic nuclear migration in the neural tube. *Proc Soc Exp Biol Med*. 1959 Jul;101(3):557-60.

Seiradake, E.; Del Toro Ruiz, D.; Nagel, D.; Cop, F.; Härtl, R.; Ruff, T.; Seyit-Bremer, G.; Harlos, K.; Border, E. C.; Acker-Palmer, A. et al.: FLRT structure: Balancing repulsion and cell adhesion in cortical and vascular development. *Neuron* 84 (2), pp. 370 - 385 (2014) .

Sekine, K.; Kubo, K.; Nakajima, K. How does Reelin control neuronal migration and layer formation in the developing mammalian neocortex? *Neurosci.Res.*2014,*86*, 50–58.

Shao W, Yang J, He M, Yu XY, Lee CH, Yang Z, Joyner AL, Anderson KV, Zhang J, Tsou MB, Shi H, Shi SH. Centrosome anchoring regulates progenitor properties and cortical formation. *Nature*. 2020 Apr;580(7801):106-112.

Shin DM, Korada S, Raballo R, Shashikant CS, Simeone A, Taylor JR, Vaccarino F. Loss of glutamatergic pyramidal neurons in frontal and temporal cortex resulting from attenuation of FGFR1 signaling is associated with spontaneous hyperactivity in mice. *J Neurosci*. 2004;24:2247–2258.

Shinmyo Y, Terashita Y, Dinh Duong TA, Horiike T, Kawasumi M, Hosomichi K, Tajima A, Kawasaki H. Folding of the Cerebral Cortex Requires Cdk5 in Upper-Layer Neurons in Gyrencephalic Mammals. *Cell Rep*. 2017 Aug 29;20(9):2131-

2143.

Spalice A, Parisi P, Nicita F, Pizzardi G, Del Balzo F, Iannetti P. Neuronal migration disorders: clinical, neuroradiologic and genetics aspects. *Acta Paediatr*. 2009 Mar;98(3):421-33.

Spear PC, Erickson CA. Interkinetic nuclear migration: a mysterious process in search of a function. *Dev Growth Differ*. 2012 Apr;54(3):306-16.

Stahl R, Walcher T, Romero CDJ, Pilz GA, Cappello S, Irmler M, Sanz-Aquela JM, Beckers J, Blum R, Borrell V, et al. Trnp1 regulates expansion and folding of the mammalian cerebral cortex by control of radial glial fate. *Cell*, 153(3):535–549, 2013.

Stevens HE, Smith KM, Maragnoli ME, Fagel D, Borok E, Shanabrough M, Horvath TL, Vaccarino FM. Fgfr2 is required for the development of the medial prefrontal cortex and its connections with limbic circuits. *J Neurosci*. 2010;30:5590–5602.

Stocker, A. M., and Chenn, A. (2015). The role of adherens junctions in the developing neocortex. *Cell. Adh. Migr*. 9, 167–174.

Storm EE, Rubenstein JL, Martin GR. Dosage of Fgf8 determines whether cell survival is positively or negatively regulated in the developing forebrain. *Proc Natl Acad Sci U S A.* 2003;100:1757–1762.

Striedter GF, Srinivasan S, Monuki ES. Cortical folding: when, where, how, and why? *Annu Rev Neurosci*. 2015 Jul 8;38:291-307.

Subramanian L, Calcagnotto ME, Paredes MF. Cortical Malformations: Lessons in Human Brain Development. *Front Cell Neurosci*. 2020 Jan 24;13:576.

Sun T, Hevner RF, Growth and folding of the mammalian cerebral cortex: from molecules to malformations. *Nature Reviews Neuroscience* 15, 217 (2014).

Tabata H, Nakajima K. Multipolar migration: the third mode of radial neuronal migration in the developing cerebral cortex. *J Neurosci.* 2003 Nov 5;23(31):9996-10001.

Tallinen, T., Chung, J., Rousseau, F. et al. On the growth and form of cortical convolutions. *Nature Phys* 12, 588–593 (2016).

Tanos BE, Yang HJ, Soni R, Wang WJ, Macaluso FP, Asara JM, Tsou MF. Centriole distal appendages promote membrane docking, leading to cilia initiation. *Genes Dev* 2013 Jan 15;27(2):163-8.

Tavano, S., Taverna, E., Kalebic, N., Haffner, C., Namba, T., Dahl, A., et al. (2018). Insm1 induces neural progenitor delamination in developing neocortex via downregulation of the adherens junction belt-specific protein Plekha7. *Neuron* 97:e1298.

Taverna, E., Götz, M., and Huttner, W. B. (2014). The cell biology of neurogenesis: toward an understanding of the development and evolution of the neocortex. *Annu. Rev. Cell. Dev. Biol* 30, 465–502.

Taverna, E. & Huttner, W. B. Neural progenitor nuclei IN motion. *Neuron* 67, 906–914 (2010).

Thomson RE, Kind PC, Graham NA, Etherson ML, Kennedy J, Fernandes AC, Marques

CS, Hevner RF, Iwata T. Fgf receptor 3 activation promotes selective growth and expansion of occipitotemporal cortex. *Neural Dev*. 2009;4:4.

Thornton GK, Woods CG (2009) Primary microcephaly: do all roads lead to Rome? *Trends Genet* 25: 501–510.

Turrero García M, Chang Y, Arai Y, Huttner WB. S-phase duration is the main target of cell cycle regulation in neural progenitors of developing ferret neocortex. *J Comp Neurol* 2016 Feb 15;524(3):456-70.

Urness LD, Paxton CN, Wang X, Schoenwolf GC, Mansour SL. FGF signaling regulates optic placode induction and refinement by controlling both ectodermal target genes and hindbrain Wnt8a. *Dev Biol* 2010 Apr 15;340(2):595-604.

Vaccarino FM, Schwartz ML, Raballo R, Nilsen J, Rhee J, Zhou M, Doetschman T, Coffin JD, Wyland JJ, Hung YT. Changes in cerebral cortex size are governed by fibroblast growth factor during embryogenesis. *Nat Neurosci* 1999 Mar;2(3):246-53.

Valence S, Poirier K, Lebrun N, Saillour Y, Sonigo P, Bessieres B, Attie-Bitach T, Benachi A, Masson C, Encha-Razavi F, Chelly J, Bahi-Buisson N (2013) Homozygous truncating mutation of the KBP gene, encoding a KIF1B-binding protein, in a familial case of fetal polymicrogyria. *Neurogenetics* 14: 215–224.

Wang, J., Li, T., Wang, J. L., Xu, Z., Meng, W., and Wu, Q. F. (2020). Talpid3-Mediated Centrosome Integrity Restrains Neural Progenitor Delamination to Sustain Neurogenesis by Stabilizing Adherens Junctions. *Cell. Rep* 33:108495.

Wang L, Hou S, Han YG. Hedgehog signaling promotes basal progenitor expansion and the growth and folding of the neocortex. *Nat Neurosci* 2016 Jul;19(7):888-96.

Wang X, Tsai JW, LaMonica B, Kriegstein AR. A new subtype of progenitor cell in the mouse embryonic neocortex. *Nat Neurosci* 2011 May;14(5):555-61.

Wilsch-Bräuninger M, Huttner WB. Primary Cilia and Centrosomes in Neocortex Development. *Front Neurosci* 2021 Oct 21;15:755867.

Wilsch-Bräuninger, M., Florio, M., and Huttner, W. B. (2016). Neocortex expansion in development and evolution - from cell biology to single genes. *Curr. Opin. Neurobiol* 39, 122–132.

Wilson SW, Houart C. Early steps in the development of the forebrain. *Dev Cell* 2004 Feb;6(2):167-81.

Xavier M. Effect of the Genetic Background on the Phenotype of Mouse Mutations. Journal of the American Society of Nephrology 11(suppl_2):p S101-S105, November 2000.

Yamagishi S, Hampel F, Hata K, Del Toro D, Schwark M, Kvachnina E, Bastmeyer M, Yamashita T, Tarabykin V, Klein R, Egea J. FLRT2 and FLRT3 act as repulsive guidance cues for Unc5-positive neurons. *EMBO J* 2011 Jun 14;30(14):2920-33.

Yamamoto T, Kato Y, Karita M, Kawaguchi M, Shibata N, Kobayashi M (2004) Expression of genes related to muscular dystrophy with lissencephaly. *Pediatr Neurol* 31: 183–190.

Yin, Y., Bangs, F., Paton, I. R., Prescott, A., James, J., Davey, M. G., et al. (2009). The Talpid3 gene (KIAA0586) encodes a centrosomal protein that is essential for primary cilia formation. *Development* 136, 655–664.

Yoon, K., Nery, S., Rutlin, M.L., Radtke, F., Fishell, G., and Gaiano, N.(2004). Fibroblast growth factor receptor signaling promotes radial glial identity andinteracts with Notch1 signaling in telencephalic progenitors. *J. Neurosci* 24,9497–9506.

Yu TW, Mochida GH, Tischfield DJ, Sgaier SK, Flores-Sarnat L, Sergi CM, Topcu M, McDonald MT, Barry BJ, Felie JM, Sunu C, Dobyns WB, Folkerth RD, Barkovich AJ, Walsh CA (2010) Mutations in WDR62, encoding a centrosome-associated protein, cause microcephaly with simplified gyri and abnormal cortical architecture. *Nat Genet* 42: 1015–1020.

AUTHOR CONTRIBUTIONS

Gönül Seyit-Bremer contributed to imaging analysis of Figures 3.1 B,D and 3.3. D. Santiago Diaz Almeida contributed to imaging and statistical analysis of Figures 3.2 C,D and 3.8 A,B,C,D, and tracking neurons of time-lapse movies Figures 3.7.2 F. F' and 3.13.2 F, F'. Mihail Todorov Ivilinov contributed to imaging of Figures 3.4 B and 3.10 B. Tobias Ruff contributed to migration speed analysis of Figures 3.7.2 G and 3.12.2 G. Mouse genotyping was done by D. Santiago Diaz Almeida, Tania Reiser, Leonhard Schaffmayer, and Yasmin Alieva. Embryo genotyping was done by D. Santiago Diaz Almeida.

ACKNOWLEDGEMENTS

I would first like to express my great appreciation to my supervisor, Rüdiger Klein for the opportunity to work in a great environment with firm support on my research. Also, I would like to give great thanks to my thesis committee members, Laura Busse for valuable and constructive advice on my PhD journey, and Silvia Cappello for insightful scientific inputs and help with all kinds of scientific questions. I am also grateful to Daniel del Toro for endless inspiring thoughts and valuable scientific discussion and input to my project.

Many thanks to my great collaborator, Mihail Todorov Ivilinov, for helping with 3DiSCO imaging and for thoughtful suggestions on imaging analysis in IMARIS. Another wonderful collaborator, Tobias Ruff for helping with time-lapse movie experiments and migration speed analysis. Also, Songhai Shi for providing *Cep83*cKO mouse lines and insight scientific discussion.

Special thanks to D. Santiago Diaz Almeida for all his contribution to embryo genotyping and a lot of technical support on my research. Also, I would like to thank all my HiWis: Tania Reiser, Leonhard Schaffmayer, and Yasmin Alieva for mouse house work and our technician, Gönül Seyit-Bremer for technical support.

I also want to thank to Yi-Ju Shen, a great colleague in the FLRT team for having insightful scientific discussions and being a good friend in the lab. Also, thanks to all my fantastic colleagues, Kerstin Völkl, Hansol Lim, and Ylenia Mastrodicasa for having wonderful times both in and outside of the lab.

I also would like to acknowledge in the MPI-BI animal facility and transgenic center, Soo Jin Min-Weissenhorn for providing great support for our tremendous amount

of animals. Also, in the imaging facility of the MPI-BI, Robert Kasper for all the support for confocal and time-lapse movie imaging.

I also would like to thank Sonia Paixao for constructive and valuable scientific discussions, input and advice on my research and PhD. life. Thanks to Pilar Lucia Alcalà Morales and Louise Gaitanos for all the technical support during my studies and English editing.

I also would like to thank my friend, Minkyung Shin for thoughtful and supportive advice that enlighten my PhD life, and Yoona Kim and Minsun Kim for wonderful support and belief in me.

Also, thanks to Yeongseok Jeong and Eunjae Cho for having a lot of fun and great memories in Germany.

I also would like to thank my parent, Hyungsup Chun, and Meok Kim for their endless support and belief to allow me to pursue my passion for science during my BSc, MSc, and Ph.D. As great mentors in my life, I sincerely appreciate their devotion, love, and trust in me. Without their support and wise advice, I would not able to overcome the difficult times during my studies. Also, thanks to my sister, SangHee Chun who has always been a good mentor and friend in my life journey.

Finally, I am grateful to all the members of the Klein lab for having great times during my PhD journey.